Carleton University

Master's Thesis

Simulation of an Organic Memristor

Author:
Cem Bonfil

Supervisor:
Dr. Tom Smy
Dr. Steven P. McGarry

A thesis submitted in fulfilment of the requirements
for the degree of Master's of Science in Electrical and Computer Engineering

in the

Carleton University

December 2013

"Quote"

Cem Bonfil

CARLETON UNIVERSITY

Abstract

Faculty of Engineering
Department of Electronics

Master's of Science in Electrical and Computer Engineering

Simulation of an Organic Memristor

by Cem Bonfil

The device that is simulated in this thesis has a conducting PEDOT:PSS sheet with two metal contacts and an electrolyte solution containing lithium and perchlorate ions is placed on top of the conducting sheet. When a potential is applied at both ends of the conducting polymer, lithium ions, which act as reversible counter doping agents, travel into the PEDOT and modify the conductivity of the sheet. Overall this system mainly consists 4 different charge carriers, 3 (holes, lithium and perchlorate ions) mobile and 1 stationary (electrons).

Acknowledgements

The acknowledgements and the people to thank go here, don't forget to include your project advisor...

Contents

List of Figures

List of Tables

Abbreviations

BTE	Boltzmann Transport Equations
CFL	Courant-Friedrichs-Lewy
ClO_4^-	Perchlorate
DD	Drift Diffusion
FD	Finite Difference
Li^+	Lithium
PEDOT	Poly(3,4-ethylenedioxythiophene)
PSS	Poly(styrenesulfonate)
SG	Scharfatter-Gummel

Physical Constants

Boltzmann Constant	k	=	$8.6173324\ 10^{-5}$ eV/K
Elementary Charge	q	=	$1.6021765\ 10^{-19}$ C
Vacuum Permittivity	ϵ_0	=	$8.8541878\ 10^{-12}$ F/m

Symbols

D	Diffusivity	m^2/s
E	Electric Field	V/m
h	Unit Distance	m
I	Current	A
J	Current Density	A/m^2
L_D	Debye Length	m
l_f	Mean Free Path	m
M	Memristance	Ω
n	Electron Density	m^{-3}
N_A	Acceptor Density	m^{-3}
N_D	Donor Density	m^{-3}
n_i	Intrinsic Carrier Density	m^{-3}
T	Temperature	K
t	Time	s
t_{dr}	Dielectric Relaxation Time	s
U	Generation Recombination Rate	$m^{-3}s^{-1}$
V	Potential	V
V_{th}	Thermal Voltage	V

Δ	Unit Distance	m
ε_r	Relative Permittivity	unitless
μ	Mobility	$m^2/(Vs)$
φ	Flux Linkage	Wb
ρ	Charge Density	C/m^3
υ	Drift Speed	m/s

For/Dedicated to/To my...

Chapter 1

Introduction

1.1 Thesis Objectives

The purpose of this thesis is to create a numerical simulation which captures the phyiscs behind the operation of a memristor. The memristor simulation developed in this thesis could be used for researching the physics behind the actual device through further modeling or it could be used as a tool for designing memristors for a specific use. (maybe few more sentences)

1.2 Thesis Overview

Background section briefly talks about the history of memristor and how it was discovered before introducing the challenges and obstacles in research of memristors. It emphasizes the need for better physical modeling and lack of simulation tools required for further analysis and research.

In chapter 2 , Boltzmann Transport Equations (BTE) are shortly introduced. This introduction is followed by explanation of transport mechanisms captured through BTE. Additionally drift diffusion equations (simplified form of BTE) which will be used for the simulation of the memristor are discussed. Finally few analytic solutions to drift diffusion equations, such as charged particles moving over an infinite line and PN junction, are generated.

A numerical solution to drift diffusion equations is formed to calculate the movement of all the charged particles in chapter 3. First finite difference method, which is the basis for all the simulations in this thesis,is introduced. Then it is applied to drift diffusion equations. Additionally, a Poisson solver to be used with drift diffusion equations is

developed in order to calculate the electric field generated by charged particles and metal contacts. Also, boundary conditions necessary for the solution of both drift diffusion and Poisson solver are introduced. All the equations and boundary conditions combined generates a set of equations to be solved. Various schemes for solving these differential equations as well as the problems numerical and physical limitations are discussed in detail.

In chapter 4, the numerical solver developed in chapter 3 is tested against analytic solutions as well as a commercially available simulator called COMSOL Multiphysics. A mechanism to limit the maximum density of any particle, which is essential for memristor simulation, is developed and tested.

After the stability and accuracy of the simulation scheme was tested in chapter 4, a memristor model is introduced in chapter 5. The difficulties in the simulation due to physical an numerical restrictions were discussed. A possible approximation 1-D approximation for a 2-D memristor simulation was proposed and simulated. After demonstrating that the simulations produced reasonable results, the validity of the approximations made for 1-D and 2-D simulations are investigeted.

A full simulation 2-D is made in chapter 6. A memristor with various PEDOT thicknesses were simulated. The simulation with thinnest PEDOT is compared to 1-D simulations made in previous chapters. This chapter ends with comparison of simulation results with experimental data and shows how parameter fitting can be used to match expermental data.

The conclusion chapter summarizes the findings of the thesis, discusses advantages and disadvantages of the proposed simulation methods and provides suggestions for improvements on the model and opportunities further research.

1.3 Background

The term memristor was first used by Chua in 1971 in his paper called "Memristor The Missing Circuit Element" [1]. He theorized that there is a fourth passive circuit element yet to be discovered in addition to resistor,capacitor and inductor. He said that we already know and use five out of six possible combinations that can be made out of four fundamental circuit variables, current I, voltage V, charge q and flux linkage φ. Chua claimed that we were missing a circuit element which produces a relationship between flux linkage(time integral of the potential) and charge. He introduced a new variable named memristance which has units of resistance and it is a function of charge.

The relationship between the current and the potential of a memristor is calculated by replacing the resistance by memristance in ohms law:

$$v(t) = M(q(t))i(t) \tag{1.1}$$

Theoretically memristor retains its resistance in the absence of any power source. When a potential is applied the resistance can be influenced by the direction and the magnitude of the current. If the current flows in one dirfection resistance increases and if it flows in the other direction resistance decreases. This produces an I-V response which looks like a pinched hysteresis curve. This response is the main characteristic of a memristor.

This new element remained mostly a theory and did not get much academic attention until a group of researchers in Hewlett Packard developed a fully functioning memristor. They successfully fabricated a nano scale memristor using TiO_2 (titanium dioxide). After the discovery in HP labs there was an increase of interest in different types of memristors due to their potential applications for data storage and addition of learning capabilities into passive circuits.

Recently it has been suggested that organic based memristors could be fabricated (ref). This thesis will be concerned with such devices. They are usually constructed on a larger scale than the ones fabricated in HP labs. The memristor studied in this thesis is in millimeter rather then nano meter scale and uses a conductor made out of a polymer called PEDOT:PSS. It is made of two polymer chains, PEDOT and PSS attached together and conducts electricity via hole transport. Unfortunately the conduction mechanism is not perfectly understood and needs further research due to the complexity of the material(ref).

Unlike a semiconductors like silicon, the structure of a polymer is quite irregular. Polymers have individual molecules with different chain lengths and a variable amount of defects. Additionally, they can be amorphous or partially crystalline and further differences occur through aging. The conduction and electronic properties depend the orientation of polymer chains which can change in x,y and z directions. These irregularities in the structure makes these conducting polymers resemble amorphous inorganic semiconductors. Following the concept of charge transport in amorphous inorganic semiconductors, the conduction mechanism of conducting polymers is commonly explained by variable range hopping. This mechanism was first introduced by Mott in 1968. He proposed a model for charge transport in systems that are randomly disordered. In variable range hopping charge transport occurs via jumps between available sites. Every charge carrier has a probability of jumping between two sites depending on its energy

and the distance to the next available site. Temperature has a big impact on conductivity since it changes the structure of the molecules and increases the energy of charge carriers.

Apart from temperature there are other ways to change the conductivity of PEDOT. It is possible to affect conductivity by either doping or counter doping. Depending on the method used, doping can be reversible or permanent. When reversible doping is employed, resulting device behaves like a memristor since its resistance is now dependent on charge. All these effects make physical modeling, experimentation and simulation very challenging.

There are few approximate analytic solutions for inorganic memristors similar to the one produced in HP labs. These solutions are mostly based on parameter fitting and some basic physics. Studies on organic memristors are even more sparse than studies on inorganic ones. The physics behind the conduction mechanism and the changes in conductivity due to doping requires further research and development of a computer model can help in various ways. First of all it is very difficult to get experimental data on the movement of ions and holes inside PEDOT due its disordered structure. The thickness of PEDOT:PSS (usually in μm scale) complicates the tracing of the ion in all dimensions. Theories that explain the movement of charged particles and their interactions with each other are difficult to formulate since it is hard to obtain required experimental data. A simulation can be a useful tool in testing various theories without having to set up and perform complicated experiments. Also once a solid understanding of the conduction mechanism has been achieved, simulations can be very useful to test different device structures and optimize them before fabrication.

(add lack of simulations for memristor)

Chapter 2

Theory

2.1 Carrier Transport Equations

We will be solving drift-diffusion equations, which are based on BTE, in order to model the complex behaviour of the memristor. Drift-diffusion equations can be obtained by simplifying BTE equation via approximations. These simplifications dictate the limits of the drift-diffusion model. The approximations also serve as guidelines for where this model can and can not be used, therefore they need to be well understood.

Derivation of Boltzmann transport equation starts by stating that charged particles can be defined by their position in space **r** and momentum **k** at time **t** using a probability distribution function f(k,r,t). We get the most general form of Boltzmann transport equation. [8]

$$\frac{d}{dt}f(k,r,t) = 0 \tag{2.1}$$

This general form of BTE needs to be expanded and relevant physical equations need to be plugged in to get an appropriate equation describing specific a problem or device. Many different device simulators use some sort of approximation to BTE. In a semiconductor device we are usually interested in the movement and the density distribution of charge carriers, holes (p) and electrons (n).

After this brief introduction to BTE, rather than going through the tedious mathematical derivation of the drift diffusion model we can directly discuss the approximations that are made along the process of derivation in order to get a better insight on the model. As a particle travels in a solid state device it collides with other particles as well as the atoms in the device. For drift-diffusion equations individual lattice scattering events or

collisions are averaged and the particles have an average constant velocity under the effects of an electric field. This means that all the particles respond instantaneously to the changes in the electric field. The movement of the particles due to electric field is called the drift current. The relationship between drift velocity and the electric field is given by the following equation:

$$v = \mu E \tag{2.2}$$

μ is called mobility constant and it determines the speed at which the particles are going to move when subject to an electric field. Based on drift velocity we can get a term for drift current density.

$$J_E = qn\mu E = qnv \tag{2.3}$$

Where q is the elementary charge and n is the electron density. In addition to the previous assumptions, we assume that the lattice is perfectly uniform, has a uniform temperature distribution and all the particles are close to the temperature of the lattice. Based on this assumption we can say that all the particles that move due to thermal effects has the same thermal velocity (v_{th}) and mean free path (l_f). These quantities can be combined into one single coefficient called diffusion constant.

$$D = v_{th}\, l_f \tag{2.4}$$

Drift and diffusion coefficients are related to each other via Einstein relationship:

$$D = \frac{\mu kT}{q} \tag{2.5}$$

Where k is the Boltzmann constant and T is the lattice temperature. Now we have a second term which contributes to carrier movement which is called the diffusion current density.

$$J_D = qD\frac{dn}{dx} \tag{2.6}$$

Unlike the drift current density, which is directly related to the carrier density, diffusion current density is related to the carrier density's first order derivative in space.

Combining these two terms we get the current density equation for electrons in one dimension.

$$\vec{J_n^x} = q\mu_n n\vec{E_x} + qD_n\frac{dn}{dx} \tag{2.7}$$

This equation can be easily extended to more dimensions by simply using the appropriate terms.

$$\vec{J_n^y} = q\mu_n n\vec{E_x} + qD_n\frac{dn}{dy} \tag{2.8}$$

At this point we can also note that anisotropic drift and diffusion coefficients can also be handled with ease by using different coefficients for different directions. Current density equation works equivalently well for positively or negatively charged particles.

$$\vec{J_p^x} = q\mu_p p\vec{E_x} - qD_p\frac{dp}{dx} \tag{2.9}$$

Current density equations by themselves are not enough to solve a time dependent problem. For this we need to account the movement of charge over time which is captured in the continuity equation. It is basically a statement of conservation of particle density over time. The change in the amount of carriers over time in a particular area must be equal to the difference in current density over the same area. Additionally the amount of charge can change due to generation-recombination of charged particles.

$$\frac{\partial n}{\partial t} = \frac{1}{q}\nabla \cdot \vec{J_n} + U_n \tag{2.10}$$

$$\frac{\partial p}{\partial t} = -\frac{1}{q}\nabla \cdot \vec{J_p} + U_p \tag{2.11}$$

U_n and U_p are net generation recombination rates.

We must keep in mind that electric field in an area can be generated in two different ways. One is through the distribution of net charge over the area and the other one is an externally applied field. It is possible calculate the potential distribution over an area by using Poisson's equation. Once the potential is known the electric field can be obtained by just calculating the negative gradient of the electric potential.

$$\nabla \cdot (\varepsilon \nabla V) = -\rho = -q(p - n + N_D^+ - N_A^-) \tag{2.12}$$

$$\vec{E} = -\nabla V \tag{2.13}$$

We can split the electric field into two components $\vec{E_x}$ and $\vec{E_y}$.

$$\vec{E_x} = -\frac{\partial V}{\partial x} \tag{2.14}$$

$$\vec{E_y} = -\frac{\partial V}{\partial y} \tag{2.15}$$

It is possible to see that through the electric field and net charge distribution, Poisson's equation and drift-diffusion equations are coupled and non linear. The strength of the non linearity depends on the size of the device and charge density which determines the total amount of charge over an area.

Usually we are particularly interested in finding the amount of current in a device. This can be easily calculated by integrating the current density over an area.

$$I = \int_s \vec{J_{tot}} \cdot ds = \int_s (J_n + J_p + \varepsilon \frac{\partial E}{\partial t}) ds \tag{2.16}$$

Overall the main equations for the drift-diffusion model can be compactly written as:

$$\nabla \cdot (\varepsilon \nabla V) = -q(p - n + N_D^+ - N_A^-) \tag{2.17}$$

$$\vec{J_n} = q\mu_n n\vec{E} + qD_n \nabla n \tag{2.18}$$

$$\vec{J_p} = q\mu_p p\vec{E} - qD_p \nabla p \tag{2.19}$$

$$\frac{\partial n}{\partial t} = \frac{1}{q}\nabla \cdot \vec{J_n} + U_n \tag{2.20}$$

$$\frac{\partial p}{\partial t} = -\frac{1}{q}\nabla \cdot \vec{J_p} + U_p \tag{2.21}$$

Unfortunately even after so many approximations and simplifications to BTE, drif diffusion equations have analytical solutions for only few isolated cases. The simplicity of these analytical solutions makes them a good candidate for testing any numerical methods that is created to solve drift diffusion equations.

2.2 Analytic Solutions

2.2.1 Steady State Solution Over a Finite Domain

The simplest problem we can solve using drift diffusion model is charge enclosed over a finite area. Basically there is no flow in or out of the area we are solving for. There is a finite amount of charge and a uniform electric field which does not get affected by the enclosed charge. Now to get an analytic solution we assume that everything is at steady state and all the transients have died. In this case the total current density in the device must be zero. It is important to note here that the initial distribution of the charge density does not matter in this problem since everything will be redistributed in steady state. We only need to know the total amount of charge over the entire area.

$$J_p(x) = q\mu_p pE - qD_p\frac{dp}{dx} = 0 \tag{2.22}$$

Total current density will only be zero when the drift current density generated by the electric field is completely balanced by the diffusion current density.

$$q\mu_p pE = qD_p\frac{dp}{dx} \tag{2.23}$$

$$\frac{\mu_p E}{D_p}p = \frac{dp}{dx} \tag{2.24}$$

Here we have a very simple differential equation that can be solved by assuming that it has the following form:

$$p(x) = Ce^{ax} \tag{2.25}$$

C and **a** are arbitrary constants. Now we can plug equation (2.25) into (2.24)

$$\frac{\mu_p E}{D_p}Ce^{ax} = aCe^{ax} \tag{2.26}$$

$$a = \frac{\mu_p E}{D_p} \tag{2.27}$$

Plugging **a** back to equation (2.25) we get a general form for the solution.

$$p(x) = Ce^{\frac{\mu_p E}{D_p}x} \tag{2.28}$$

It is possible to solve for **C** by observing that the total number of charges at steady state must be equal to the initial number of charges. So the integral of charge density at time zero must be equal to the integral of charge density at steady state.

$$\int_0^L Ce^{\frac{\mu_p E}{D_p}x}dx = \int_0^L p(t=0,x)dx$$

$$C = \frac{\int_0^L p(t=0,x)dx}{\int_0^L e^{\frac{\mu_p E}{D_p}x}dx}$$

$$C = \frac{\int_0^L p(t=0,x)dx}{\frac{D_p}{\mu_p E}[e^{\frac{\mu_p E}{D}L} - 1]} \tag{2.29}$$

So the full solution takes the following form:

$$p(x) = \frac{\int_0^L p(t=0,x)dx}{\frac{D_p}{\mu_p E}[e^{\frac{\mu_p E}{D}L} - 1]}e^{\frac{\mu_p E}{D_p}x} \tag{2.30}$$

By examining the solution we can tell that increasing electric field will concentrate the charge density at the edge of the area. Physically this makes perfect sense since the force that is pushing the particles is getting greater and it is making the charges accumulate more in one side.

Since this solution does not have any time dependence it is not suitable for testing a numerical methods transient response but it is quite good for testing the accuracy of a steay-state solution as well as the conservation of mass over time.

2.2.2 Transient Solution Over an Infinite Domain

This time, in order to find a transient solution, we need to use the continuity equation (2.10). The problem we are going to solve consists of an initial particle density distribution subject to a uniform electric field over an infinitely long conductor. Same as the steady state problem we solved earlier, the particle density's effect on the electric field is negligible therefore we do not need to solve for Poisson's equation at the same time.

We start our solution by plugging (2.7) into (2.10) and assuming that generation/recombination rate is zero, so $U_n = 0$.

$$\frac{\partial n}{\partial t} = \frac{1}{q}\nabla \cdot (\vec{J_n}) \tag{2.31}$$

$$\frac{\partial n}{\partial t} = \frac{1}{q}\nabla \cdot (q\mu_n n\vec{E} + qD_n\frac{dn}{dx}) \tag{2.32}$$

For 1-D above equation can be simplified to:

$$\frac{\partial n}{\partial t} = \mu_n E\frac{dn}{dx} + D_n\frac{d^2n}{dx^2} \tag{2.33}$$

Here we make use of separation of variables which assumes that the solution can be separated into a time and space dependent functions.

$$n(t,x) = n(t)n(x) = n_t n_x \tag{2.34}$$

Plugging equation (2.34) into (2.33) and dividing by n(t,x),

$$\frac{1}{n_t}\frac{dn_t}{dt} = \mu_n E\frac{1}{n_x}\frac{dn_x}{dx} + D\frac{1}{n_x}\frac{d^2n_x}{dx^2} \tag{2.35}$$

Assuming both sides of the equation are equal to a constant -k, time dependent part of the problem becomes a simple first order differential equation.

$$\frac{1}{n_t}\frac{dn_t}{dlt} = -k$$

$$\frac{dn_t}{dt} = -kn_t$$

Based on the above differential equation we can get a general form for n_t:

$$n_t = C_1 e^{-kt} \tag{2.36}$$

Now for n_x assume a solution in the following form,

$$n_x = C_2 e^{-j\omega x} \tag{2.37}$$

Plug (2.37) into (2.35)

$$\omega^2 D C_2 e^{-j\omega x} - j\omega\mu_n E C_2 e^{-j\omega x} + k C_2 e^{-j\omega x} = 0 \tag{2.38}$$

Simplifying equation (2.38) and solving for k gives,

$$k = \omega^2 D + j\omega\mu_n E \tag{2.39}$$

Combining equation (2.36), (2.37) and (2.39) to get the initial form of the solution. ($C = C_1 C_2$)

$$n = n_t n_x = C e^{(-\omega^2 D + j\omega\mu_n E)t} e^{-j\omega x} \tag{2.40}$$

Using superposition principle we get,

$$n = n_t n_x = \int_{-\infty}^{\infty} C(\omega) e^{(-\omega^2 D + j\omega\mu_n E)t} e^{-j\omega x} d\omega \tag{2.41}$$

The distribution of n_x is known at t=0.

$$n(x, t = 0) = \int_{-\infty}^{\infty} C(\omega) e^{-j\omega x} d\omega \tag{2.42}$$

$C(\omega)$ is just the inverse fourier transform of $n(x, 0)$.

$$C(\omega) = \int_{-\infty}^{\infty} n(x, 0) e^{-j\omega x} dx \tag{2.43}$$

Plugging equation (2.43) into (2.41) we get the final form of the solution,

$$n = \int_{-\infty}^{\infty} \int_{-\infty}^{\infty} n(z,0) e^{j\omega z} dz e^{(\omega^2 D - j\omega\mu_n E)t} e^{-j\omega x} d\omega \tag{2.44}$$

Rearranging equation (2.44),

$$n = \int_{-\infty}^{\infty} \int_{-\infty}^{\infty} n(z,0) e^{(\omega^2 D - j\omega\mu_n E)t} e^{-j\omega x} e^{j\omega z} dz d\omega \tag{2.45}$$

If the initial distribution is a gaussian distribution then we get,

$$n(x,0) = e^{-(\frac{x-x_o}{\sigma})^2} \tag{2.46}$$

$$n(x,t) = \frac{1}{\sqrt{4D_n\sigma^{-2}t+1}} e^{-\frac{(t\mu_n E - x + x_o)}{4D_n t + \sigma^2}} \tag{2.47}$$

If the initial distribution is a rectangular distribution then we get,

$$n(x,0) = \prod(w(x)) \tag{2.48}$$

$$n(x,t) = \frac{1}{2} erf(\frac{w + 2t\mu_n E - 2x}{4\sqrt{D_n t}}) - \frac{1}{2} erf(\frac{-w + 2t\mu_n E - 2x}{4\sqrt{D_n t}}) \tag{2.49}$$

2.2.3 PN Junction

Previous analytical solutions involved the solution of Poisson's equation and continuity equation which were not coupled. Now we can look at an example where these equations are tightly coupled. There are usually no direct analytical solution for coupled equation but it is possible to get a closed form solution by making use of certain approximations. One simple example of this situation is an abrupt p-n junction. An abrupt p-n junction is created when two materials of uniform opposite doping,p type and n type, are brought together. A p type material has an excess number of acceptors N_A and an n type material has an excess number of donors N_D. The junction is defined at the interface where $N_A = N_D$.

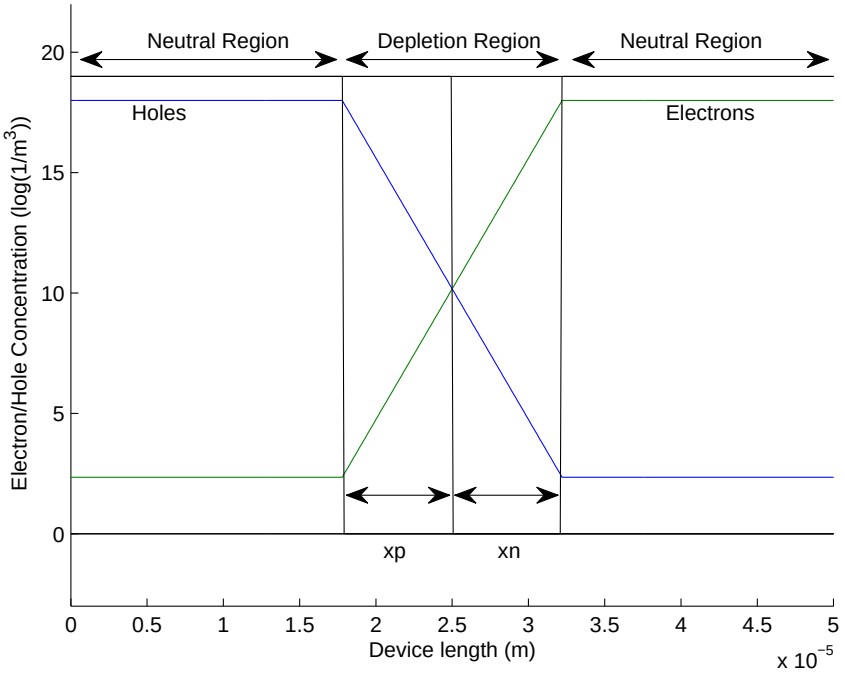

FIGURE 2.1: PN junction electron/hole density

In this example we will be deriving an analytical solution for an abrupt p-n junction. In order to get a solution for this problem we can make use of the depletion region approximation. This approximation starts by assuming that the charges are fully depleted around the junction. All the electric field is confined in the depletion region and regions far away from the junction are neutral. Based on this the net charge density over the entire region is:

$$\frac{d\vec{E}}{dx} = \frac{\rho}{\varepsilon} = \frac{q}{\varepsilon}(-N_A + N_D) \tag{2.50}$$

$$\rho = \begin{cases} 0 & \text{for } x < -x_p \\ -qN_A & \text{for } -x_p \leq x \leq 0 \\ qN_D & \text{for } 0 \leq x \leq < x_n \\ 0 & \text{for } x > x_n \end{cases} \tag{2.51}$$

The electric field over the entire region can be calculated by integrating ρ.

$$E = \begin{cases} \int \frac{-qN_A}{\varepsilon} dx + C_1 & \text{for } -x_p \leq x \leq 0 \\ \int \frac{qN_D}{\varepsilon} dx + C_2 & \text{for } \ 0 \leq x \leq x_n \end{cases} \tag{2.52}$$

We can solve for C_1 and C_2 since electric field must go to zero at x_p and x_n.

$$E(x = -x_p) = 0 \ \ \Rightarrow \ \ C_1 = \frac{-qN_A}{\varepsilon} x_p \tag{2.53}$$

$$E(x = x_n) = 0 \ \ \Rightarrow \ \ C_1 = \frac{qN_D}{\varepsilon} x_n \tag{2.54}$$

Then E(x) becomes:

$$E(x) = \begin{cases} \frac{-qN_A}{\varepsilon}(x + x_p) & \text{for } -x_p \leq x \leq 0 \\ \frac{qN_D}{\varepsilon}(x - x_n) & \text{for } 0 \leq x \leq x_n \end{cases} \tag{2.55}$$

Additionally, we know that the electric field must be continuous across the interface therefore the electric field in the p-type side and the n-type side must equal each other at the interface or when x = 0.

$$\frac{-qN_A}{\varepsilon}(x_p) = \frac{qN_D}{\varepsilon}(-x_n) \tag{2.56}$$

$$N_A x_p = N_D x_n \tag{2.57}$$

This equation makes physical sense since it states that the total charge on one side of the junction must be the same as the total charge on the other. In other words, the net charge on each side keeps the electric field confined to the depletion region.

To find the voltage as a function of distance, we can make use of equation 2.13 and integrate the electric field.

$$V(x) = \begin{cases} \int -E(x)dx = \int \frac{qN_A}{\varepsilon}(x + x_p)dx = \frac{qN_A}{\varepsilon}(\frac{x}{2} + x_p) + C_3 & \text{for} - x_p \leq x \leq 0 \\ \int -E(x)dx = \int \frac{qN_D}{\varepsilon}(x - x_n)dx = \frac{qN_D}{\varepsilon}(-\frac{x}{2} + x_n) + C_4 & \text{for } 0 \leq x \leq x_n \end{cases} \tag{2.58}$$

We are usually interested in the potential difference across the junction and can arbitrarily set one side to zero. Here we define the voltage on the p type side as zero, such that at x= x_p, V=0. This gives the constant C3 as:

$$C_3 = \frac{qN_A}{2\varepsilon}x_p^2 \tag{2.59}$$

$$V(x) = \frac{qN_A}{2\varepsilon}(x + x_p)^2 \quad \text{for} - x_p \leq x \leq 0 \tag{2.60}$$

We can find C4 by using the fact that the potential on the n-type side and p-type side are equal at the interface, such that:

$$V_p(x = 0) = \frac{qN_A}{2\varepsilon}x_p^2 = V_n(x = 0) = \frac{qN_A}{2\varepsilon}(x_n - \frac{x}{2})x + C_4 \tag{2.61}$$

$$C_4 = \frac{qN_A}{2\varepsilon}x_p^2 \tag{2.62}$$

Now we can get an overall expression for V(x).

$$V(x) = \begin{cases} \frac{qN_A}{\varepsilon}(x + x_p)^2 & \text{for} - x_p \leq x \leq 0 \\ \frac{qN_D}{\varepsilon}(-\frac{x}{2} + x_n)x & \text{for } 0 \leq x \leq x_n \end{cases} \tag{2.63}$$

The maximum voltage across the junction is at $x = x_n$, which is:

$$V_{bi} = \frac{q}{2\varepsilon}(N_D x_n^2 + N_A x_p^2) \tag{2.64}$$

Using (2.57) in the above equation and rearranging allows x_p and x_n to be determined. They are:

$$x_n = \sqrt{\frac{2\varepsilon V_{bi}}{q}\frac{N_A}{N_D(N_D + N_A)}} \tag{2.65}$$

$$x_p = \sqrt{\frac{2\varepsilon V_{bi}}{q} \frac{N_D}{N_A(N_D + N_A)}} \tag{2.66}$$

The value of the built in potential can also be calculated using fermi levels of p and n doped materials.

$$E_{FN} - E_i = kT\ ln(\frac{N_D}{n_i}) \tag{2.67}$$

$$E_i - E_{FP} = kT\ ln(\frac{N_A}{n_i}) \tag{2.68}$$

E_{FN} and E_{FP} are fermi energy levels of electrons and holes respectively. The difference between the fermi levels divided by the single electron charge gives us the built in potential of the pn junction.

$$E_{FN} - E_{FP} = qV_{bi} = kT\ ln(\frac{N_D}{n_i}) + kT\ ln(\frac{N_A}{n_i}) = kT\ ln(\frac{N_A N_D}{n_i^2}) \tag{2.69}$$

$$V_{bi} = \frac{kT}{q}\ ln(\frac{N_A N_D}{n_i^2}) \tag{2.70}$$

With the calculation of the built in potential we have all the information we need for the analytical solution of the pn junction without any external bias. Following graphs shows the plots of approximate solutions for net charge, electric field and the junction potential.

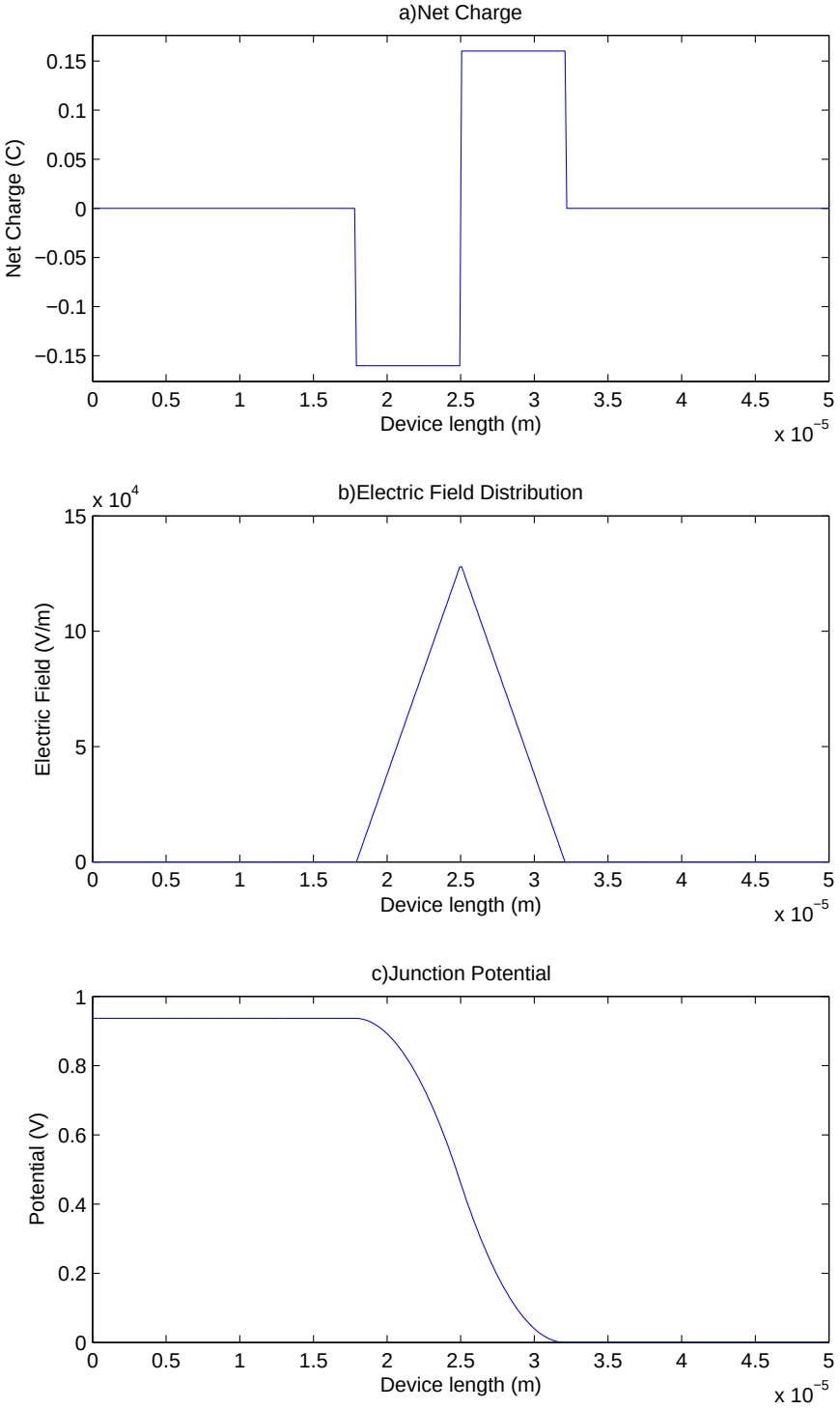

FIGURE 2.2: Approximate Solution of a PN Junction

Chapter 3

Numerical Solution of Drift-Diffusion Equation

3.1 Finite Difference Method

There are many different methods that can be used to solve drift diffusion equations such as finite elements, finite difference or meshless methods. We will be using finite difference method which uses an approximation for the derivative of a function based on the mathematical definition of the derivative.

$$\frac{df}{dx} = \lim_{h \to 0} \frac{f(x+h) - f(x)}{h} \tag{3.1}$$

We can get a numerical approximation for the first derivative by dropping the limit and assuming that h is small enough to get a value for the derivative reasonably close to the actual value. Of course as h gets smaller the approximation becomes more and more accurate. The difference between the calculated value and the real value is called the truncation error and it is captured using $O(h^n)$ notation. n signifies the order of h which determines how fast the approximation is approaching the real solution as h decreases.

$$\frac{df}{dx} = \frac{f(x+h) - f(x)}{h} + O(h) \tag{3.2}$$

It is possible to uniformly discretise the entire region over which a function is defined in order to calculate its derivative. We start by dividing the region over which the function is defined into *n-1* segments therefore there will be n number of points. Then we can find the length of each segment using the following relationship:

$$h = \frac{L}{n} \tag{3.3}$$

The function we are interested in is defined on the edge of every segment. We can label each point consecutively, $x_0, x_1, x_2 \ldots x_{n-1}$ where $x_i = ih$. Our function is discretely defined on $f_i = f(x_i)$ where *i=0,1,2..n-1*. It is possible to use equation 3.2 to discretely calculate the first derivative of the function with respect to x.

$$\frac{df(x_i)}{dx} = \frac{f(x_{i+1}) - f(x_i)}{h} + O(h) \tag{3.4}$$

Above equation is called forward difference because the derivative for point x_i was calculated using the point that is coming right after it, x_{i+1}.

$$f_i^{'} = \frac{f_{i+1} - f_i}{h} + O(h) \tag{3.5}$$

Forward difference is not the only way to calculate a discrete derivative. Here are a few more ways calculate the same derivative by making use of different points.

$$f_i^{'} = \frac{f_i - f_{i-1}}{h} + O(h) \tag{3.6}$$

$$f_{i+\frac{1}{2}}^{'} = \frac{f_{i+1} - f_i}{h} + O(h^2) \tag{3.7}$$

Equation 3.6 is called backward difference and equation 3.7 is called central difference. One important thing to note here is that in the central difference formula the derivative falls exactly in the middle of two points. It also gives more accurate results using the same number of points as forward and backward difference.

Using finite difference formulas it is possible to construct higher derivatives. Lets look at how to get a formula for a second order derivative at point x_i using central difference. First step is to calculate the first order derivative on $x_{i-\frac{1}{2}}$, x_i and $x_{i+\frac{1}{2}}$

$$f_{i+\frac{1}{2}}^{'} = \frac{f_{i+1} - f_i}{h} \tag{3.8}$$

$$f_{i-\frac{1}{2}}^{'} = \frac{f_i - f_{i-1}}{h} \tag{3.9}$$

$$f_i^{'} = \frac{f_{i+\frac{1}{2}} - f_{i-\frac{1}{2}}}{h} \tag{3.10}$$

We can take the second derivative of the last function and plug in the first two.

$$f_i^{''} = \frac{f_{i+\frac{1}{2}}^{'} - f_{i-\frac{1}{2}}^{'}}{h}$$

$$f_i^{''} = \frac{\frac{f_{i+1}-f_i}{h} - \frac{f_i-f_{i-1}}{h}}{h}$$

$$f_i^{''} = \frac{f_{i+1} - f_i - f_i + f_{i-1}}{h^2}$$

After some algebra we get the final form of the second derivative.

$$f_i^{''} = \frac{f_{i+1} - 2f_i + f_{i-1}}{h^2} + O(h^2) \tag{3.11}$$

Overall these finite difference equations are enough to solve drift diffusion equations. Even though all the derivations were done in 1-D it is trivial to extend them to higher dimensions. Now we can use finite difference method to solve Poisson's equation and drift diffusion equations.

3.2 Solving Drift-Diffusion Equations

3.2.1 Poisson Solver

Since we are dealing with electronic devices there is usually going to be an electric field in the system generated by an external source or generated within the device through charged particles. Either way we need to solve Poisson's equation in order find the potential distribution as well as the electric field inside the device. We can start by simplifying the equation through assumptions and then we can employ finite difference to solve this simplified equation. The first step of simplification is assuming that the permittivity is isotropic, then we can get:

$$\nabla \cdot (\varepsilon \nabla V) = -\rho \tag{3.12}$$

$$\nabla \cdot (\varepsilon \nabla V) = \varepsilon \nabla^2 V \tag{3.13}$$

We can also move the permittivity to the right hand side and get,

$$\nabla^2 V = -\frac{\rho}{\varepsilon} \tag{3.14}$$

Expanding the left hand side,

$$\nabla^2 V = \frac{\partial^2 V}{\partial^2 x} + \frac{\partial^2 V}{\partial^2 y} \tag{3.15}$$

After discretizing electric potential over a 2-D uniform grid and using the second order central finite difference formula (3.11) we get the following equation,

$$\nabla^2 V_{i,j} = \frac{V_{i+1,j} - 2V_{i,j} + V_{i-1,j}}{\Delta x^2} + \frac{V_{i,j+1} - 2V_{i,j} + V_{i,j-1}}{\Delta y^2} \tag{3.16}$$

Since the grid is uniform we can use the same value for the distance between the nodes in each direction.

$$\Delta = \Delta x = \Delta y \tag{3.17}$$

Of course the net charge density and the permittivity is also discretized over the same uniform mesh. Putting all this information together we have generated a numerical approximation for Poisson's equation.

$$\nabla^2 V_{i,j} = \frac{V_{i-1,j} + V_{i,j-1} - 4V_{i,j} + V_{i+1,j} + V_{i,j+1}}{\Delta^2} = -\frac{\rho_{i,j}}{\varepsilon_{i,j}} \tag{3.18}$$

If we rearrange this equation by keeping all the known values on the right hand side and all the unknown values on the left hand side we get the following equation.

$$\varepsilon_{i,j}(V_{i-1,j} + V_{i,j-1} - 4V_{i,j} + V_{i+1,j} + V_{i,j+1}) = -\Delta^2 \rho_{i,j} \tag{3.19}$$

Above equation is valid for almost all the nodes in the system except two cases, boundary nodes and interface nodes. We can have two different types of boundary conditions which determine how the boundaries are going to be handled. The first one is Dirichlet boundary condition which forces a particular value for the potential at the boundary.

$$V_{i,j} = V_b \tag{3.20}$$

Where V_b is the value of the potential at the boundary. The other possible boundary condition is called Neumann boundary condition which states that the derivative of the potential at the boundary is zero. This gives us the following equation:

$$\frac{\partial V}{\partial x} = \frac{V_{i+1,j} - V_{i,j}}{\Delta} = 0 \tag{3.21}$$

So for a boundary over y axis we get:

$$V_{i+1,j} = V_{i,j} \tag{3.22}$$

Following the same procedure we can get Neumann boundary condition over x axis:

$$V_{i,j+1} = V_{i,j} \tag{3.23}$$

After we have handled all the boundary conditions we have to figure out how to handle interfaces. These interfaces occur when two materials with different permittivities come into contact. So when we have a node at the interface the permittivity of that node is ambiguously defined. We need a special way to solve this ambiguity. It is possible to derive a finite difference equation that handles dielectric interfaces properly starting

from Gauss's Law.

$$\oint \varepsilon \vec{E} \cdot \vec{ds} = Q \tag{3.24}$$

After piecewise integration around the boundary we can get an equation for a horizontal interface and a vertical interface respectively:

$$(\varepsilon_1 + \varepsilon_2)V_{i-1,j} + (\varepsilon_1 + \varepsilon_2)V_{i+1,j} - 4(\varepsilon_1 + \varepsilon_2)V_{i,j} + 2\varepsilon_1 V_{i,j+1} + 2\varepsilon_2 V_{i,j-1} = Q_{i,j} = \Delta^2 \rho_{i,j} \tag{3.25}$$

$$(\varepsilon_1 + \varepsilon_2)V_{i,j-1} + (\varepsilon_1 + \varepsilon_2)V_{i,j+1} - 4(\varepsilon_1 + \varepsilon_2)V_{i,j} + 2\varepsilon_1 V_{i+1,j} + 2\varepsilon_2 V_{i-1,j} = Q_{i,j} = \Delta^2 \rho_{i,j} \tag{3.26}$$

Now that we have all the equations we need for all the nodes over the simulation domain it is possible to combine them ((3.19),(3.20),(3.25), (3.26)) into a matrix and turn Poisson's equation, which is a second order differential equation, into a linear equation.

$$D_2 \vec{V} = -\Delta^2 \vec{\rho} - \vec{V_b} \tag{3.27}$$

One can easily get the potential distribution by simply solving the matrix equation obtained. Due to the nature of the problem the matrix we end up with is quite sparse and using a sparse LU decomposition dramatically increases the computational efficiency.

$$\vec{V} = D_2^{-1}(-\Delta^2 \vec{\rho_{i,j}} - \vec{V_b}) \tag{3.28}$$

After solving for the potential distribution it is easy to calculate the electric field distribution discretely using the relationship between electric field and electric potential (2.13) and central difference equation (3.7).

$$E_{i,j}^{\vec{x}} = -\frac{V_{i+1,j} - V_{i-1,j}}{2\Delta} \tag{3.29}$$

$$E_{i,j}^{\vec{x}} = -\frac{V_{i,j+1} - V_{i,j-1}}{2\Delta} \tag{3.30}$$

3.2.2 Current Density Equations

After we have calculated the electric field distribution over the entire region we can now figure out how the particles move. Both drift and diffusion currents can be calculated over the entire grid. There are few different methods that can be used to calculate the current density. The accuracy of the methods we will look at change based on the physics of the device.

3.2.2.1 Finite Difference Method

The first method involves simply applying finite difference to calculate drift and diffusion currents. Drift current is quite simple since it does not involve any differentials and the diffusion current can be calculated using first order central difference. The current density is calculated in such a way that it falls between two points which simplifies the application of the boundary conditions.

$$J^x_{i+\frac{1}{2},j,k} = q\mu_n n_{i+\frac{1}{2},j,k} E^x_{i+\frac{1}{2},j,k} + D_n \frac{n_{i+1,j,k} - n_{i,j,k}}{\Delta} \tag{3.31}$$

The electric field was calculated exactly on the nodes but we can use linear interpolation in order to get a value between the nodes. Same argument is also valid for particle densities p and n. They were defined on the nodes but can be linearly interpolated.

$$n_{i+\frac{1}{2},j,k} = \frac{n_{i+1,j,k} + n_{i,j,k}}{2}$$

$$E^x_{i+\frac{1}{2},j,k} = \frac{E^y_{i+1,j,k} + E^y_{i,j,k}}{2}$$

We can follow the same method in order to calculate the current density in y direction:

$$J^y_{i,j+\frac{1}{2},k} = q\mu_n n_{i,j+\frac{1}{2},k} E^y_{i,j+\frac{1}{2},k} + D_n \frac{n_{i,j+1,k} - n_{i,j,k}}{\Delta} \tag{3.32}$$

$$n_{i,j+\frac{1}{2},k} = \frac{n_{i,j+1,k} + n_{i,j,k}}{2}$$

$$E^y_{i,j+\frac{1}{2},k} = \frac{E^y_{i,j+1,k} + E^y_{i,j,k}}{2}$$

Same current density equations can be used for positively charged particles by replacing n by p and changing the sign of the diffusion term.

3.2.2.2 Boundary Conditions

For a drift diffusion problem there are two different possibilities for boundary conditions. The first one is when the particles cannot go past through a certain boundary, no flow boundary condition. This can be achieved by using Dirichlet bounday condition and setting the flow at the boundary to zero.

$$J = 0 \tag{3.33}$$

This boundary condition can also be used conditionally. A straightforward example is when there is a particle density limit over an area. This condition can be used to cut the flow of particles into an area when a certain particle concentration is reached.

Dirichlet boundary condition can also be used in cases where there is a flow through the boundary. A good example is a metal contact. It is assumed that metal contact has infinite amount of charge and the boundary is always charge neutral. For example if we have holes, electrons, positive and negative doping we can assume that at the boundary positive charge concentration will be equal to the negative charge concentration.

$$N_D + p = N_A + n \tag{3.34}$$

If we are dealing with a semiconductor the amount of holes and electrons has to obey mass action law at equilibrium.

$$np = n_i^2 \tag{3.35}$$

n_i here is the concentration of the semiconductor at equilibrium before getting doped. Solving (3.35) and (3.34) together we get,

$$n = \frac{1}{2}(N_D - N_A + \sqrt{(N_D - N_A)^2 + 4n_i^2}) \tag{3.36}$$

Once electron concentration is obtained it is possible to calculate the hole concentration using mass action law.

$$p = \frac{n_i^2}{n} \tag{3.37}$$

During simulation, the application of this boundary condition differs from the no flow boundary which was applied implicitly. All the boundaries are simulated using a no flow condition but their values are set to the appropriate value at the end of every time step. Lack of charge is compensated and excess charge is taken off by the metal contact. The difference between the boundary value of the charge density and its actual value is used to calculate the derivative of the current density with respect to time.

$$\frac{dn}{dt} = \frac{n_{cr} - n_{ct}}{\Delta t} \tag{3.38}$$

n_{cr} is the excess carrier density and n_{ct} is the equilibrium carrier density at the contact. Using these boundary conditions for holes and electrons and the following two equations it is possible to calculate incoming and outgoing currents.

$$Q = An \tag{3.39}$$

$$I = \frac{dQ}{dt} \tag{3.40}$$

Equation 3.39 is an approximate relationship between charge and charge density where Q is total charge, A is the area holding that charge. Equation 3.40 is simply the general definition of current. By combining these two equations it is possible to derive a formula for calculating current at any metal contact.

$$I = A\frac{dn}{dt} \tag{3.41}$$

3.2.3 Continuity Equation

Continuity equation is needed to calculate a transient solution for drift diffusion equations. The equation is simple to discretize using finite difference method. There are two terms that need to be discretized, a first order derivative in time and space. We can first start by evaluating the divergence term in equation (2.10).

$$\nabla \cdot J = \frac{\partial J}{\partial x} + \frac{\partial J}{\partial y} = \frac{dJ_x}{dx} + \frac{dJ_y}{dy} \tag{3.42}$$

It is possible to replace the derivative with central finite difference terms.

$$\frac{dJ_x}{dx} = \frac{J^x_{i+\frac{1}{2},j,k} - J^x_{i-\frac{1}{2},j,k}}{h} \tag{3.43}$$

$$\frac{dJ_y}{dy} = \frac{J^y_{i,j+\frac{1}{2},k} - J^y_{i,j-\frac{1}{2},k}}{h} \tag{3.44}$$

$$\nabla \cdot J_{i,j,k} = \frac{J^x_{i+\frac{1}{2},j,k} - J^x_{i-\frac{1}{2},j,k}}{h} + \frac{J^y_{i,j+\frac{1}{2},k} - J^y_{i,j-\frac{1}{2},k}}{h} \tag{3.45}$$

This is the general form of the divergence of the current density. We can plug in the current density equations from either finite difference or Scharfatter-Gummel approach. Collecting everything in a matrix gives rise to the following equation:

$$\nabla \cdot J_k = B \tag{3.46}$$

The time derivative can also be replaced by a forward or backward finite difference terms respectively.

$$\frac{\partial \vec{n}_k}{\partial t} = \frac{\vec{n}_{k+1} - \vec{n}_k}{\Delta t} \tag{3.47}$$

$$\frac{\partial \vec{n}_k}{\partial t} = \frac{\vec{n}_k - \vec{n}_{k-1}}{\Delta t} \tag{3.48}$$

It is possible to find a numerical transient solution for the drift-diffusion problem by combining finite difference form of the time derivative ((3.47) or (3.48)) and the divergence of the current density equations (3.46).

Using forward difference approximation we get,

$$\frac{\vec{n}_{k+1} - \vec{n_k}}{\Delta t} = B$$

$$\vec{n}_{k+1} = \vec{n_k} + \Delta t B \tag{3.49}$$

Both forward and backward difference formulas work sequentially in order to generate a transient solution. In order to calculate the next time step we need the solution of the previous time step. Forward difference gives us an explicit solution which has few advantages. This solution can be implemented without forming any matrices, just by directly calculating the divergence of the current density for each node and then marching through time using equation 3.49. Additionally, unlike backward difference, there are no equations to be solved for every time step. These two properties ease the computational load of the problem and speed up the solution process. Unfortunately this scheme has very strict stability conditions which has to be met in order to get a reasonable solution.

Using backward difference approximation we get,

$$\frac{\vec{n}_k - \vec{n}_{k-1}}{\Delta t} = \frac{1}{q}(qB)$$

$$\vec{n}_k - \Delta t B = \vec{n}_{k-1}$$

Since all the equations in B matrix are linear we can pull n out ($B = Cn$) and rearrange the equation.

$$\vec{n}_k - \Delta t C \vec{n}_{k-1} = \vec{n}_{k-1}$$

$$\vec{n}_k = (I - \Delta t C)^{-1} \vec{n}_{k-1} \tag{3.50}$$

Now we have an implicit solution which seem quite similar to the previous solution but in fact they are quite different. This solution needs a matrix inversion every time step but it is unconditionally stable. The decision to use implicit or explicit solution is not very simple and it will be discussed in detail the next section.

3.2.4 Stability and Computational Efficiency

Before we go into numerical limitations of solving drift diffusion equation via finite difference we should look into physical limitations of the problem. These limitations persist no matter what kind of numerical scheme is employed to solve drift diffusion equations.

3.2.4.1 Physical Limitations

Debye length is the length over which mobile charge carriers screen out an external electric field. It determines how steeply charges will accumulate over a certain distance when subject to an electric field.

$$L_D = \sqrt{\frac{\varepsilon V_{th}}{qn}} \tag{3.51}$$

Debye length limits how coarse the grid can be since we need to be able to accurately capture the distribution of charge density. As it can bee seen from the formula above the higher the charge density is the steeper the charge will accumulate. This can become a major problem for device sizes in millimetre range or higher and high charge concentrations since the mesh density needs to be extremely high.

The amount if time it takes for charge fluctuations to disappear is called Dielectric relaxation time. It limits the maximum time step of a simulation since the fluctuations that are not properly resolved over time will make the simulation unstable.

$$t_{dr} = \frac{\varepsilon}{qn\mu} \tag{3.52}$$

Dielectric relaxation time is only important when electric potential is highly affected by redistribution of charge over time. Otherwise it has minimal impact on the stability of the problem.

3.2.4.2 Numerical Limitations

There are also numerical limits which can affect convergence and stability of a solution when using an explicit scheme. These are called Courant-Friedrichs-Lewy (CFL)conditions. We can look at CFL conditions for pure diffusion and pure drift.

$$\frac{\Delta^2}{2D_n} > \Delta t \tag{3.53}$$

Above condition is for pure diffusion and it restricts the maximum time step. Following condition is for drift dominated systems:

$$\frac{2\Delta}{\mu E} > \Delta t \tag{3.54}$$

This is the second numerical restriction on our simulation. Interestingly the condition for drift depends on the electric field therefore it needs to be satisfied as the electric field changes over time during simulation.

Now we have all the conditions we need to ensure the stability of the simulation. Both physical and numerical constraints have to be evaluated and mesh density and time step need to be selected in order to satisfy all these conditions discussed above. Particularly mesh density have a very strong effect on the accuracy, stability and computational efficiency of the simulation. Increasing mesh density increases the computational time needed to calculate every time step since we have more points. Additionally because of the CFL condition for diffusion time step is related to the square of the mesh size. This means that maximum allowed step size decreases much quicker than the mesh density. Also, increasing charge density can decrease the maximum mesh size to a very small value. This can be somewhat fixed by using a non uniform mesh which can dramatically decrease the amount points needed for the simulation. Unfortunately this is usually not very straightforward to implement in a finite difference scheme.

3.2.4.3 Explicit vs. Implicit Solution

Overall explicit and implicit solutions have their advantages and disadvantages. Choosing one over the other requires careful analysis of the problem. Implicit solution by itself is unconditionally stable therefore it can support very large time steps without any stability issues. However with increased time step, the accuracy of the transient solution decreases but the steady state solution does not get affected. So for steady state solutions it is better to use an implicit method which can reach steady state very quickly. This advantage disappears when particle densities are high enough to affect the electic field and Poisson's equation needs to be solved for every time step. In this scenario the maximum step size is determined by dielectric relaxation time which tends to be around the same order as CFL conditions. Now since the time step is going to be around the same order for both implicit and explicit methods it makes sense to use the explicit one because it is computationally less expensive.

We can sum this brief analysis by stating that implicit solution is preferable when there is no coupling between Poisson's equation and drift diffusion equations and the transient

response is not very important. Explicit solution have an edge over the implicit solution due to its lower computational resource requirement when the equations are coupled and the time steps for both schemes are restricted to fairly small values.

3.2.5 Simulation Procedure

Over the past section we have gone through different equations and schemes that are used to solve drift diffusion and Poisson's equation. Using all this information we can create a general strategy to solve a drift diffusion problem.

First of all we need to define the geometry and physical properties of the problem as well as all initial and boundary conditions. Initialization sets up the first time step of the problem at $t = 0$. Once this first step is done we can generate required vectors and matrices and solve the problem for the next time steps, $t = t_i$.

The solution process starts by solving Poisson's equation using the charge distribution at current time step. Once it is solved we can calculate the electric field distribution and use it in drift diffusion equations to calculate current density distribution. One important choice to make here is to either use finite difference method or Scharfatter-Gummel method in order to calculate current density. The conditions that favor one or the other are not simple to determine and will be discussed in detail in the next chapter. The next decision to be made is either to use an implicit or explicit solution which will determine if we can directly calculate the next step or need to solve a matrix. Finally once we have the carrier distribution for the next step we can check for a stopping criterion. If this criterion is not met then the whole process will start all over again with a small difference. If the charge concentration is so small that the equations are decoupled then we can skip solving Poisson's equation again. This can significantly speed up the simulation since we only need to solve for the continuity equation after this point.

There are two different criteria that can be used to decide weather to finish the simulation or not. We can stop if we intend to solve for a certain time frame and we reached the final time. This is quite simple since we look at the current time and if it is equal or greater than the required simulation time we can just stop the simulation. We could also be interested in reaching a steady state solution. This can be determined by comparing the current carrier distributions with distribution at the previous time step. If the difference is very small then we can conclude that the simulation has reached steady state and it is time stop the solution process. This makes physical sense since it makes sure that the time derivative of the carrier densities are close to zero. The flowchart in figure 3.1 summarizes the solution procedure.

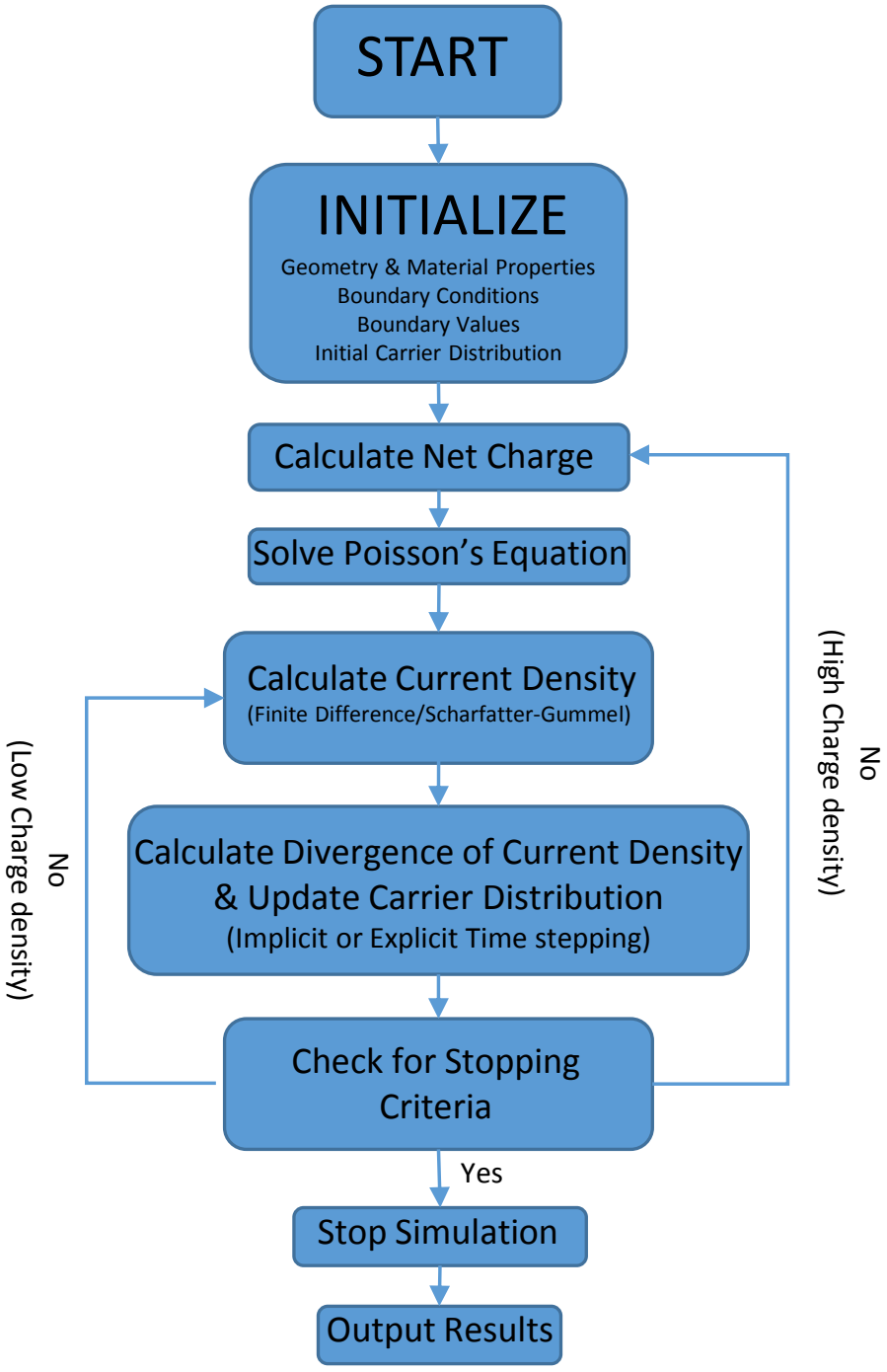

FIGURE 3.1: Finite Difference Drift-Diffusion Scheme Flowchart

Chapter 4

Testing of the Drift Diffusion Solver

In the past chapter we have gone through the details of how to solve drift-diffusion and Poisson's equation using finite difference method. Now we can do steady state and transient analysis and compare the results with analytical solutions as well as a commercially available simulator called 'COMSOL Multiphysics' which uses finite element method instead of finite difference. Following test cases were made to ensure that the key parts of the finite difference scheme runs properly and does not produce unexpected results.

4.1 Solution for Closed Boundary

In this test case we will examine the accuracy of the finite difference solution in steady state. In order to do this we can use a simple 1-D problem where we have a finite number of negatively charged particles over a certain distance subject to constant electric field. This is the same problem we have solved analytically in section 3.3.1. We also assume that the charge density is very low and does not affect the electric field. Both ends of the simulation domain have no flow boundary conditions for charged particles. The solution process requires an initial distribution for charge density over the area. For this problem the density of the negative particles was initialized to be uniform over the entire area. Since our differential equations are uncoupled solving Poisson's equation only once is sufficient to determine the electric field over the course of the entire simulation. Figures 4.2 and 4.1 show the potential and the electric field distribution over the entire simulation area calculated from Poisson's equation using finite difference.

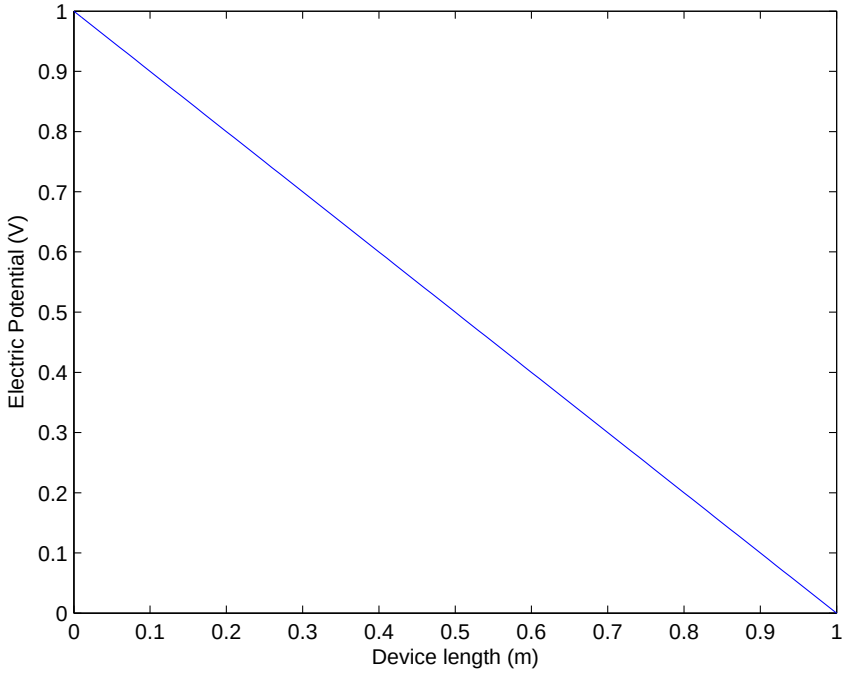

FIGURE 4.1: Potential Distribution

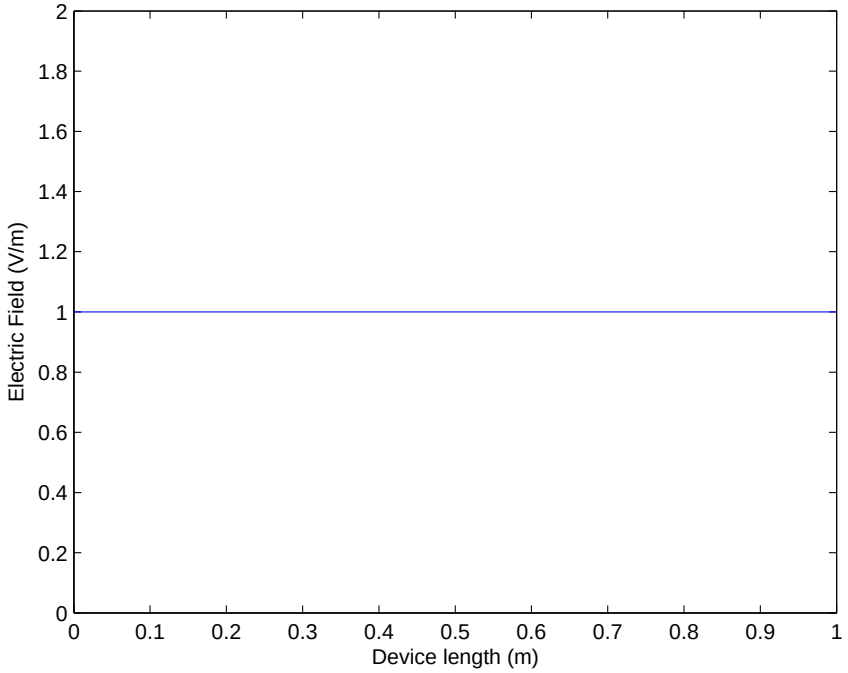

FIGURE 4.2: Electric Field Distribution

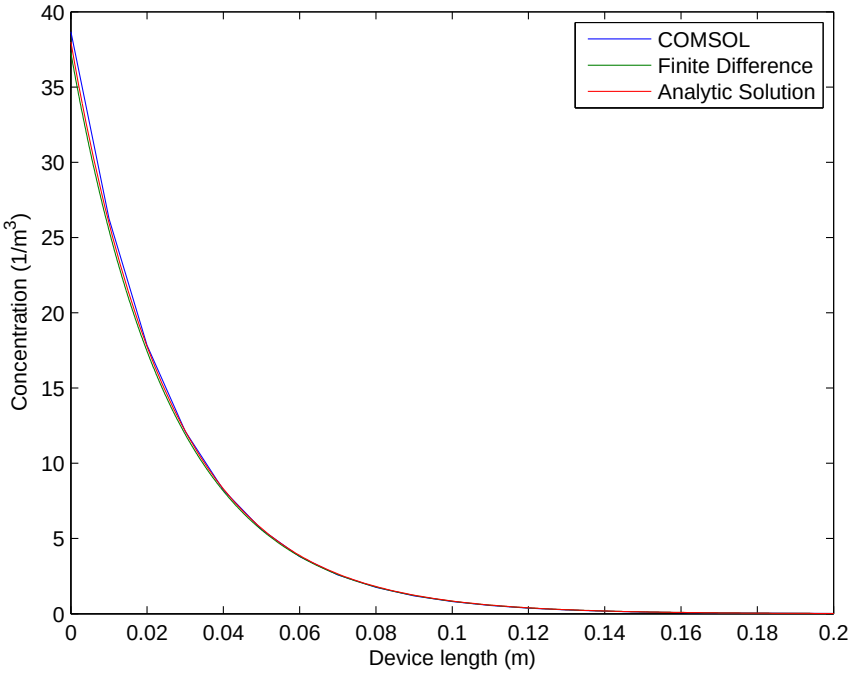

FIGURE 4.3: Steady State Negative Charge Density

Figure 4.3 has two simulation results as well as the exact solution of this problem. The green line represents the result given by the finite difference method once the transient response reaches steady state. It can be seen from the graph that the steady state solution generated by both COMSOL and finite difference matched the analytical solution.

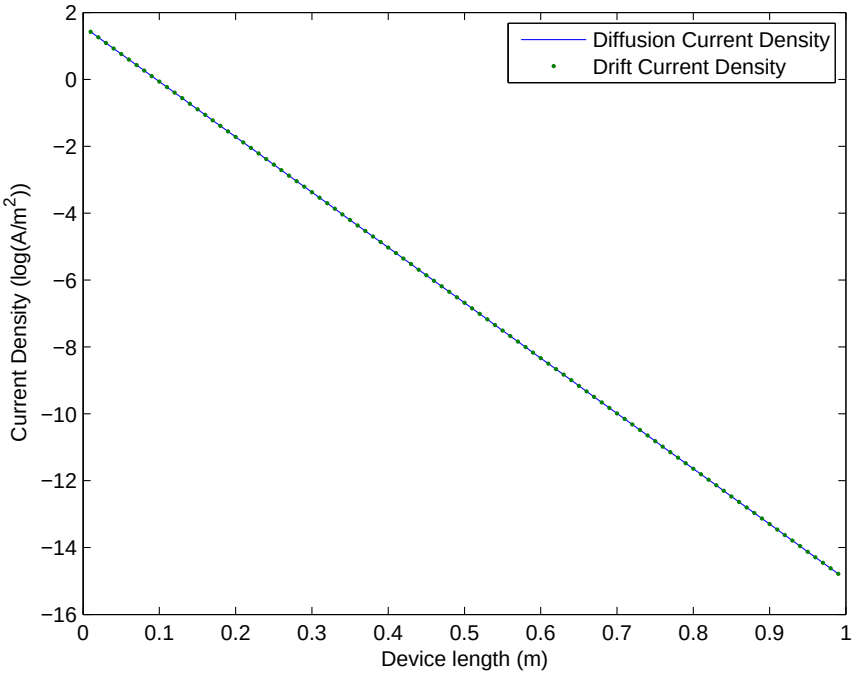

FIGURE 4.4: Finite Difference Drift and Diffusion Current Densities

While deriving an analytical solution for this problem we have assumed that at steady state the drift current density must be equal to the diffusion current density. In figure 4.4 we see drift and diffusion current densities in log scale. Overall both currents match quite tightly.

4.2 Solutions for Open Boundary

Another very important aspect of drift-diffusion simulation is its transient response. Like the previous test case, we can use a closed form solution to test the accuracy of the transient response. In section 3.3.2 we have found two different analytic solutions for a similar drift diffusion problems which involved infinite boundaries and a uniform electric field. The only difference between two cases are their initial carrier distribution. One has a rectangular and the other one has a gaussian initial carrier distribution. Since we have not implemented any way to deal with infinite boundaries we will just simulate these two problems until the carrier distributions gets close to one boundary.

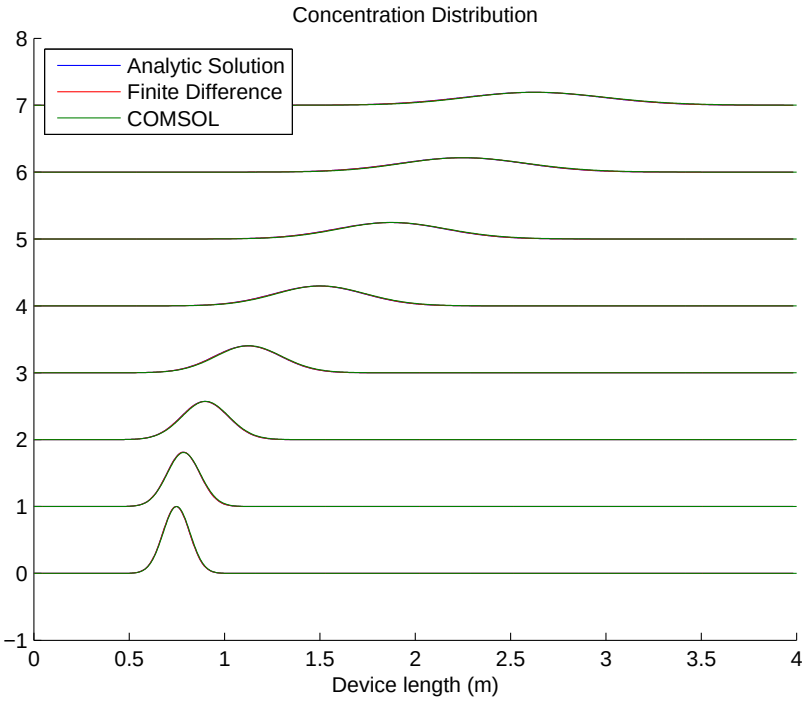

FIGURE 4.5: Gaussian Carrier Distribution Evolving Over time

Figure 4.5 has the transient response from COMSOL, finite difference and analytical solution. Snapshots of the carrier distributions were taken for each method at different time steps and they were superposed on top of each other. Increasing levels on y axis represent a carrier distributions at a different time starting from the bottom and moving forward in time towards the top. Figure 4.5 has a gaussian initial carrier distribution. It can be seen from that the transient solution generated by both COMSOL and finite difference are quite close to the analytical solution.

4.3 PN Junction

In previous sections of this chapter we have put finite difference drift diffusion model to test. In all the cases we ran before, Poisson's equation was not coupled with drift diffusion equations. In this example we will be testing both drift diffusion and Poisson's equation to see how well they work when they are coupled together. A simple pn junction is quite adequate for this task since it has analytical solutions, under certain assumptions, for electric potential, electric field and net charge.

For the simulation ,the initial hole and electron distributions were determined using mass action law and they were assumed to be constant at the boundaries. Keeping carrier concentrations constant at the boundaries creates a mechanism in which the charge can move in and out of the simulation domain. If the charge density at any time step is higher than the fixed density then the difference will move out of the system. If there is a lack of charge at the boundary then carriers will move in to fill in the gap. Following figure (4.6) shows the final result of bringing p and n type materials together.

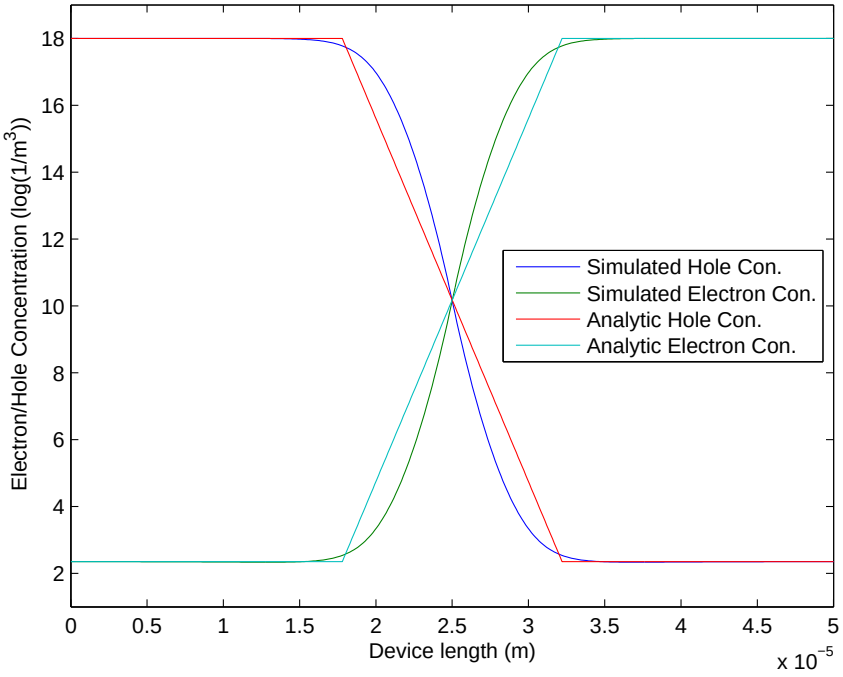

FIGURE 4.6: Electron/hole Concentration of a PN Junction

We can see a little mismatch between simulated and analytic concentration densities. Analytic solution have sharp edges and simulated solution does not. This is due to all the assumptions made in order to find an analytic solution. We will be seeing this little mismatch also for electric field, electric potential and net charge .

Since the purpose of this problem is to test Poisson's equation as well, we can look at the final potential distribution due to pn junction. Figure 4.7 shows the potential distribution for simulated and analytic solution. Close match in electric potential distribution shows that coupled equations can generate fairly accurate solutions.

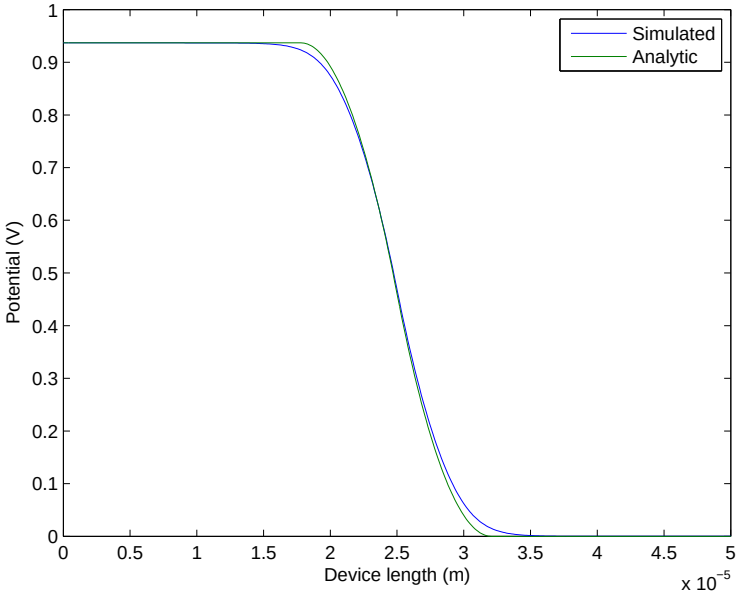

FIGURE 4.7: Potential Distribution of a PN Junction

Calculation of the electric field involves one basic derivative. Since simulated potential is matching the analytic solution quite nicely the electric field should follow a similar pattern. Figure 4.8 shows that this is indeed the case, simulated electric field matches the calculated electric field.

Finally we can look at the total charge distribution at steady state(4.9). Simulated net charge density follows the analytic one except the abrupt changes at two ends.

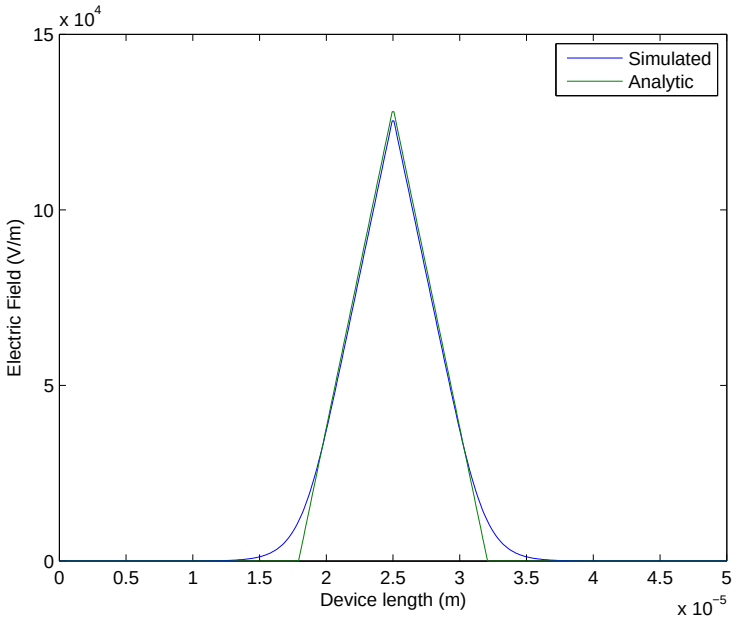

FIGURE 4.8: Electric Field Distribution of a PN Junction

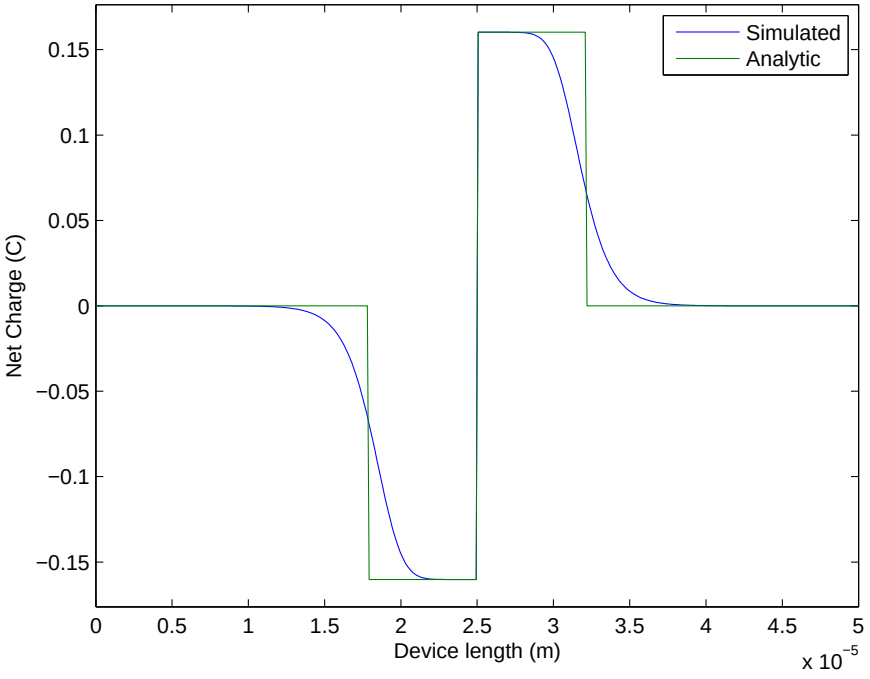

FIGURE 4.9: Total Charge Distribution of a PN Junction

4.4 Region Specific Particle Density Limit

In section 4.2.2.3 we have talked about using a Dirichlet boundary condition (J=0) to stop the particle flow into a node. This can be done by precalculating the particle density of concentration restricted nodes at the next time step, setting any influx to zero if the concentration is going to go over the limit and finally calculating the concentration at the next time step using the updated current densities.

In order to test this method we can use a simple example where we have two particles of the same charge initialized like the figure below (4.10). One set of particles has a concentration limit of 2 10^{10} m^{-3} on the right side of the simulation area and no limit on the left side. The other set has no restrictions.

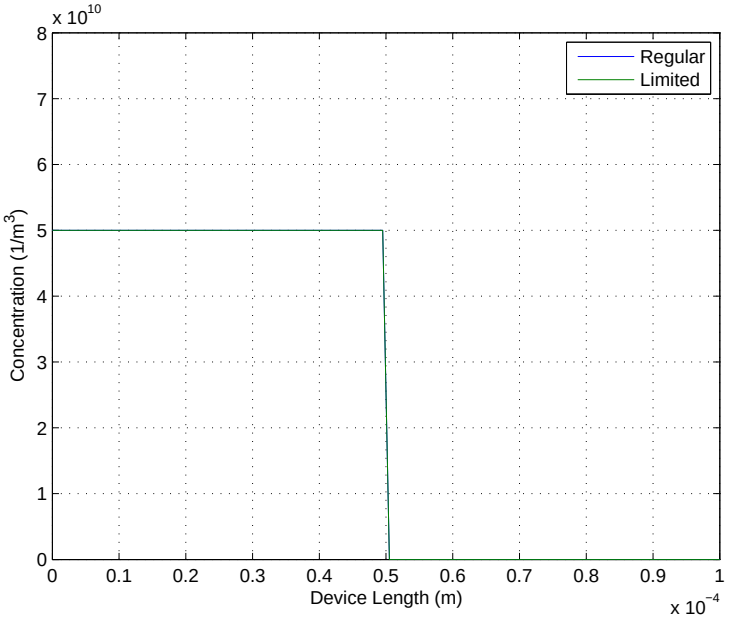

FIGURE 4.10: Initial Particle Density

This transient simulation was done using a potential as a function of time. For the first half of the simulation applied potential was positive and for the second half it was negative. Figure 4.10 shows how two simulations differ when the particles are pushed towards the right wall due to the electric field created by the positive potential. Particles with no limit on the right side move freely and accumulate on the right side. The limit for the other particles is effectively stopping them from going in and accumulating freely. Once the limit is reached at a certain node the concentration cannot increase any further and that node becomes a no flow wall.

When the potential is switched all the particles accumulate freely to the left side of the simulation domain since there are no restrictions on this side (figure 4.12).

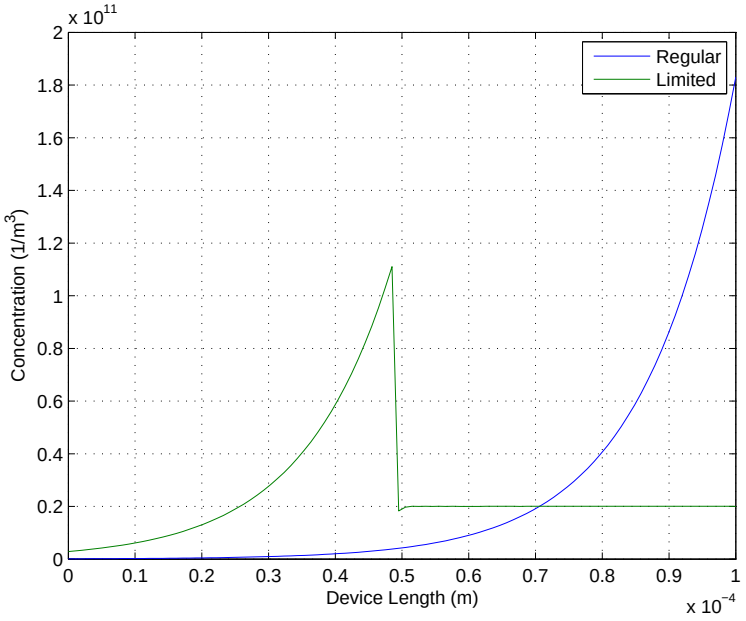

FIGURE 4.11: Limited Concentration Accumulation on the Right Side

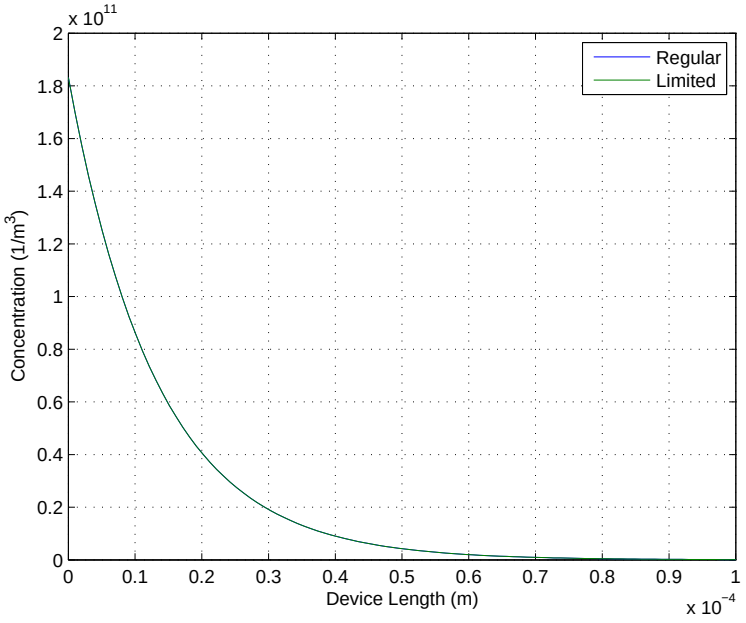

FIGURE 4.12: Limited Concentration Accumulation on the Left Side

This last figure (4.13) shows the transient response over time of a single node on the right side. The potential is positive for the first 1.5 seconds and it is switched to negative for the last 1.5 seconds. The node without limit keeps accepting charge until steady state has been reached but the node with a limit on stops accepting charged particles once the limit is reached. After the potential is switched density limited node has no problem releasing the particles.

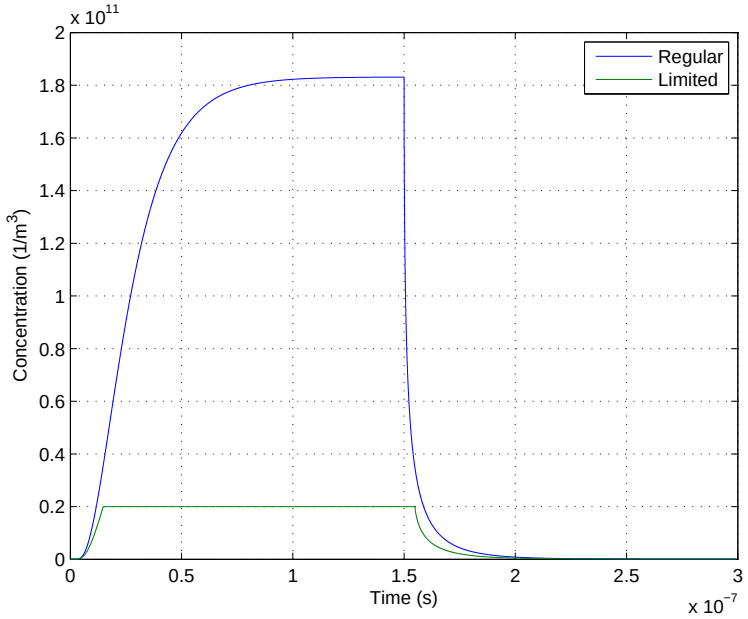

FIGURE 4.13: Accumulation at the right wall over time

Additional to the test we ran using finite difference we can also try to simulate the exact same behaviour in COMSOL.

COMSOL does not have a built in option that allows limiting particle density. One possible solution to this is making particle mobility and diffusivity a function particle density. It is possible to use a sigmoid function which switches from 1 to 0 very quickly when particle density is close to its limit. Here is the equation of the sigmoid function used to limit the particle flow:

$$\mu = \frac{\mu_0}{1 + e^{\sigma(n-n')}} \tag{4.1}$$

μ_0 is the original mobility of the charge carrier. σ controls the sharpness of the switch and n' determines the density at which the switch will be.

Another problem with COMSOL was the definition of mobility and diffusion coefficients over different areas. If these constants are defined as one single value per area it works just fine but if they are defined as a function of concentration it causes convergence

issues. This can be overcome by defining using two more sigmoid functions to distinguish between two areas with different mobilities and diffusion constants. Left sigmoid in figure 4.14 was multiplied by the mobility/diffusivity of the left side of the area and the right sigmoid was multiplied by the mobility/diffusivity of the right side of the area. Both functions were summed to obtain a function which describes the characteristics of the entire area.

$$\mu = \frac{\mu_l}{1 + e^{\sigma_x(x-x')}} + \frac{\mu_r}{1 + e^{-\sigma_x(x-x')}} \tag{4.2}$$

In this problem μ_r is the same as equation 4.1 since the region on the right side has a particle density limit. A sharp switch between right and left side mobility using the function above would be ideal for this simulation but unfortunately it causes convergence issues in COMSOL therefore there is a gradual change between two mobilities.

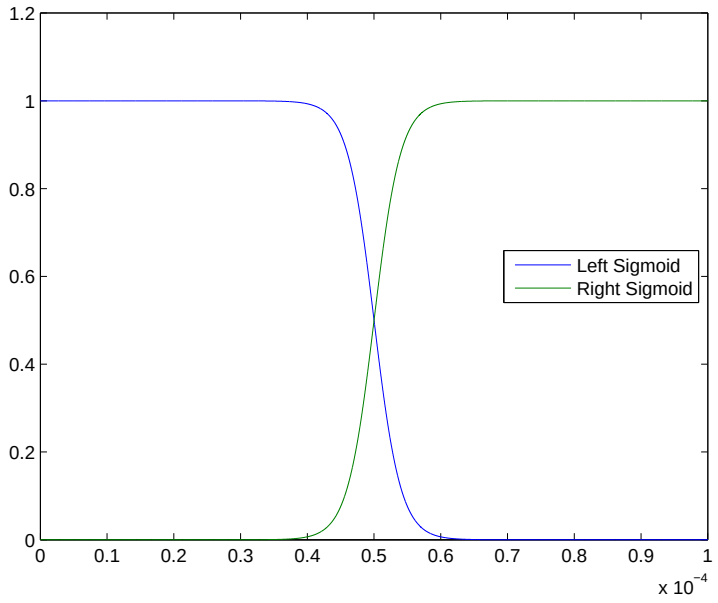

FIGURE 4.14: Mobility change from left to right side

The initial carrier distribution for COMSOL was set to be exactly the same as finite difference simulation. Figures 4.15 and 4.16 show results for both COMSOL and finite difference simulations at steady state before the potential switch. The plot on the left side gives insight on how COMSOL simulation behaves for limited and limitless accumulation on the right wall. Due to the gradual change of mobility and diffusion constants between two areas we end up with concentration on the right side higher than the limit which is 2 10^{10}. Additionally, the particle density goes over its limit near the right wall. In figure 4.16 the difference between COMSOL and finite difference becomes

more visible. In FD simulation the accumulation goes much higher due to higher electric field and unlike COMSOL it does not penetrate the right half of the simulation domain.

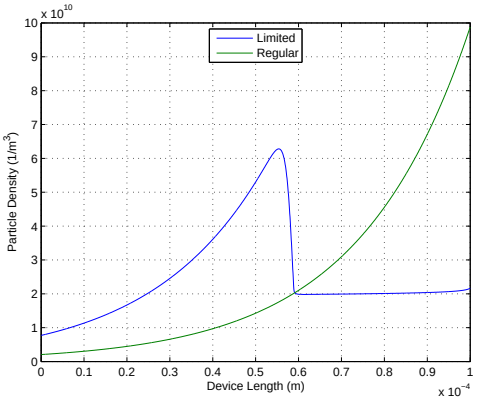

FIGURE 4.15: COMSOL Simulation for Particle Density Limit

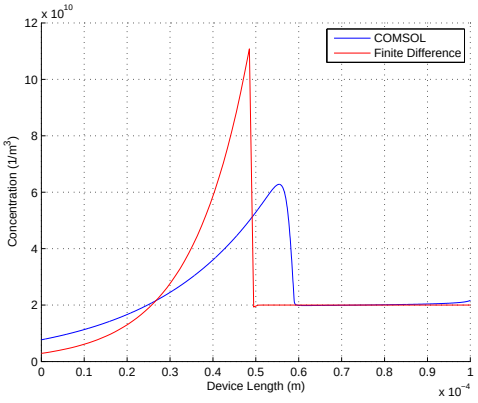

FIGURE 4.16: COMSOL and Finite Difference Simulation

In figure 4.17 we can see the accumulation of charge near the middle after the potential is switched. This is due to mobility being a function of distance and concentration. As the ions move from left to right they go from a low mobility region to a high mobility region and they slowly accumulate around the area where the change in mobility occurs. Figure comparing both COMSOL and finite difference shows that the accumulation does not happen in the case of finite difference due to the way concentration limiting mechanism was implemented.

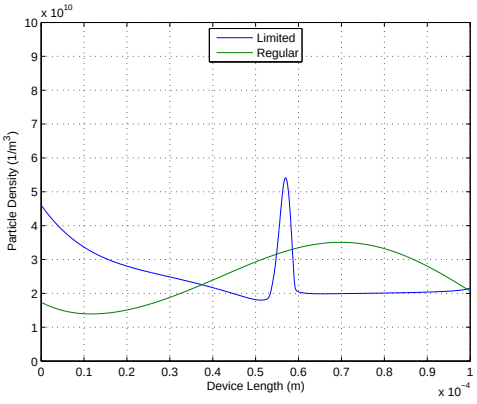

FIGURE 4.17: COMSOL Simulation for Particle Density Limit

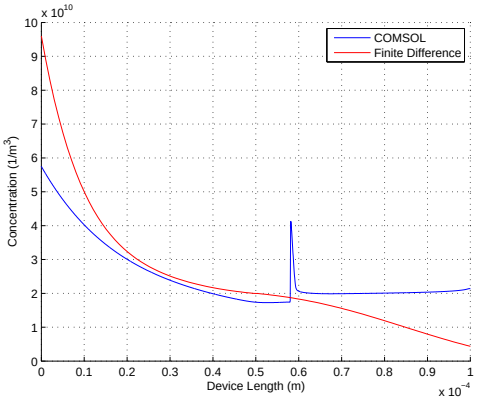

FIGURE 4.18: COMSOL and Finite Difference Simulation

With the decrease of ion concentration on the limited region the difference between low and high mobility regions diminish. Once the concentration on the limited side is low enough the whole system behaves as if there was no limit and ion mobility becomes equal for all regions and the ions freely accumulate on the left wall (figure 4.19). Aside from the difference in electric field strength both simulations behave the same way as they approach steady state. Figure 4.20 shows concentration densities at steady state.

COMSOL simulation has a lower electric field since it has convergence issues with high electric fields.

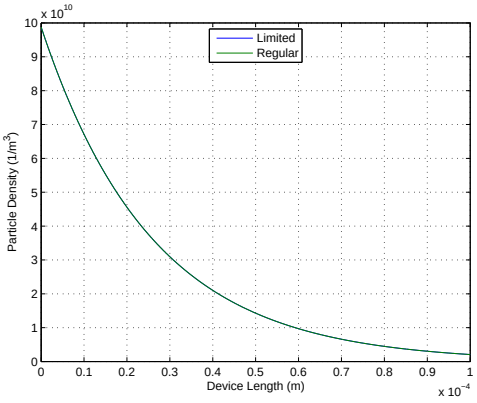

FIGURE 4.19: COMSOL Simulation for Particle Density Limit

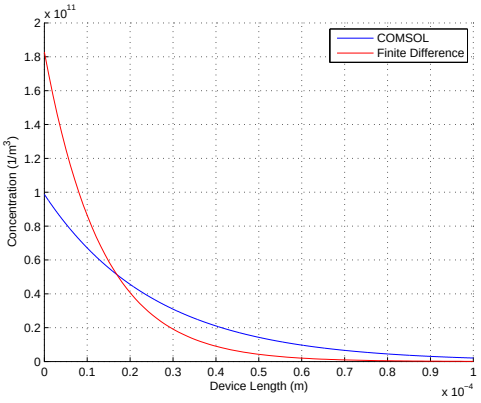

FIGURE 4.20: COMSOL and Finite Difference Simulation

To finish our comparison we can look at the particle density transient response of the rightmost node. For the first half of the simulation everything is the same as the finite difference case except COMSOL goes a little bit over the limit. When the potential is switched node without the limit has no noticeable difference in behaviour. The node with concentration limit has a lag when it comes to releasing the particles. This is due to the sigmoid function used to achieve a limiting behaviour. Once the limit is reached mobility and diffusivity are stuck at a very low value until the particle density starts to go lower than the limit.

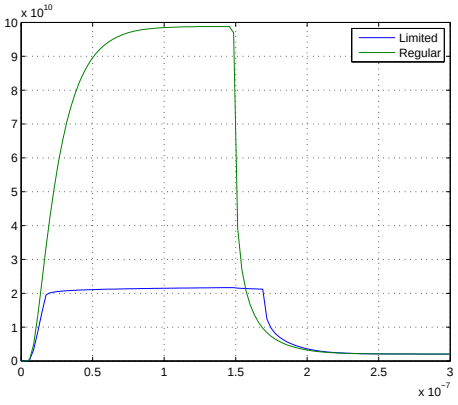

FIGURE 4.21: Density on the right wall over time using COMSOL

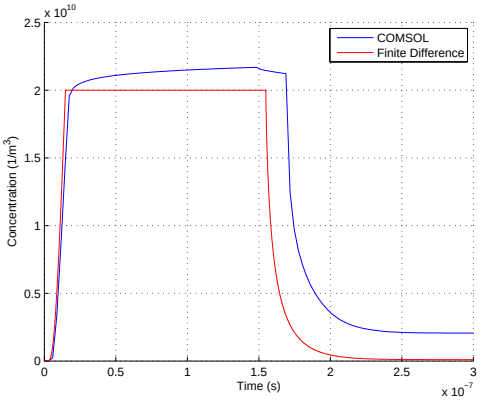

FIGURE 4.22: Density on the right wall over time,COMSOL vs. Finite Difference

In this example we have seen that it is possible to impose a density limit over any area using a simple no flow boundary condition in finite difference. For COMSOL we had to use some workarounds in order to simulate the same behavior but the results were not very satisfying because of convergence issues.

Chapter 5

Memristor Simulation

A numerical method for a memristor simulation was developed and tested in previous chapters based on drift-diffusion equations and finite difference. This chapter introduces the memristor's structure and physical parameters used for the simulation. It continues with a preliminary problem analysis to determine required mesh density and maximum possible time step. This preliminary analysis is followed by 1-D simulations of a memristor under various conditions.

5.1 Memristor Structure

Following figure (5.1) shows the structure of a simple memristor which will be taken as a basis for all the memristor simulations presented in this thesis. It consists of 2 metal contacts, a polymer conductor (PEDOT:PSS) and an electrolyte solution which has lithium and perchlorate ions (perchlorate/lithium density $\approx 6.02\ 10^{23}\ m^{-3}$). The memristor is about 1 cm long and 1 mm wide. The thickness of the conductive layer is around 1 μm. During experimentation the electrolyte is deposited on PEDOT via a syringe so its thickness can vary drastically but as long as the amount of ions in the electrolyte solution is enough to saturate PEDOT this does not make a significant difference in the operation of the memristor. For simulation it was assumed that there were always more than enough ions to saturate the PEDOT so the electrolyte was modeled as an infinite source/sink of ions. The top boundary of the electrolyte was assumed to be charge neutral at all times which provides a mechanism for moving ions in and out of the system. This way the movement of ions near the surface of the PEDOT can still be captured without having to simulate the ion movement for the entire electrolyte solution which is variable in size.

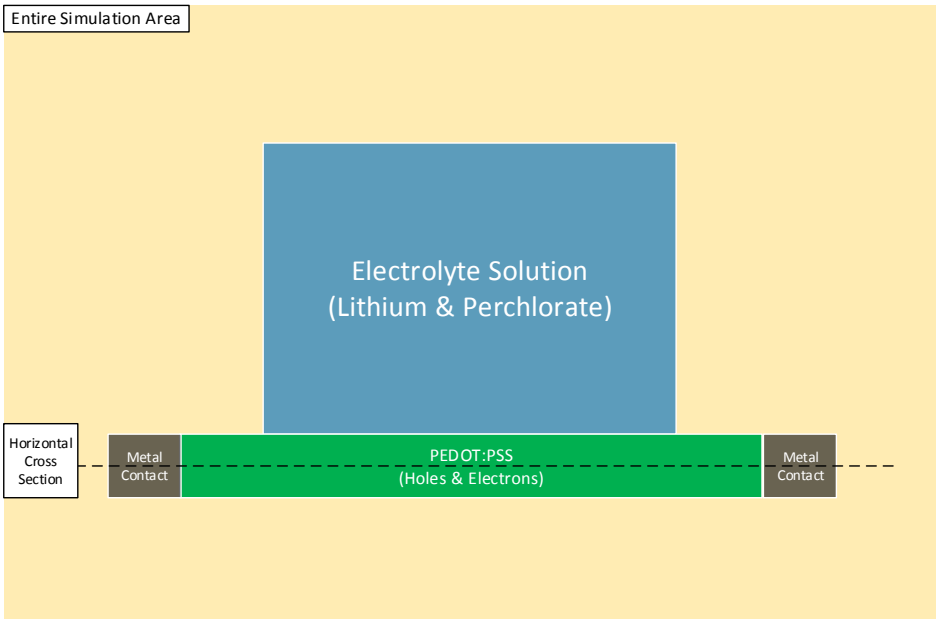

FIGURE 5.1

The initial conditions for all the charge carriers are the same. All charges are balanced and uniformly distributed but the carrier density in the electrolyte solution is higher than the carrier density in PEDOT. Perchlorate ions are not allowed to move outside the electrolyte solution so a no flow boundary condition was used around the electrolyte. Lithium ions are free to move between PEDOT and the electrolyte solution but their maximum concentration is limited inside the PEDOT. The mobility of lithium ions has further restrictions inside PEDOT. Lithium has higher mobility in PEDOT right under the electrolyte solution, wet PEDOT, than the region without any contact with electrolyte, dry PEDOT. In fact due to this difference very little amount of lithium reaches the metal contacts. This decrease in mobility was modeled by making the mobility of lithium a function of position. The mobility of lithium ions were assumed to be 100 times slower than the mobility of holes in the wet PEDOT and it is zero in the dry PEDOT($\mu_{hole} \approx 10^{-3}\ m^2/Vs$).

PEDOT:PSS is a regular conductor with fixed negative charge and mobile holes. Holes can move in an out of the PEDOT through the metal contacts which hold the charge neutrality of the initial condition throughout the simulation. The interface between PEDOT and electrolyte only allows the exchange of lithium ions. During simulation,the movement of lithium ions changes the conductivity of the PEDOT by increasing or decreasing the amount of available holes through coulomb forces. In the actual device lithium ions change the conductivity via various physical effects like changing the mobility of holes through modifying their hopping distance. Even though the mobility of

the holes can simply be made a function of time the physical details of these additional affects are beyond the scope of this thesis.

5.2 Simulation Requirements

It is important to analyze computational requirements of a simulation in order to asses the feasibility of the computation scheme. In this case, it is possible to determine spacial and temporal requirements using the equations 3.51 to 3.54 which describe physical and numerical limitations of the simulation. Following graph 5.2 shows the requirements for a memristor of the scale discussed above and a typical semiconductor device size around 1 μm. The mesh density has to be high enough in order to capture the exponential charge accumulation for charge shielding so the minimum step size was set to be 5 times smaller than the Debye length. Plots 5.2.a and 5.2.c show the amount of points required to simulate a semiconductor and a memristor based on minimum step size. It is important to note that these values are for 1-D simulation and they can be converted to 2-D and 3-D by squaring or cubing y axis values respectively. Plots 5.2.b and 5.2.d were created using CFL conditions for drift and diffusion and dielectric relaxation time. A typical simulation time was estimated using mobility and electric field. Based on the estimated simulation time the number of time steps were calculated using the minimum time step obtained from CFL conditions and dielectric relaxation time.

It can be seen from graphs 5.2.a and 5.2.c that memristor simulations require much higher mesh densities compared to a typical semiconductor simulation such as 1 μm long PN diode. This is due to the larger size and higher charge density of the memristor. Graph 5.2.a 5.2.b show that a memristor with 10^{26} m^{-3} charge density of the electrolyte would require close to 10^9 points and 10^{14} time steps to simulate in 1-D. These requirements make the simulation of the memristor extremely challenging. In order investigate and find possible solutions for this issue, first a memristor low charge density ($\approx 10^{15}$) was simulated in order to ensure that the simulation functions as designed. Then memristors with different charge densities were simulated and compared with each other to asses whether the behavior at low charge densities will be comparable to behavior at high charge densities.

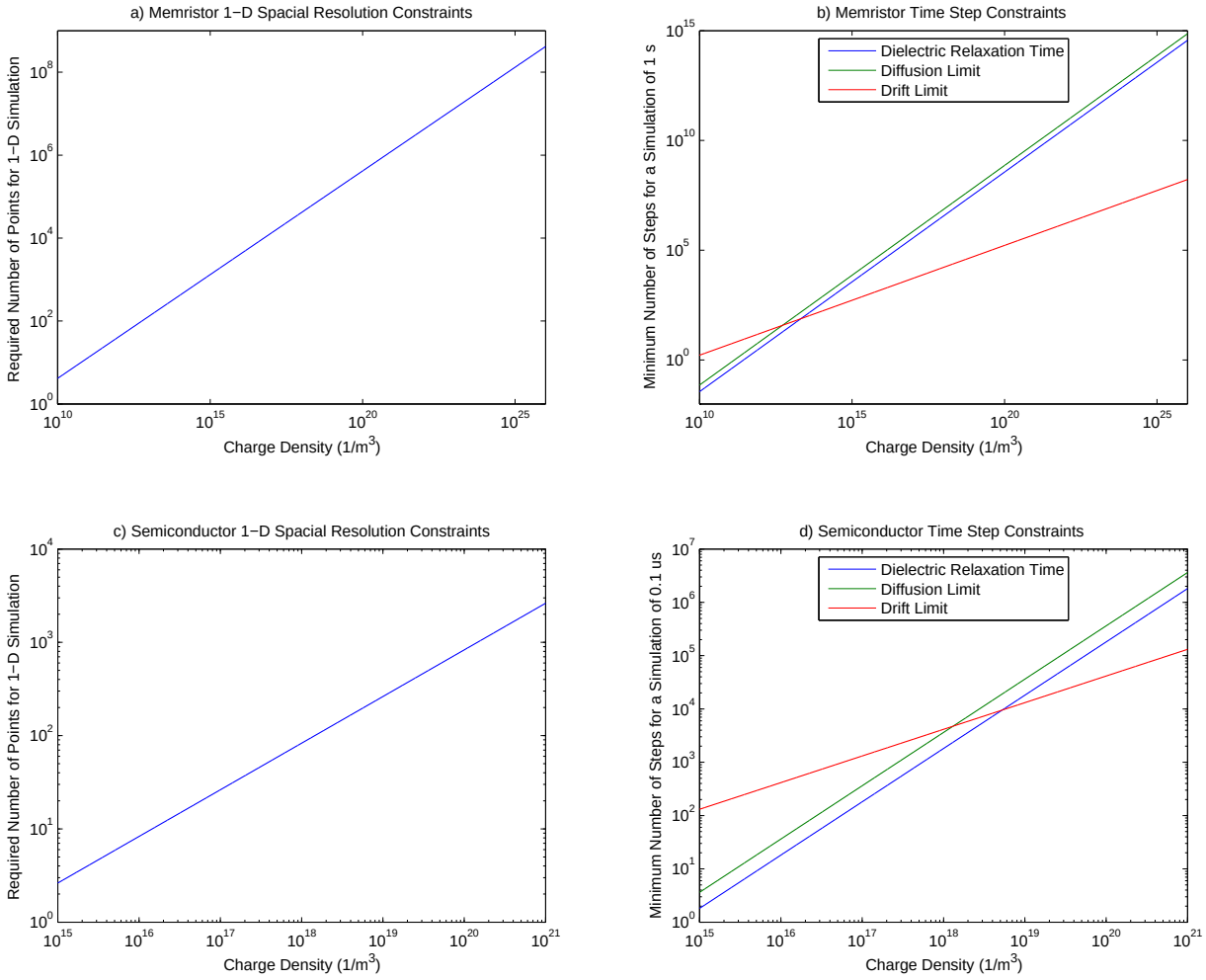

FIGURE 5.2: Spatial and temporal requirements for simulation

5.2.1 1-D Memristor Approximation

The horizontal cross section from figure 5.1 has the most crucial elements of the memristor but its simulation in 1-D is not straight forward. This cross section through the PEDOT does not include the vertical movement of lithium. Without this effect, PEDOT is just a regular conductor with a uniform current density. In order to overcome this problem a generation/recombination term for lithium ions, calculated at every time step, was added to capture the vertical movement in addition to regular drift diffusion equations which represents the horizontal movement. This generation/recombination term can be symbolized as a current source with a resistor connected to all the nodes (figure 5.3). Perchlorate ions were not included in the simulation since they do not move into the PEDOT.

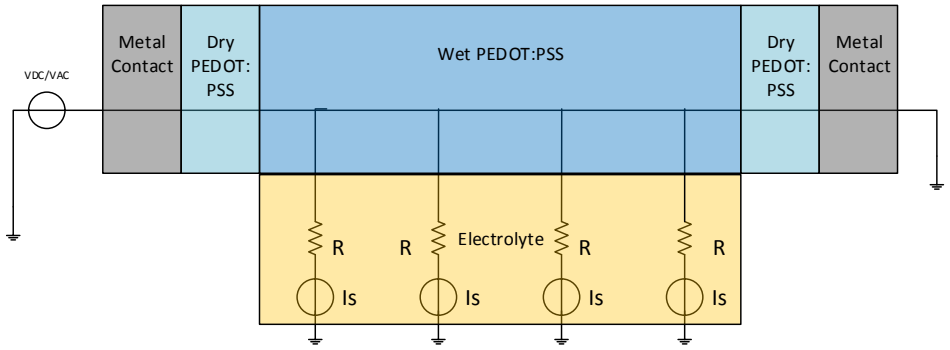

FIGURE 5.3: 1.5-D Memristor Structure

The lithium source has two different terms, one for drift and another one for diffusion. It was assumed that the concentration of lithium was always constant in the electrolyte. This way the vertical diffusion current density can be calculated using the difference between the lithium density in PEDOT and electrolyte. For the diffusion term an electric field had to be estimated between the PEDOT and the electrolyte. First the potential of the electrolyte was assumed to be half of the net applied potential. Then an electric field was calculated using the electrolyte and the instantaneous potential of the PEDOT at different positions.

Since the main characteristic of memristor is the change in resistivity over time it is important to develop a standard approach for measuring it. For the simulations in this chapter and the following one, first all the simulations were run until steady state without the movement of lithium/perchlorate ions. Lithium and perchlorate ions start to move after the steady state has been reached. The movement of ions create another transient which includes changes in resistivity. The current density (at steady state) obtained

from the initial simulation was used as a normalizing factor in order to determine the changes in resistivity after the ion movement has started.

5.2.2 1-D Memristor Simulation Using a Pulse Train

For the following simulation a potential pulse train, slow enough to let the memristor reach steady state, was applied on the left contact. Following plot 5.4 shows the resistivity measured using both contacts separately. As expected the resistance of the device more than doubled as the lithium ions move in. Additionally, it can be seen from the graph 5.4 the resistivity measurements from left and right contacts are not always the same over the duration of the simulation. This is normal since this is due to PEDOT layer losing holes on one side and gaining holes on the other which produces a difference in measured resistivity between contacts.

The resistivity in figure 5.4 shows a sudden drop when the potential is switched from 1 to 0 and vice versa. This sudden drop occurs because of the accumulation of lithium ions and holes near the negative contact which opposes the electric field generated due to the applied potential (see figure 5.8). When the potential changes suddenly, previously opposing electric field now helps the movement of holes and lithium towards the other end of the device. This additional electric field momentarily reduces the resistivity of the device.

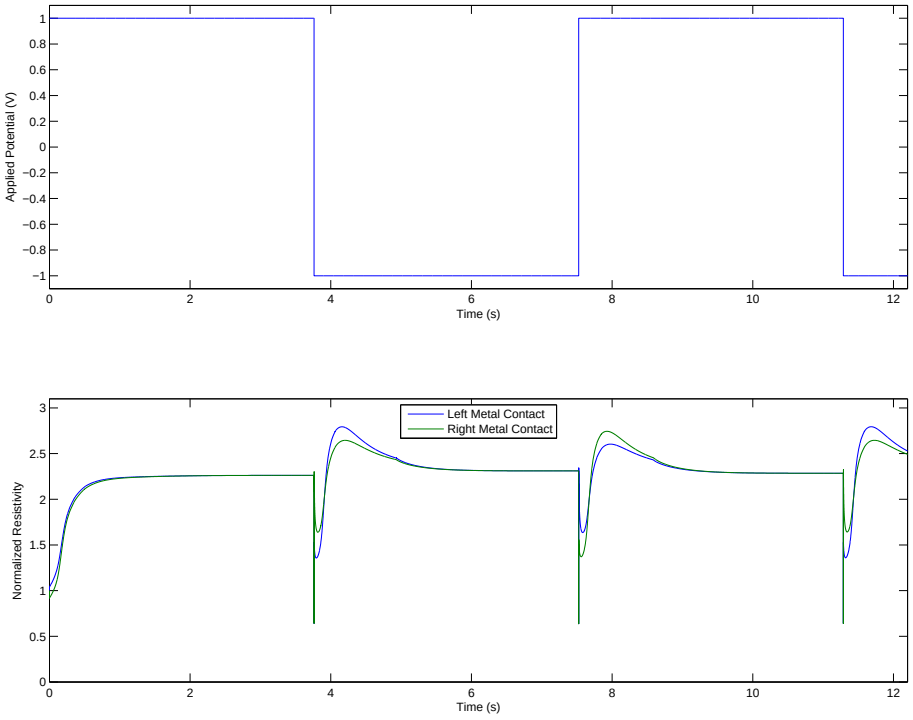

FIGURE 5.4: Change in resistivity over time due to applied potential

Figure 5.5 demonstrates the replacement of holes by lithium ions over time which directly effects resistivity seen in figure 5.6. As lithium ions get pulled in from the electrolyte toward the contact they accumulate inside PEDOT and push holes out via coulomb forces. Decreased hole concentration in the PEDOT increases the resistivity of the material. This change in resistivity over time is illustrated in figure 5.4.

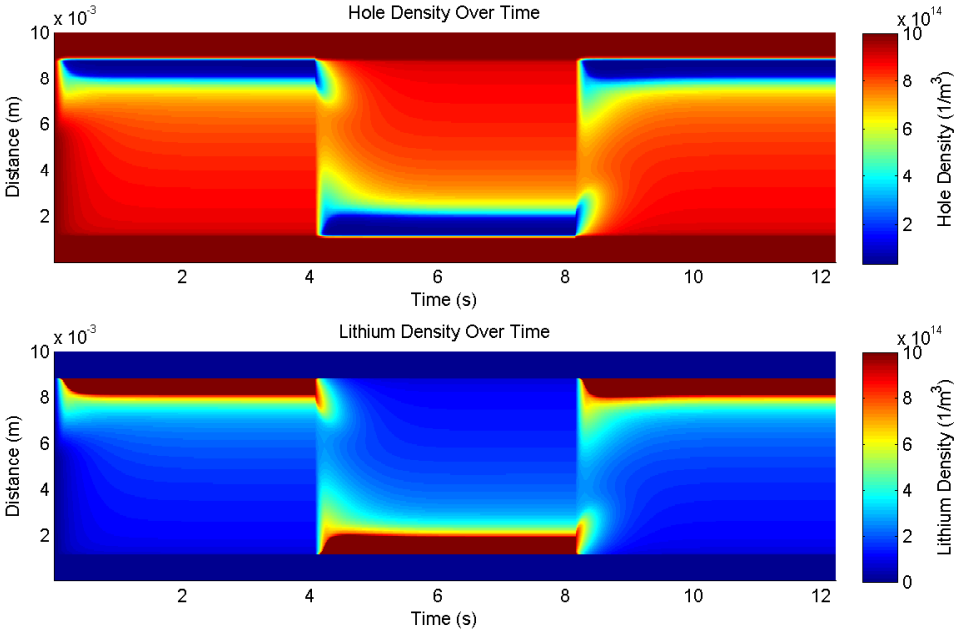

FIGURE 5.5: Lithium and hole density distribution over time

It is important to note that lithium ions are free to move in x and y direction. In figure 5.5 it can be seen that after the potential is switched as the lithium density moves from side to the other. Most of the lithium movement happens through the exchange of ions between PEDOT and the electrolyte since the distance between them is far less than the length of the PEDOT. So lithium ions, traveling from the positive to the negative contact, are pulled into the electrolyte before they reach the other side. Near the negative contact lithium ions are quickly pulled into the PEDOT and accumulate at the wet/dry interface. Figure 5.6 shows the changes in resistivity throughout PEDOT due to the accumulation of lithium. The resistivity is increased in regions where there is high lithium accumulation.

By examining the resistivity plot of PEDOT it is possible to conclude that it is composed of 3 distinct regions. 2 dry regions, where there is no contact with the electrolyte, have constant uniform resistance. Between these two resistances there is a variable non uniformly distributed resistance controlled by hole/lithium concentration and hole mobility. So this model captures the main characteristic of the memristor which is a variable resistance where the resistance at any time depends on the past of the device.

Following equation gives the total resistance for the memristor model developed for this thesis:

$$R_{tot} = 2R_{dry} + R(Li, p, \mu_{hole}) \tag{5.1}$$

The minimum resistance of this device is just the total resistance of the PEDOT without the lithium ions. The maximum resistance depends on different factors such as applied potential and the distribution and concentration of lithium ions inside PEDOT.

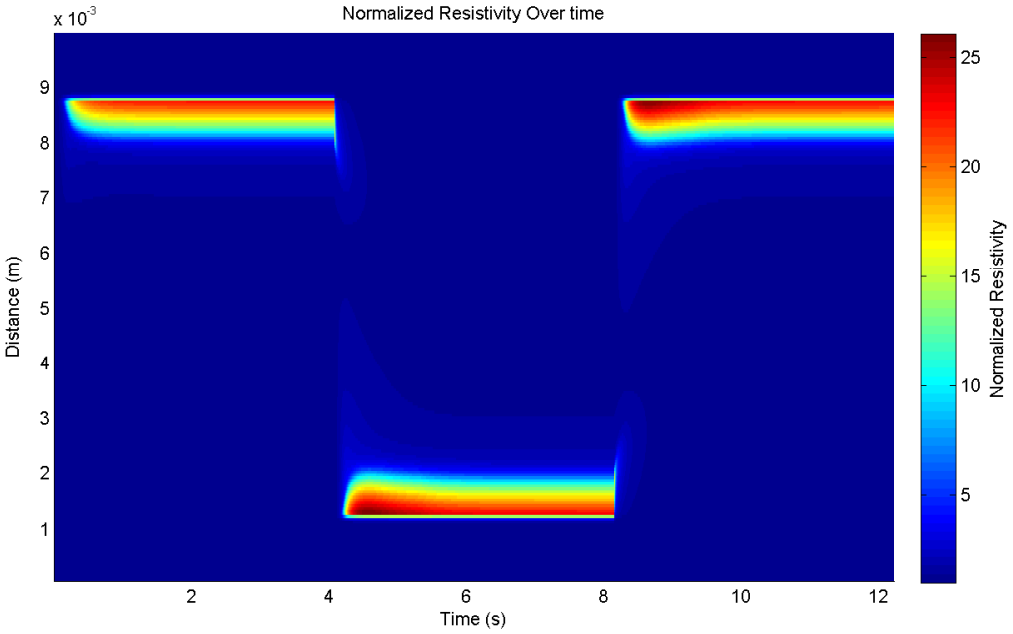

FIGURE 5.6: Normalized resistivity over time

(the following figures can go in appendix ?)

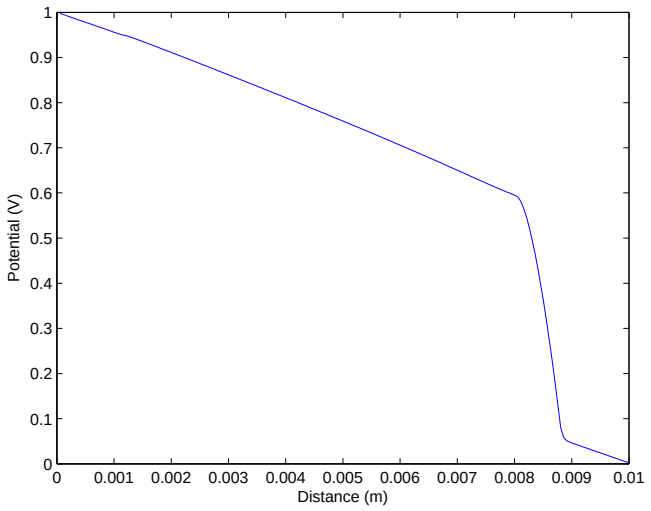

FIGURE 5.7: Potential at steady state

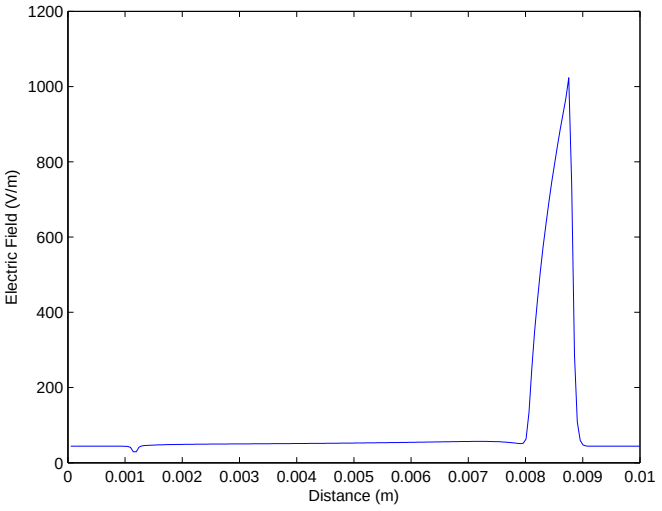

FIGURE 5.8: Electric field at steady state

5.2.3 1-D Memristor Simulation Using a Sinusoid

Memristor with a pulse train simulation showed the change in resistivity over time due to an applied potential but it does not demnostrate any memory effects. The memory effect of the memristor can be clearly demonstrated in an I-V curve using sinusoidal potential. Following four graphs (figure 5.9) were created using an AC potential with different frequencies at the contacts. All the plots show that current can have more than one value for the same potential at different times. This means that simulated memristor's past states affects its present output, therefore the device has memory.

The sudden changes in current around 0 V can be attributed to the density limiting mechanism for lithium. Instead of a slowdown in the movement of lithium ions near maximum concentration, the current flow into that region is completely blocked. Even though this makes the lithium density more responsive to changes, sudden movement block combined with large time steps can result in fast changes which can be directly seen as abrupt changes in the hole/lithium current density during transient simulations.

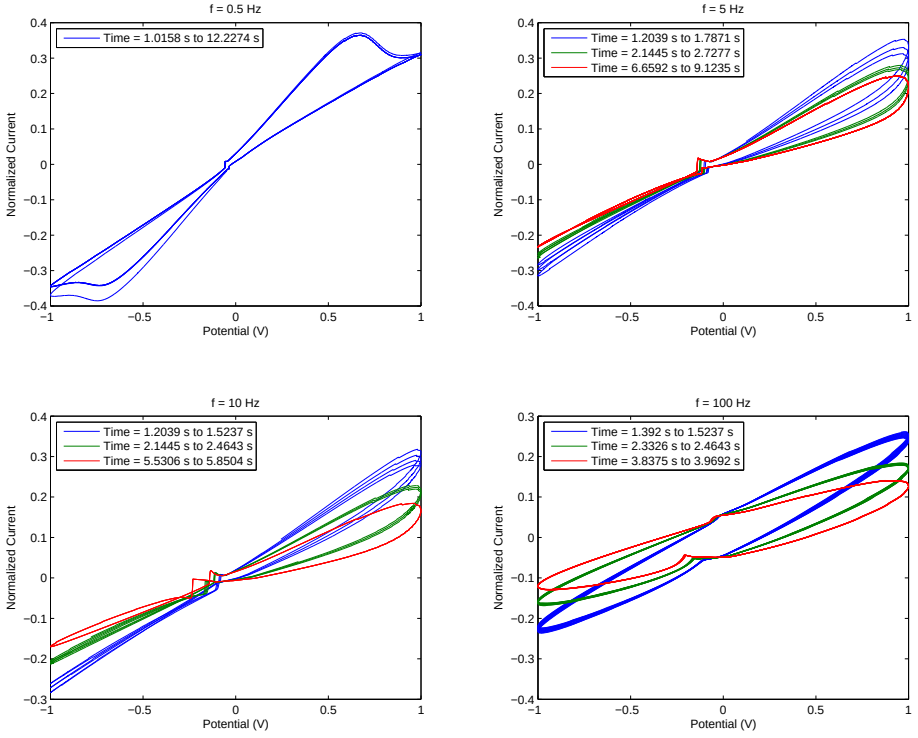

FIGURE 5.9: Normalized Current vs. applied potential at different frequencies

As AC potential pushes lithium ions from one side to the other, an equilibrium is reached over time. The changes in resistivity starts to repeat itself and after a while it becomes periodic. Figure 5.10 shows the changes in memristor current over time for the right

metal contact. At first, as lithium moves into the PEDOT there is a drop in current on average. Once enough lithium settles into the PEDOT the increase in resistiviy simply shifts from left to right but it stays fairly constant on average. The final figure (5.11) show the changes in resistivity of PEDOT over time. The maximum value of the resistivity increases over time until it reaches a steady value on either side.

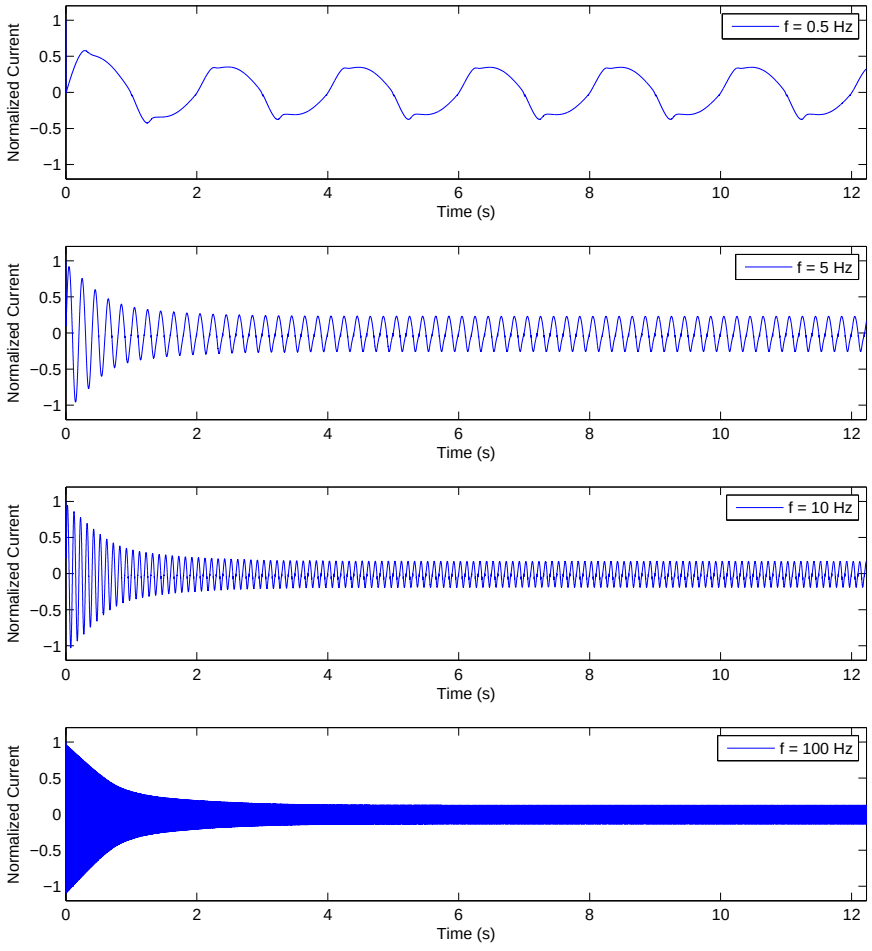

FIGURE 5.10: Normalized current over time

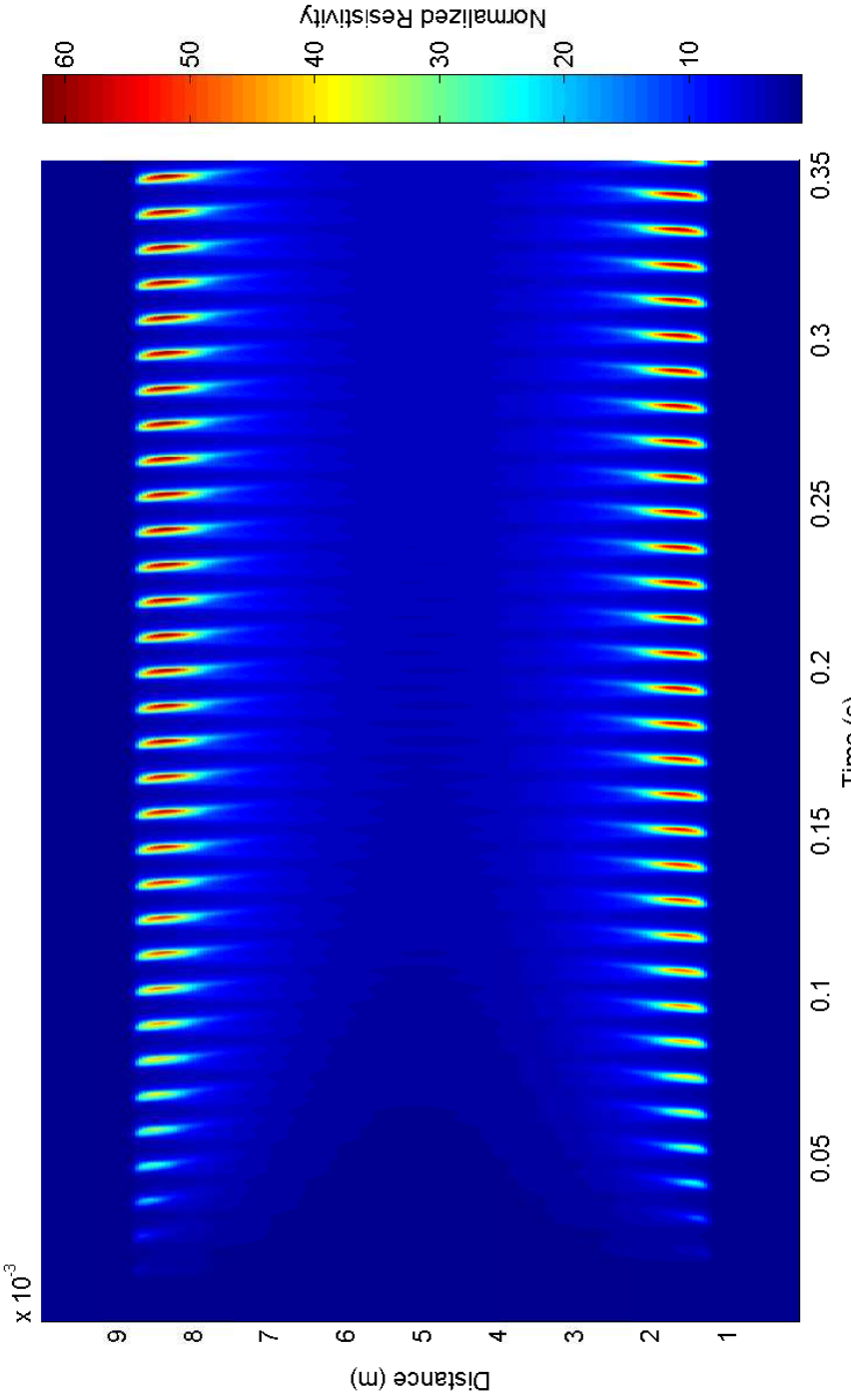

FIGURE 5.11: Normalized resistivity over time (f = 5 Hz)

5.2.4 1-D Memristor Simulation With Increasing Charge Density

After establishing that the simulation behaves appropriately it is important to investigate how charge density effects this model since the size of the device limits the maximum charge density that can be simulated. The actual device has a hole density in the range of $\approx 10^{22}\ m^{-3}$ but the simulation is restricted to $\approx 10^{15}\ m^{-3}$. In theory, if the densities used for simulation does have a limited affect on the behavior of the memristor then simulations in low densitiy can be use as a proxy for the actual device which operates in much higher carrier densities.

Following 3 graphs (5.12, 5.13 and 5.14) show hole and lithium densities at steady state as well as the current density over time at the right metal contact for various charge densities. The simulations were done on high mesh densities to allow stable simulation at high charge concentrations. 20 different simulations were made using densities ranging from 5 x $10^{15}\ m^{-3}$ to 1 x $10^{17}\ m^{-3}$ but only 5 of them were plotted for illustration purposes. All the values were normalized to the initial plot using respective hole/lithium density ratios. Following equations were used for the normalization procedure.

$$n_{norm} = \frac{n_i}{r} \tag{5.2}$$

$$J_{norm} = \frac{J_i}{r} \tag{5.3}$$

$$r = \frac{n_{initial}}{n_0} \tag{5.4}$$

n_i is the charge carrier density which could be either holes or lithium ions. J is the current density calculated from the left metal contact. r is the normalization constant which is calculated using initial carrier density ($n_{initial}$) of a simulation to be normalized and n_0 which is the carrier density of the initial plot ($5x10^{15}\ m^{-3}$). After the normalization of various variables, all the plots were placed in the same graph to visually illustrate how increasing charge density affects the simulation.

Plots for lithium ions (figure 5.13) and holes (figure 5.12) are nearly identical to each other in terms of the plot shapes. They both tend to get sharper around the area where there is a substantial accumulation of lithium. This is not unexpected since the debye length gets smaller with increasing carrier density concentration. So with increased density it is expected that the density accumulation at the wet/dry PEDOT interface will be more narrow. This affect is not as strong for lithium ions since there is a maximum concentration limit on them. Lithium and hole plots only show the difference carrier

density makes on steady state. The affect of debye length on device operation can be further explored by looking at the current density over time.

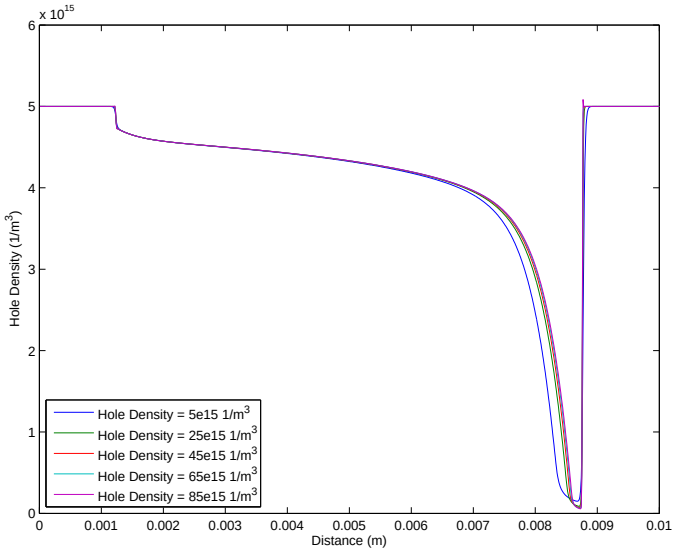

FIGURE 5.12

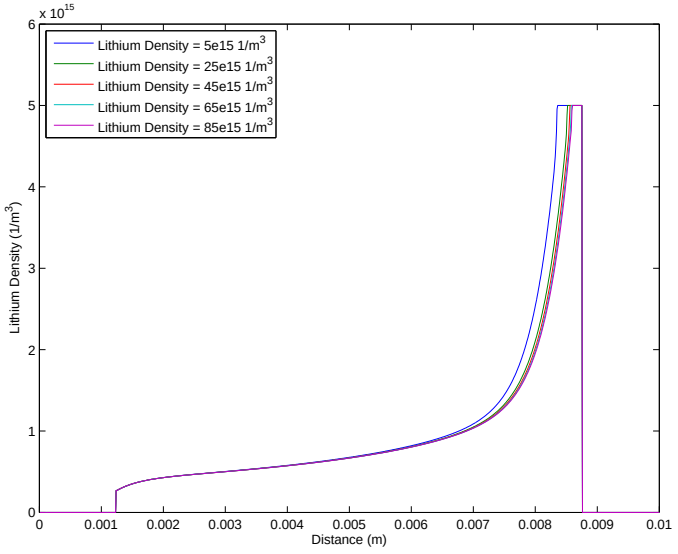

FIGURE 5.13

Like the simulation in section 5.2.2, first few miliseconds of this simulation was run without the movement of lithium ions. At this stage normalized currents are identical to each other which means a simulation with low density can be scaled up to any density without introducing any error. The introduction of lithium ions slowly deviates the current plots from each other over time but the overall behavior of the memristor remains unchanged. The current density decreases over time and reaches a steady state value.

After the first plot which has the lowest hole density, consecutive plots get closer and they are almost impossible to distinguish from each other at steady state.

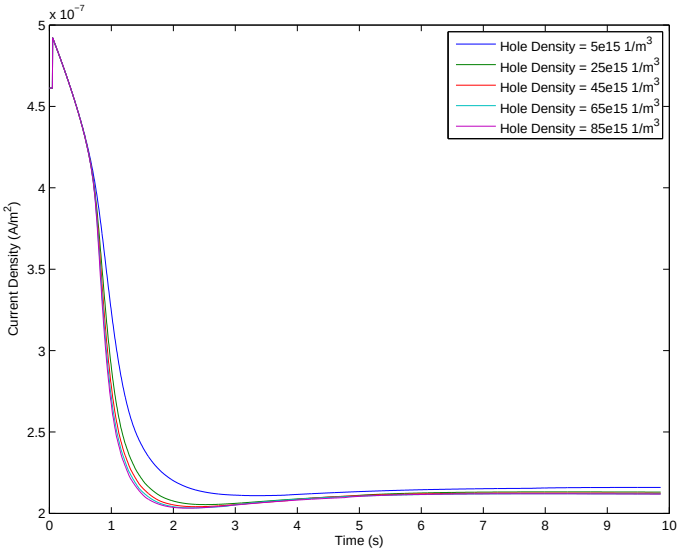

FIGURE 5.14

The impact of increasing charge density can be numerically explored using normalized plots. Following formula was used to calculate a percentage difference between different normalized carrier densities as well as normalized current densities.

$$P_i = \frac{1}{K}\sum_{k=1}^{K}|100\ \frac{n_i(x_k)/r - n_0(x_k)}{n_0(x_k)}| \tag{5.5}$$

$$P_i = \frac{1}{T}\sum_{k=1}^{T}|100\ \frac{J_i(t_k)/r - J_0(t_k)}{J_0(t)}| \tag{5.6}$$

K is for total number of points along x axis and T is the total number of time steps taken by the simulator. x_k and t_k are used to for a point in x axis and a point in time respectively. r is the normalization constant described in equation 5.4. Both equations start by taking a point in either space (lithium/hole density) or time (current density) for a simulation with a certain carrier density and normalize them. After that point is normalized its difference from the lowest carrier density simulation is calculated as a percentage. Finally all the differences are averaged and used as a measure of the difference between simulations with different charge densities. They can also be used as an error factor for scaling.(Is this paragraph clear enough ?)

Figure 5.15 shows the difference hole/lithium density makes in the simulation. Carrier densities in the dry regions of the PEODT change very little between consecutive simulations since lithium ions do not reach there. For this reason only the densities at the wet PEDOT were used to measure the difference between plots.

In all 3 cases, there is an increase in average difference for increasing carrier density. Hole density shows the most difference between plots. Since holes are free to move inside the PEDOT they directly get effected by the change in debye length due to the increase in hole density. This is not the case for lithium ions because their movement is restricted by the limit on lithium density. In contrast, current density is not as sensitive to density changes as lithium and hole distributions.

An approximate error estimation can be made for current density if a low hole/lithium density is used for simulation and then scaled up to match the actual memristor. Figure 5.15 shows around 3.3 % difference for 2 orders of magnitude increase in hole density. Assuming the error scales linearly after that point a total of 6 orders of magnitude will result in 9.9 % error introduced in order to linearly scale from 10^{15} to 10^{21}. The actual error is likely to be less since the error progresses sub linearly. Following the same procedure 6 orders of magnitude difference produces a 12 % error for lithium distribution and 48 % error for hole distribution. The difference in hole distribution looks very large but the overall shape of the plot is still reserved, most change occurs around the wet/dry PEDOT interface where lithium accumulates. Based on these error margins and previous plots it can be concluded that the behavior of the memristor simulated using low charge density is very similar to the simulation at high carrier density.

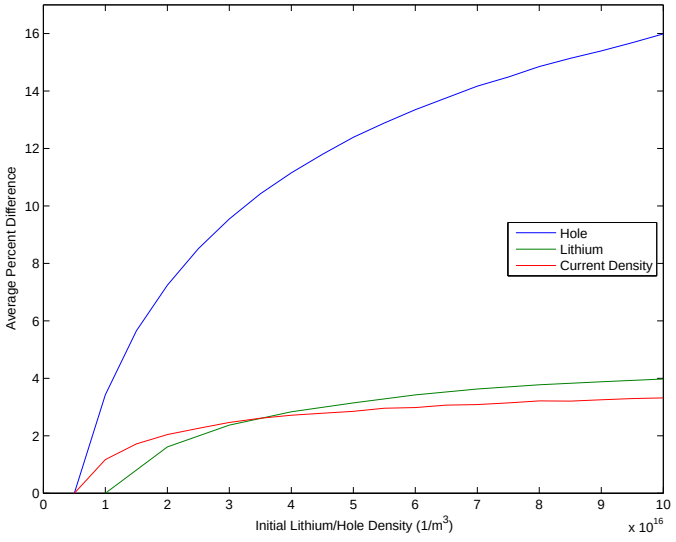

FIGURE 5.15

5.2.5 Experiment vs. Simulation

Hopping distance change due to lithium modifies hole mobility. Can be used to match maximum resistivity.

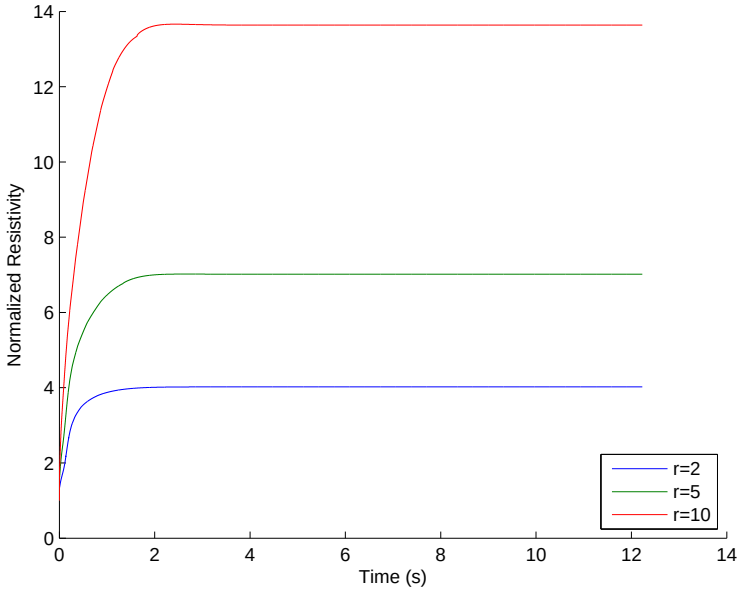

FIGURE 5.16

Lithium mobility can be scaled to match the experimental values

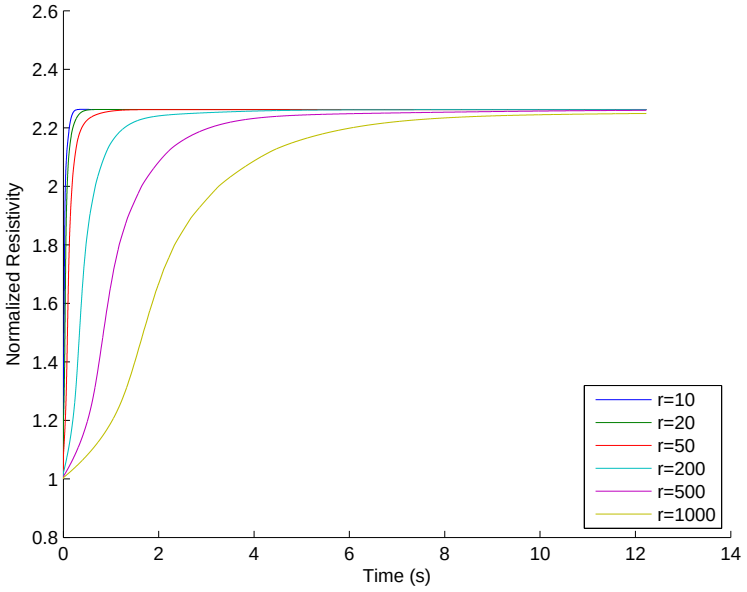

FIGURE 5.17

Resistivity change due to applied potential. This behaves unexpectedly. I thought the resistivity would go higher with increased applied potential. Probably because of 1 line approximation for the electrolyte, the vertical potential is probably off.

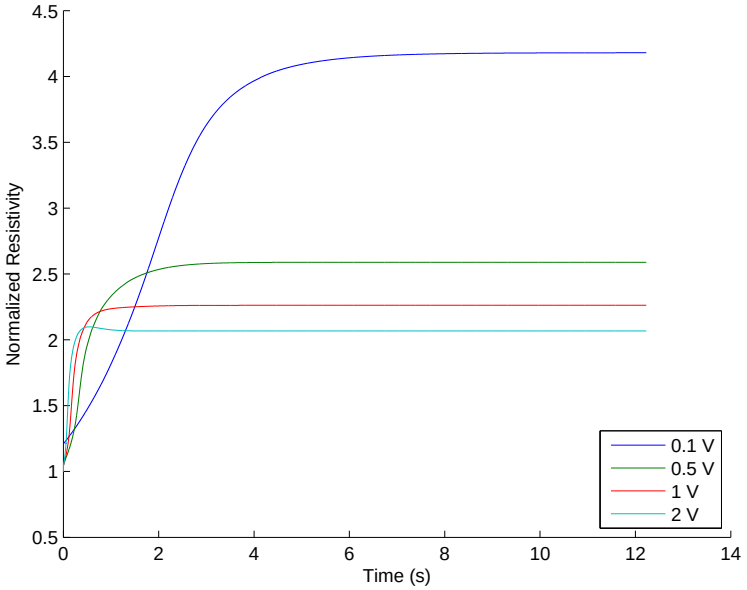

FIGURE 5.18

-Can add Notch simulation vs. notch experiment. They visually match

Chapter 6

2-D Memristor Simulation

6.1 2-D Memristor Model

After creating a method to solve drift diffusion equations using finite difference in chapter 4 and testing it in chapter 5 we can now simulate an actual memristor. The most basic memristor structure consists of a rectangular strip of PEDOT with metal/carbon contacts on both sides. On top of the strip there is a drop of electrolyte solution. In order to be able to simulate the memristor we first need to determine boundary conditions and values, initial conditions and physical constans for this device.

We have two different materials and three charge carriers that are important for this problem. The drop of electrolyte has lithium and perchlorate ions and PEDOT has holes and electrons. All the carriers are not free to move everywhere. Due to PEDOT's conduction mechanism the electrons are fixed in place and holes are mobile. Also because of PEDOT's chemistry only lithium is allowed to move in so perchlorate ions always stay in the electrolyte. When a lithium ion moves into the PEDOT, through drift or diffusion, it replaces a hole. This replacement reduces the number of available holes in the PEDOT and increases its resistance.

For the initial concentration of ions in the electrolyte we have assumed that there is no net charge and everything is uniformly distributed. Similar to electrolyte PEDOT has no net charge. All the electrons and holes are uniformly distributed and in equilibrium. Boundary conditions for all species are no flow boundary conditions with the exception of holes which can leave PEDOT through the contacts. On the contacts zero net charge is always conserved through the movement of holes in and out of the device. Lithium atoms can move between PEDOT and the electrolite but they cannot go through the contacts. Also there is a limit on the amount of lithium PEDOT can accept. Once all the holes have been replaced lithium ions cannot go into the PEDOT anymore.

The difference between the thickness of the PEDOT and electrolyte makes the simulation very difficult using uniform meshing. The thickness of the electrolyte was shortened by assuming that the amount of charge in the electrolyte is very large and more than enough to saturate PEDOT with lithium ions. Very thick electrolyte was replaced by a thinner one and the top part assumed to be an infinite source/drain for ions.

The contacts have constant potential so they have dirichlet boundary conditions. There were no constraints for the edges of the simulation domain so the potential was set to float using Neumann boundary condition.

Another important aspect of this device is the change in mobility between different materials. Lithium ions move very slowly when they get intercalated into the PEDOT. Also the regions of PEDOT that are in contact with the electrolite (wet region) has higher mobility for lithium compared to the regions that are not in contact (dry region).

6.2 Simulation vs. Experimental Results

6.2.1 Single Channel Memristor

In this section we will be looking into the transient simulation of a single channel memristor which is very similar to the last simulation of the previous section. Drift diffusion and Poisson's equations are coupled and lithium density is limited in PEDOT. In addition, the mobility of lithium is now gradually changing between wet and dry regions. This way lithium ions can penetrate the dry region but they cannot move too far. For transient simulation a constant potential has been applied until steady state. Once the memristor reached steady state the polarity of the potential has been switched and the simulation was run until it reached steady state.

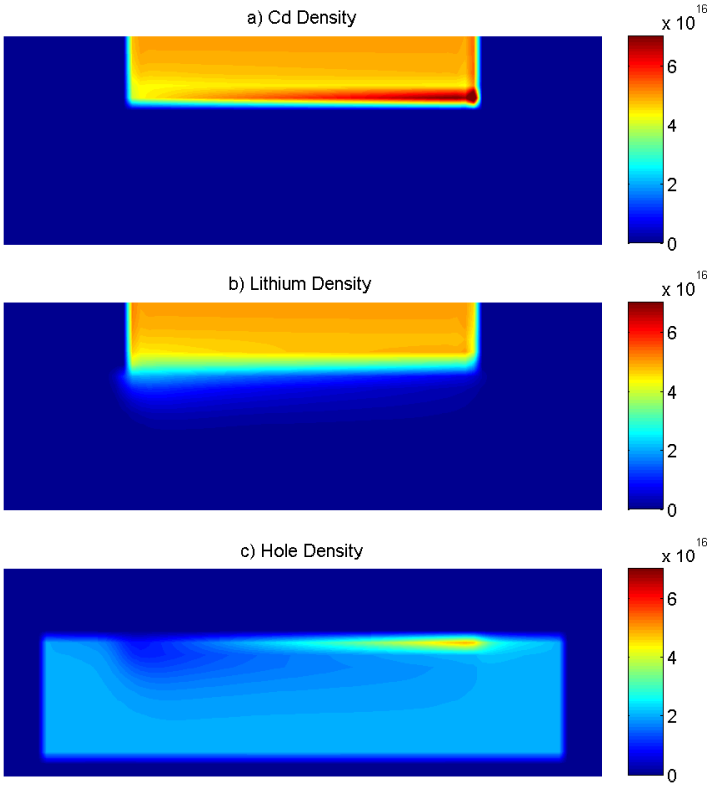

FIGURE 6.1: Particle distribution right after the simulation has started

Following graph (6.1) shows the distribution of charged particles right after the simulation has started using initial conditions described in figure **??**. We can see that perchlorate ions quickly redistribute and pile up at the bottom right corner of the electrolyte. Lithium ions drift and diffuse into the PEDOT and move as far as they can towards the contact but they cannot reach it due to the decreased mobility in the dry

region. Holes accumulate right on the interface between PEDOT and electrolyte in response to perchlorate accumulation. We can also see holes being pushed out on the left side due to the migration of lithium into PEDOT.

At steady state we can see lithium accumulating on the left side of PEDOT and creating an area with very low hole density therefore high resistance (figure 6.2).

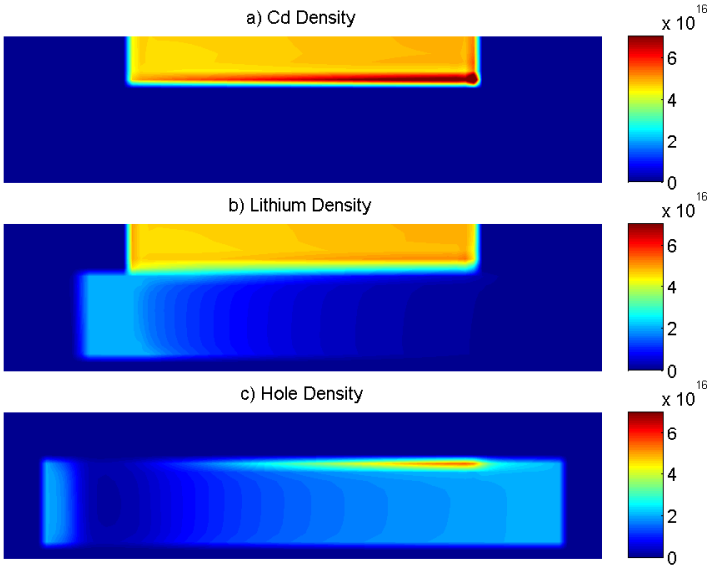

FIGURE 6.2: Particle distribution at steady state

After the potential has been flipped (figure 6.3) we can see that some lithium that got into the dry region of the PEDOT does not leave right away due to low mobility. Also, the change in potential forces lithium ions to accumulate on the right side of PEDOT.

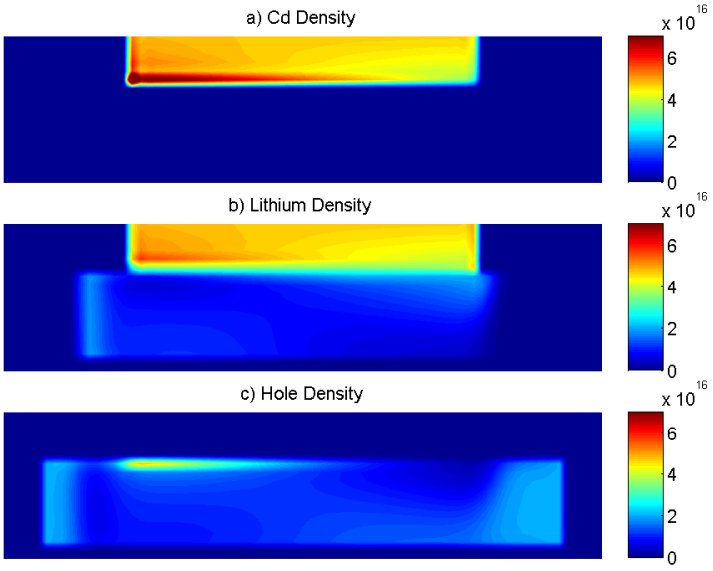

FIGURE 6.3: Particle distribution after the potential has been changed

Finally once everything reaches steady state again almost all of the lithium ions that ware stuck in the dry region of PEDOT moved away. The final distribution for all particles looks like a mirror image of the situation with opposite potential (figure 6.2). This is expected since the device is completely symmetrical.

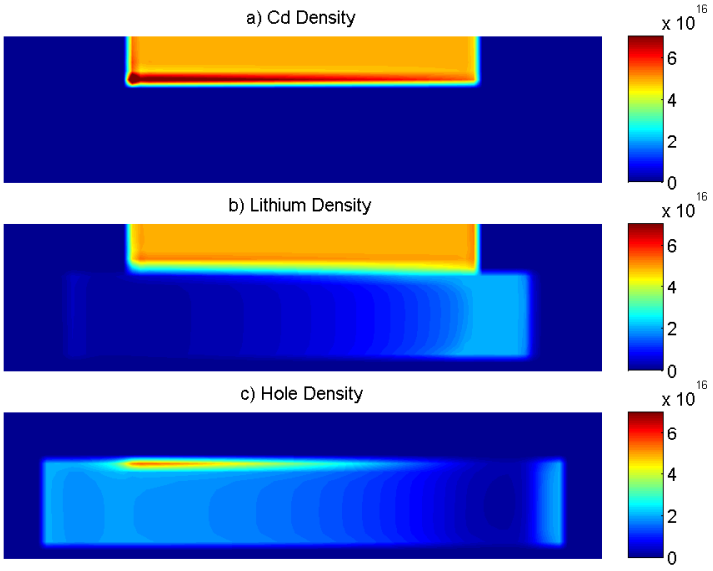

FIGURE 6.4: Particle distribution at steady state after the potential has been changed

The next five graphs show the evolution of the potential and the electric field over time. The snapshots were taken at the same time as the ones for charged particles. The first figure (6.5) shows the initial potential distribution. At te second figure (6.6) We can see the large electric field between the PEDOT and electrolyte created by the accumulation of holes and perchlorate on both sides. Additionally the electric field inside the electrolyte is getting canceled out due to separation of charge.

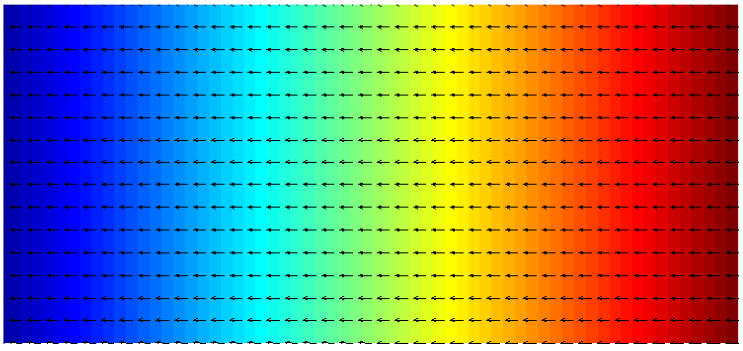

FIGURE 6.5: Electric field and potential distribution before any movement of charge

At steady state there is almost no electric field inside the electrolyte (figure 6.7). Most of the electric field inside PEDOT is also canceled out by the accumulation of lithium

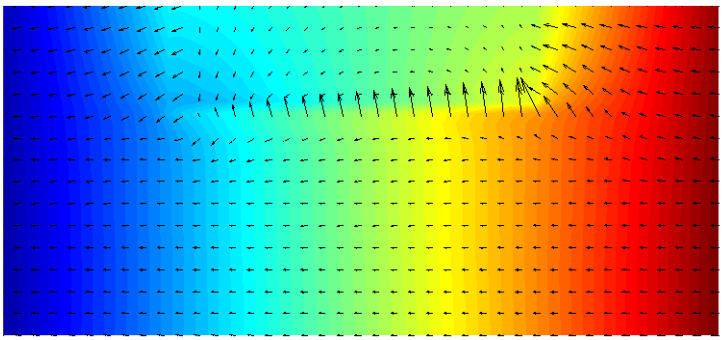

FIGURE 6.6: Electric field and potential distribution right after the simulation has started

on the left side. Almost all the electric field is concentrated around the region where lithium accumulates and forces holes out. Since the electrons are fixed in place, when holes move out they leave behind an exposed negative charge in the dry region. This strengthens the electric field even further.

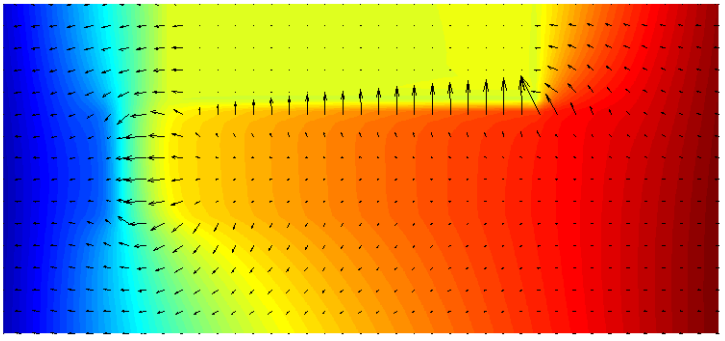

FIGURE 6.7: Electric field and potential distribution at steady state

As soon as the potential is switched we see a change in the electric field between PEDOT and electrolyte (figure 6.8). The electric field created by lithium on the left side of the PEDOT quickly disappears. The dark spot on the left side of PEDOT is due to lithium taking time to move towards the other side.

At steady state the potential distributions of 6.7 and 6.9 are mirror images of each other except the polarity of the applied potential at the contacts are opposite. This is not unexpected since charge particle distributions had the exact same behavior.

Figures 6.10 to 6.15 show the horizontal cross section of lithium around the wet dry/interface of PEDOT. The figures on the left side are simulation results and the figures on the right side are experimental results. Unfortunately we did not have any means of directly measuring the lithium density. The closest option to measuring lithium density in

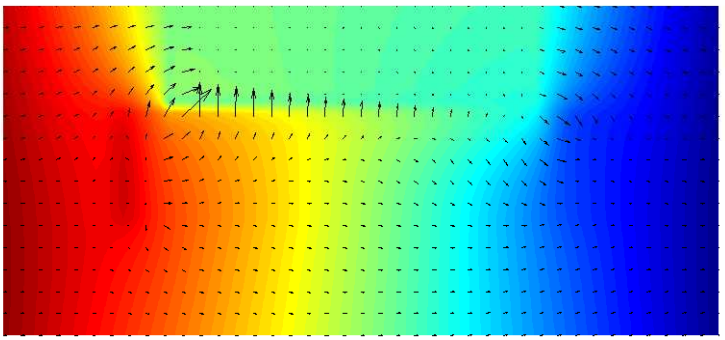

FIGURE 6.8: Electric field and potential distribution right after the applied potential has been changed

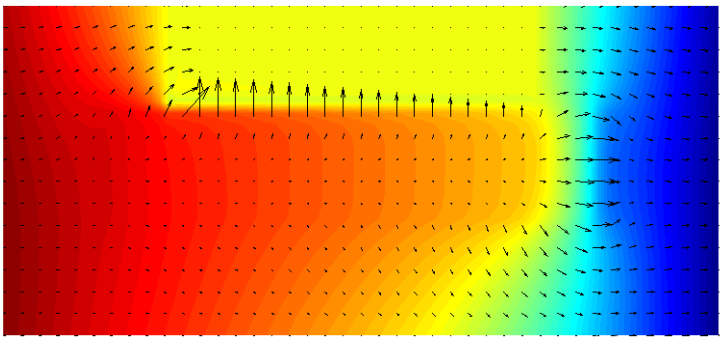

FIGURE 6.9: Electric field and potential distribution at steady state after the applied potential has been changed

PEDOT was to capture the blue coloration of PEDOT when it interacts with lithium. This was done by recording the video of the experiment as it goes through different stages. Afterwards, the images were filtered and processed to show high values for blue and low values for other colors.

The figure below shows the distribution of lithium right before the potential is flipped. We can see , from both simulation and experimental results, that as time progresses lithium moves towards the opposite side of the device and leaves behind a trail where mobility is very low.

Another phenomenon that was observed in the experiment was the change in lithium penetration into dry PEDOT due to increased applied potential. The last figure in this chapter (6.16) shows the maximum distance lithium travels into the dry region of PEDOT with increasing potential at the contacts. Both simulation and the experiment follow a similar trend but they deviate at higher voltages. There could be a few reasons for this discrepancy. First of all it is very hard to get an exact function for the change between wet and dry regions through experimentation so any function used to model this

gradual change had to be optimized by trial and error. Since the simulation for every data point takes a very long time to run, it is very difficult to find a general function that fits all the data points. Also the grid used to simulate this problem was quite coarse so there were only a few points to represent the change between two regions.

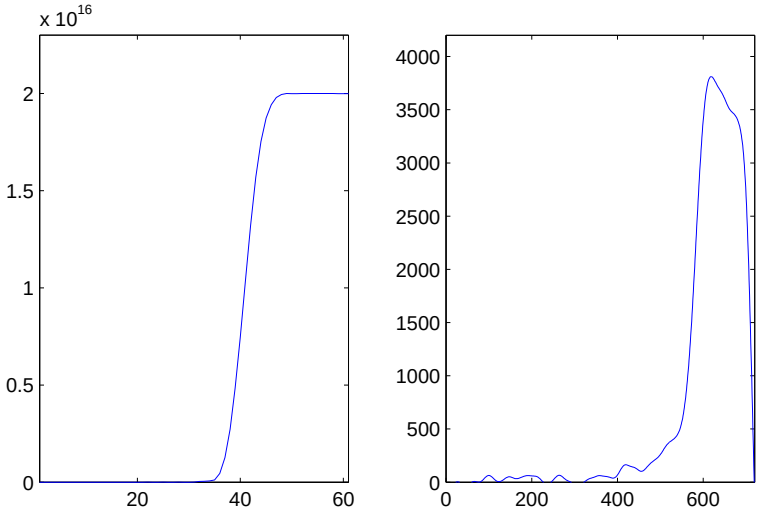

FIGURE 6.10: Lithium movement at wet/dry interface

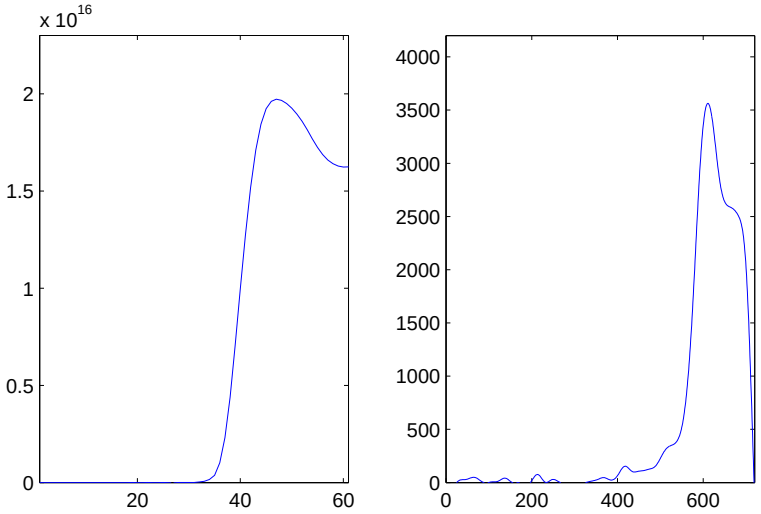

FIGURE 6.11: Lithium movement at wet/dry interface

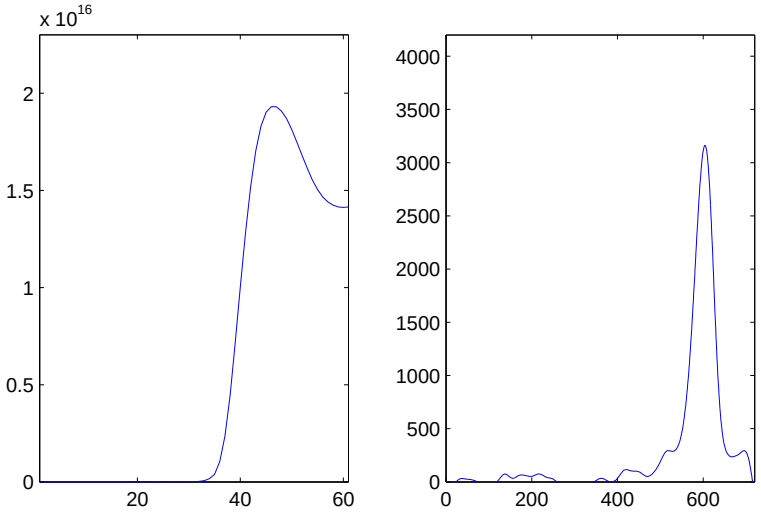

FIGURE 6.12: Lithium movement at wet/dry interface

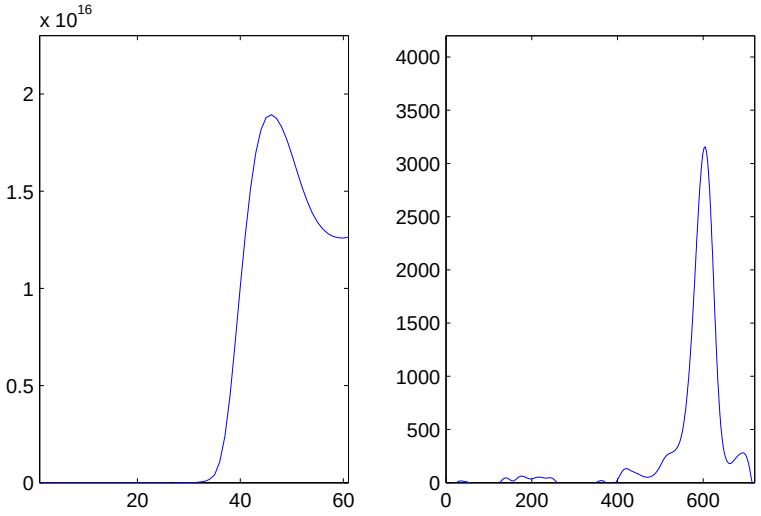

FIGURE 6.13: Lithium movement at wet/dry interface

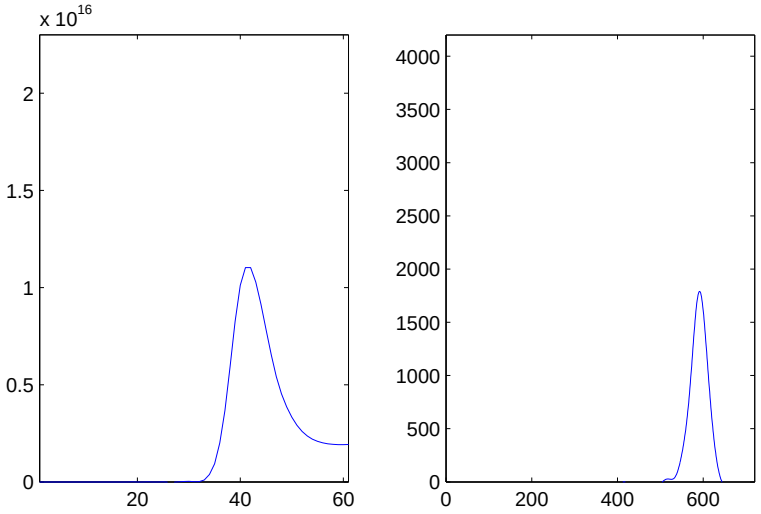

FIGURE 6.14: Lithium movement at wet/dry interface

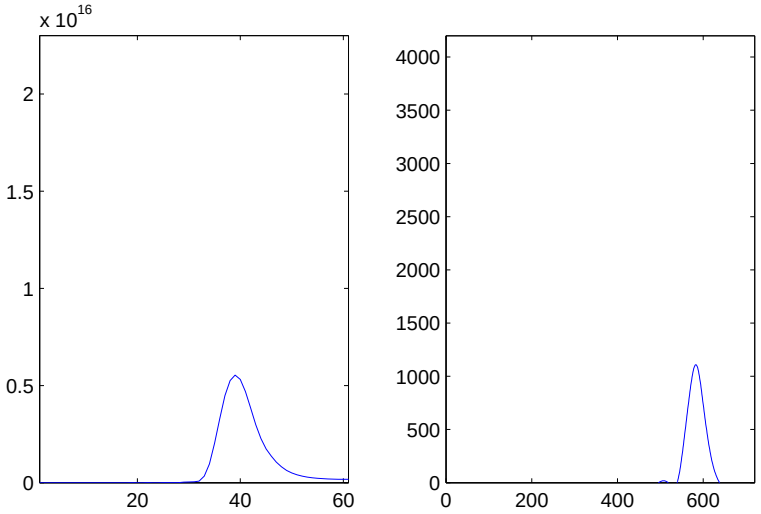

FIGURE 6.15: Lithium movement at wet/dry interface

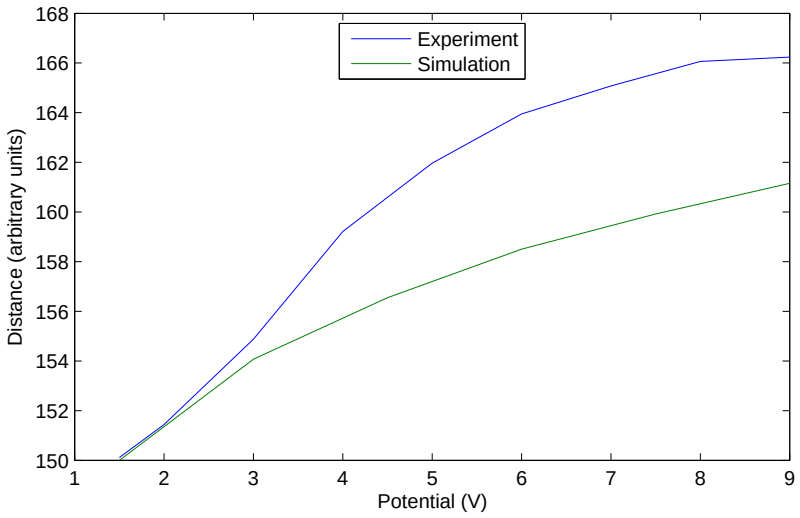

FIGURE 6.16: Penetration of lithium into dry PEDOT

6.2.2 Noteched PEDOT

In this section we will be looking at a structure which is very similar to the single channel memristor. All the boundary conditions and initial values are the same except this time there is a notch in the PEDOT (figure 6.17). So there is no hole current through the device and lithium cannot migrate into the notch. The device itself has very limited practical use but the experimental results are very suitable to test our numerical model.

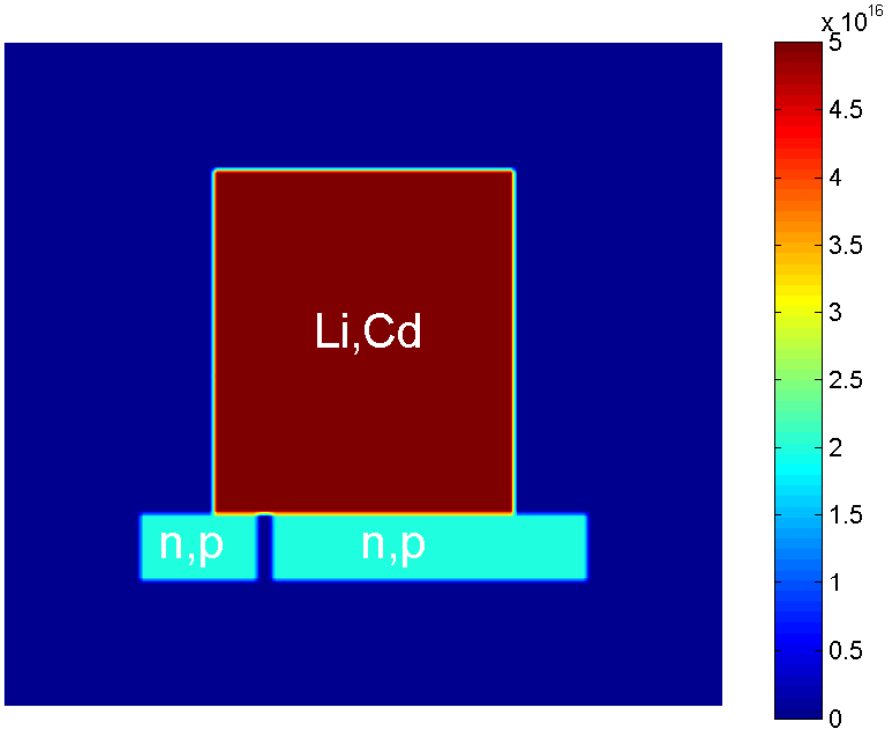

FIGURE 6.17: Initial hole, electron, perchlorate and lithium distribution for a notched memristor

The notch in the PEDOT is sandwiched between two conductive parts. This is analogous to having a simple circuit with two low and one high resistance in series. Based on this analogy we can see that almost all the potential drop is going to be on the notch. One side of the PEDOT will have a low potential and the other side will have a high potential. In figure 6.18 we can see lithium slowly moving towards the negative side of the PEDOT. At the same time perchlorate is starting to accumulate on the positive side. We can also see a significant hole accumulation inside PEDOT right before the notch.

As time goes by more lithium is pushed away from the positive side of the PEDOT and pulled into the negative side (figure 6.19). The here is a noticeable lack of lithium on the side with positive contact at the electrolyte/PEDOT interface. While lithium is pulled

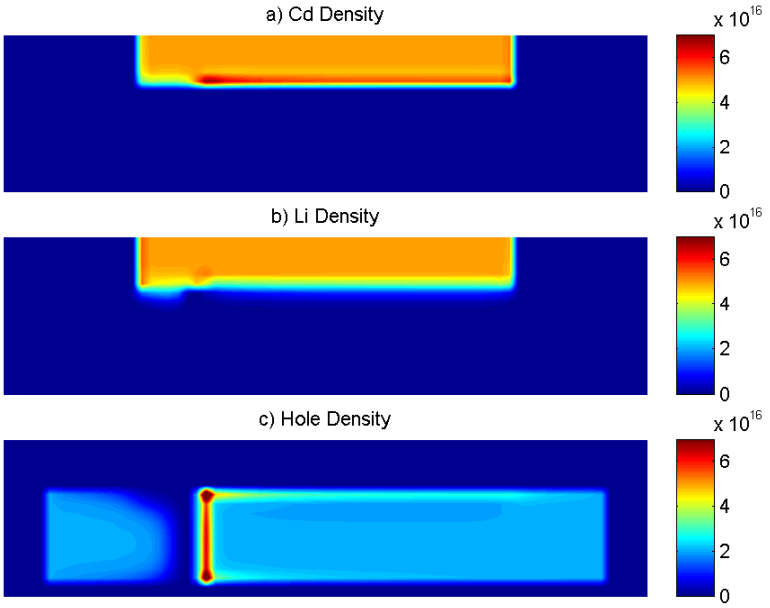

FIGURE 6.18: Particle distribution shortly after the simulation has started

into the PEDOT holes are being pushed away. Holes also accumulate at the surface of the PEDOT due to accumulation of perchlorate right across the interface.

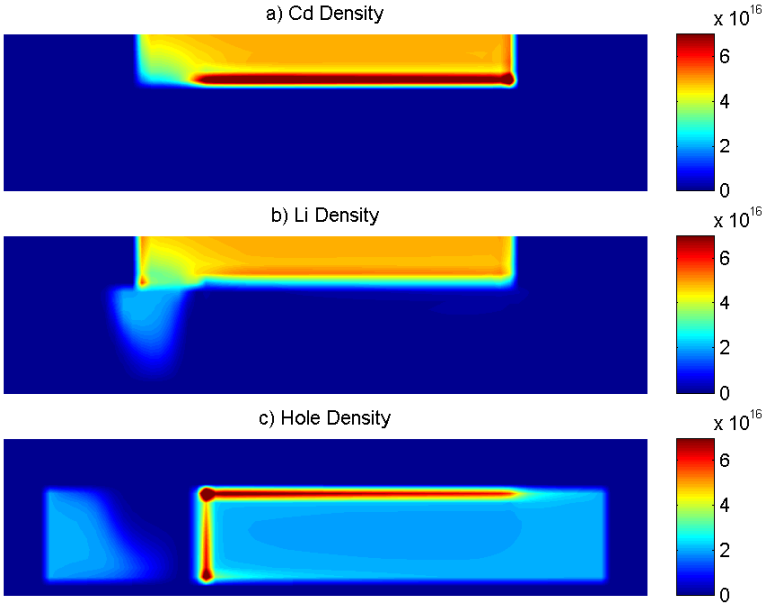

FIGURE 6.19: Particle distribution before steady state

At steady state we can see that lithium density in PEDOT is uniform and at its maximum value (6.20). At the same area we can see the lack of holes due to migration of lithium.

Once the potential is flipped everything starts to move in opposite direction (figures 6.21 and 6.22). Perchlorate moves towards the positive contact. Lithium ions start to leave

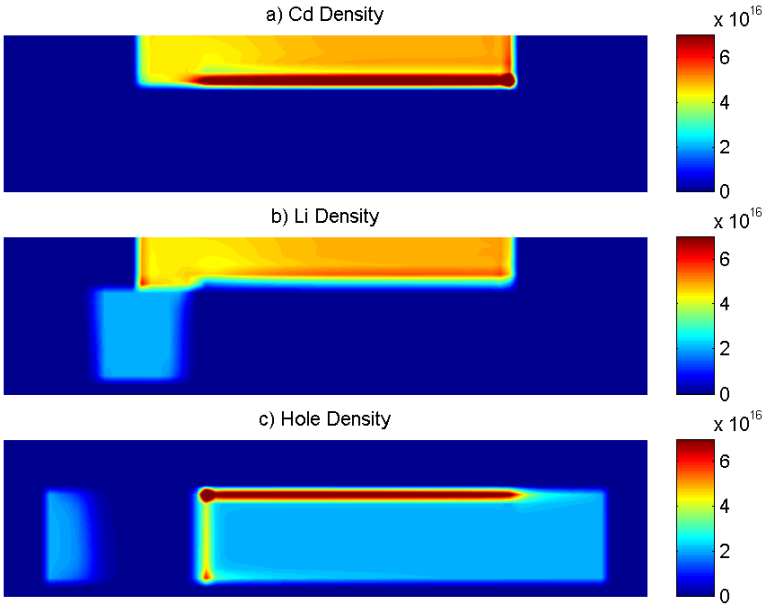

FIGURE 6.20: Particle distribution at steady state

the PEDOT on the left side of the notch and they get attracted towards the right side. Holes start to accumulate on the left side instead of the right side.

In figure 6.22 we can see that due to the strength of the electric field, holes and perchlorate ions gather on the left side of the PEDOT/electrolyte interface very quickly and leave behind a depleted region. Also as lithium settles in the right side of the PEDOT holes start to move away.

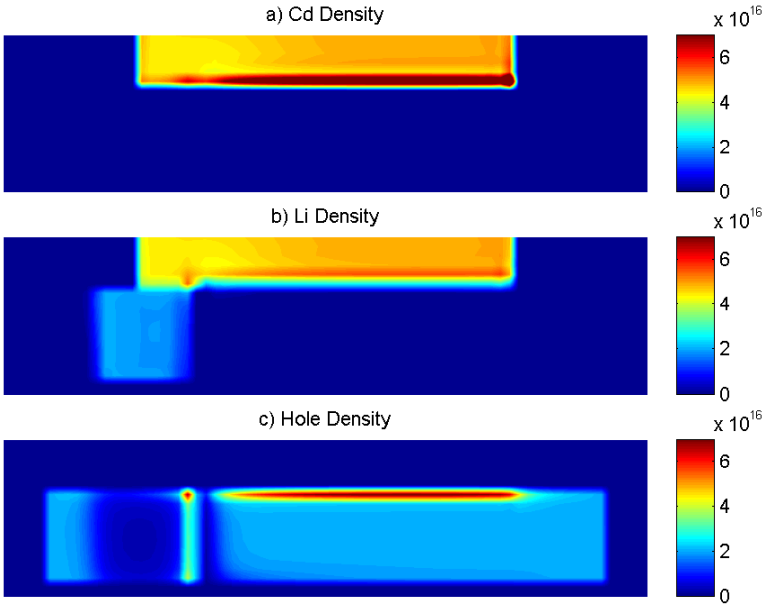

FIGURE 6.21: Particle distribution right after applied potential has been switched

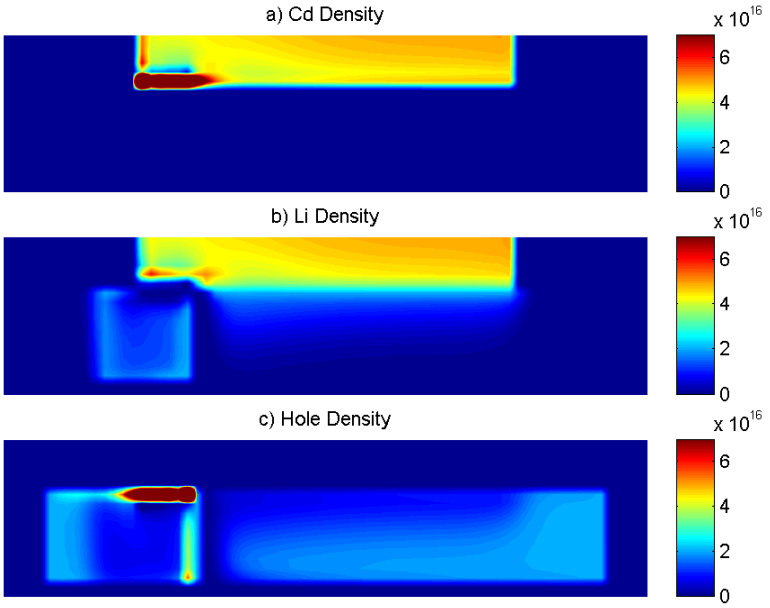

FIGURE 6.22: Particle distribution close to steady state after the potential has been switched

Steady state in figure 6.23 is the complete opposite of figure 6.20. The potential is flipped therefore everything else appears on the opposite side. In both cases lithium ions push out holes and perchlorate accumulates at the interface.

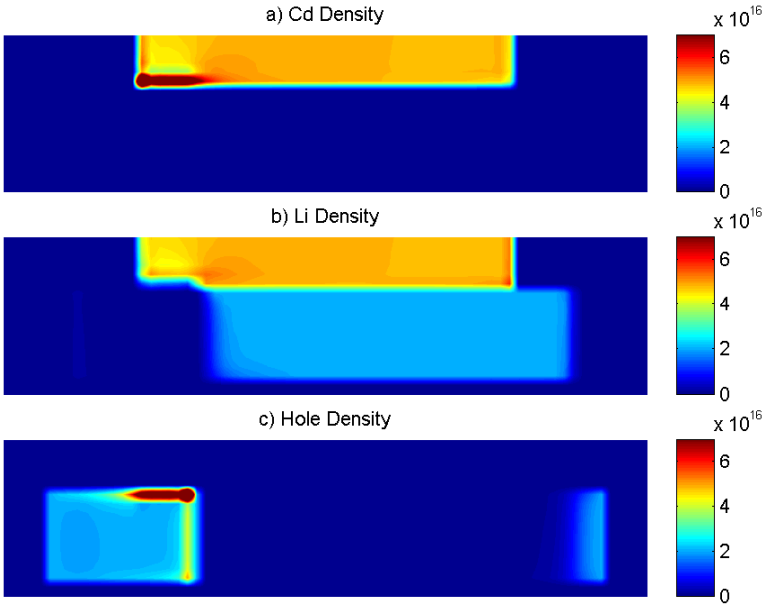

FIGURE 6.23: Particle distribution at steady state after the potential has been switched

Figures 6.24 to 6.30 show the evolution of electric field and potential over time. Right after the simulation has started we can see a large drop of potential and a large electric field at the gap (figure 6.25). There is also a large electric field forming at the

PEDOT/electrolyte interface as holes and perchlorate ions right across each other.

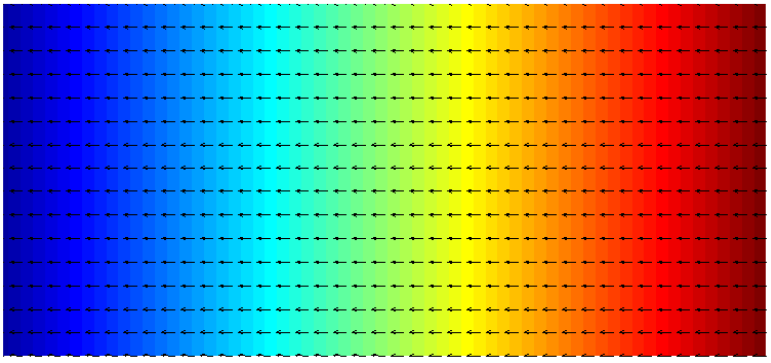

FIGURE 6.24: Electric field and potential distribution before redistribution of charge

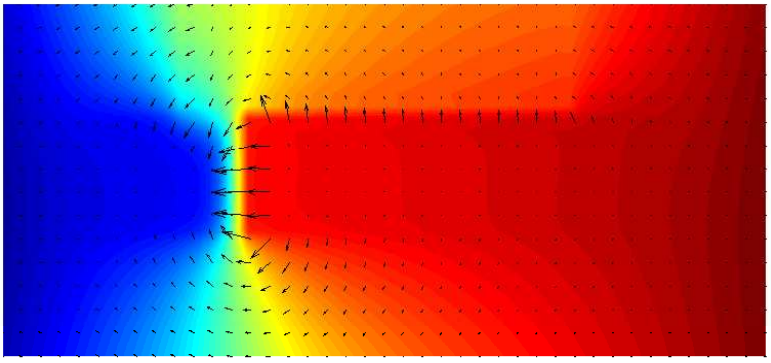

FIGURE 6.25: Electric field and potential distribution shortly after the simulation has started

In figure 6.26 we can see the cancellation of the electric field inside the electrolyte due to redistribution of charge. We can also see the effect of lithium ions moving in on the left corner of the notch.

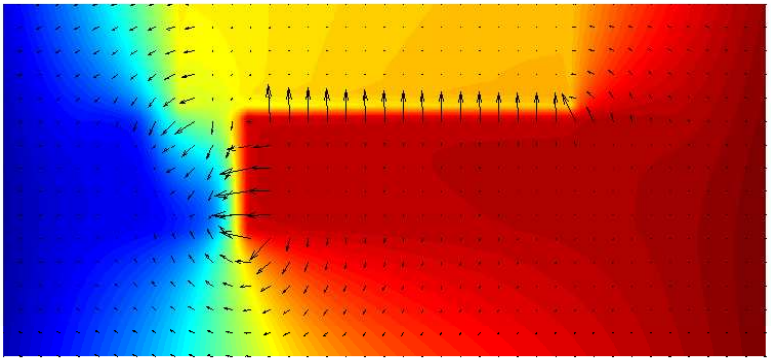

FIGURE 6.26: Electric field and potential distribution before steady state

At steady state we can see that the electric field on the right side of the notch was canceled but there is still an electric field on the left side (figure 6.27). This is due to the density limit of lithium. Holes cannot accumulate at the contact and lithium can only accumulate until a certain density so the electric field in that region does not get canceled out.

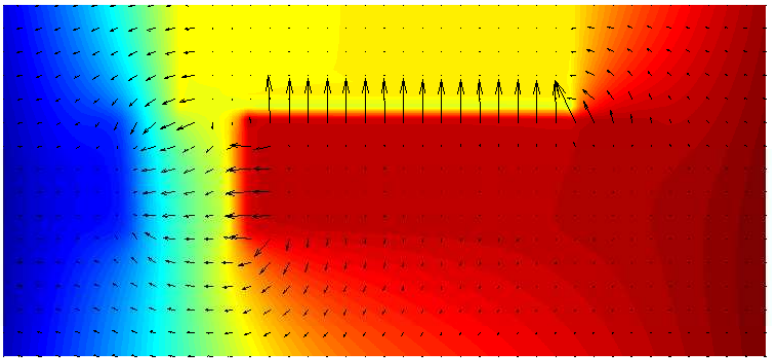

FIGURE 6.27: Electric field and potential distribution at steady state

The same process repeats itself after the applied potential has been switched (figures 6.28 to 6.30). Holes accumulate on the left side of the notch and cancel the electric field. Also there is a large electric field emerges due to the accumulation of perchlorate ions and holes at the boundaries on the left side (figure 6.30).

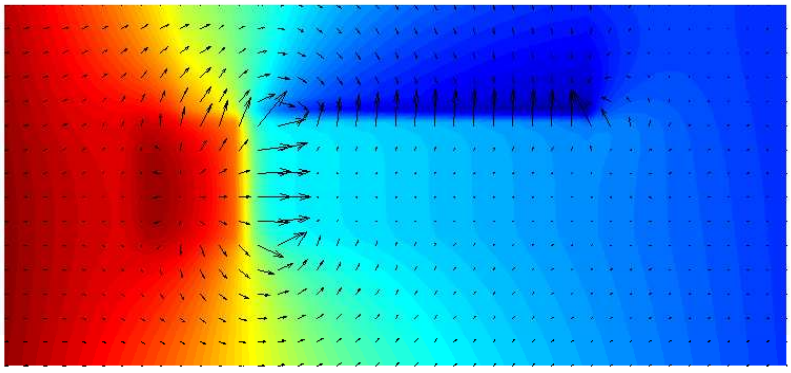

FIGURE 6.28: Electric field and potential distribution right after applied potential has been switched

The only experimental measurement directly showing the movement of lithium ions inside is the video showing the blue coloration of PEDOT. Figures 6.31 to 6.42 compare the simulation lithium movement with experimental results. Following figures show a horizontal cross section of PEDOT (only the side that is receiving lithium)near the electrolyte. The experimental results show the blue coloration of PEDOT after some

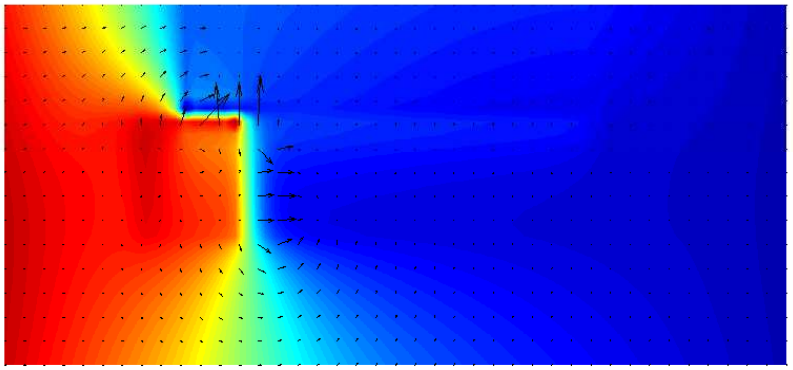

FIGURE 6.29: Electric field and potential distribution before steady state

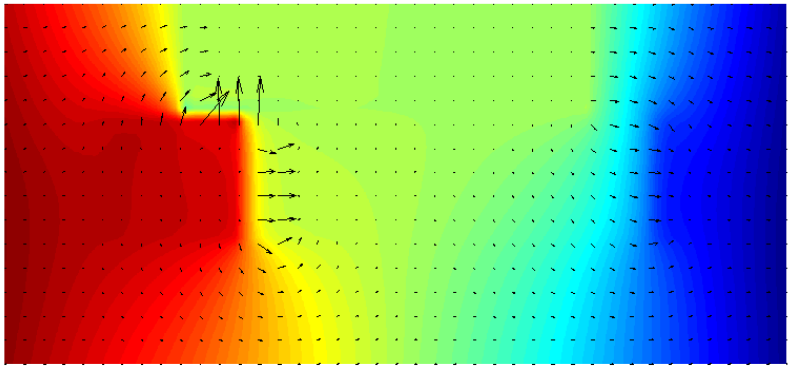

FIGURE 6.30: Electric field and potential distribution at steady state

filtering and image processing. High values in the y axis of signify blue coloration and low values are other colors.

In both experiment and simulation lithium ions start to move in from the notched side. As time progresses lithium ions move toward the contact. There are two effects contributing to this behavior. The electric field is at its highest right around the notch. So this is where the most amount of lithium is pulled into PEDOT. As lithium ions move in vertically, they drift horizontally through PEDOT due to electric field created by the contacts.

When ion movement approaches steady state, in the experiment, we can see that coloration becomes more uniform and stops changing. In the simulation lithium reaches its maximum density and PEDOT stops receiving any additional ions. Overall the behavior seen in this simulation matches the experimental observations quite well.

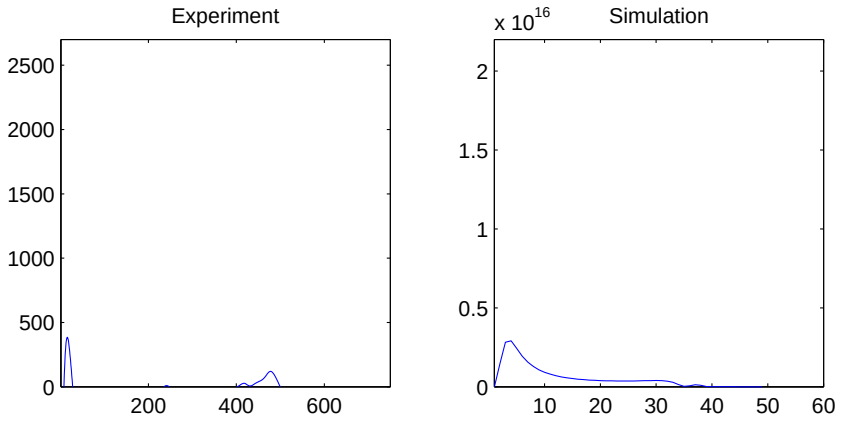

FIGURE 6.31: Movement of lithium ions into PEDOT

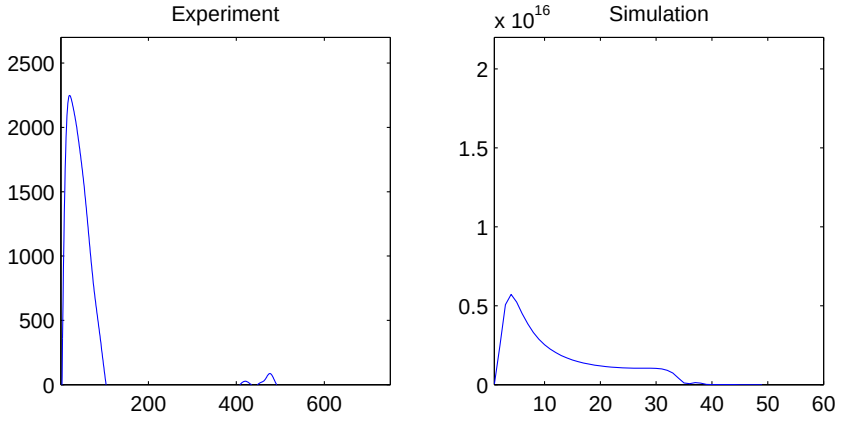

FIGURE 6.32: Movement of lithium ions into PEDOT

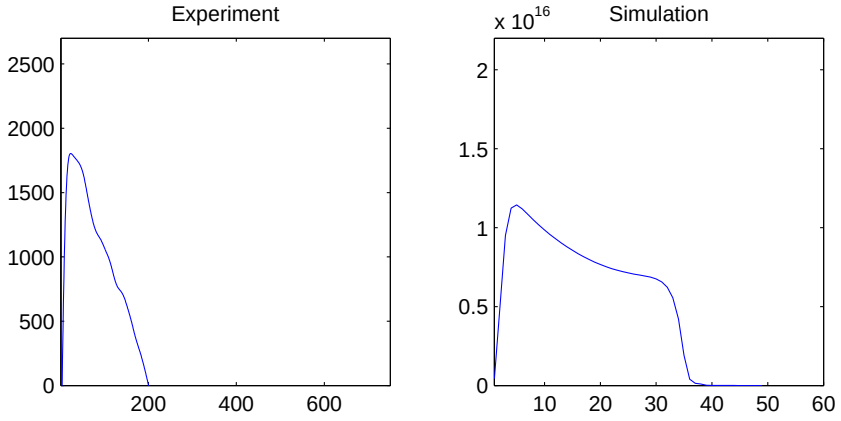

FIGURE 6.33: Movement of lithium ions into PEDOT

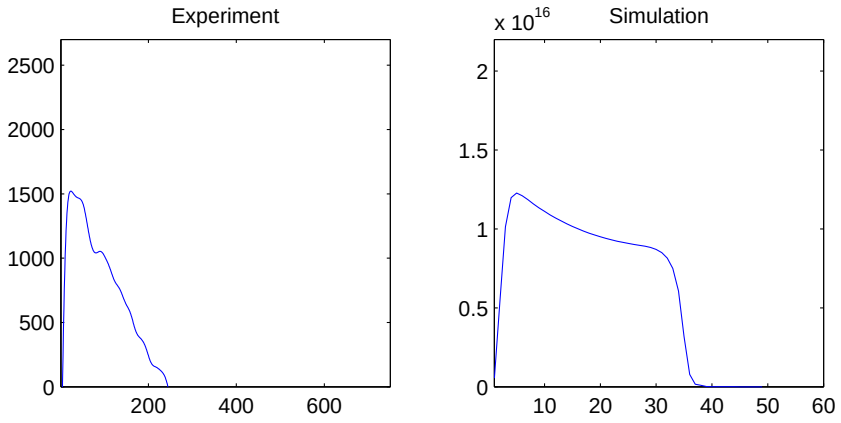

FIGURE 6.34: Movement of lithium ions into PEDOT

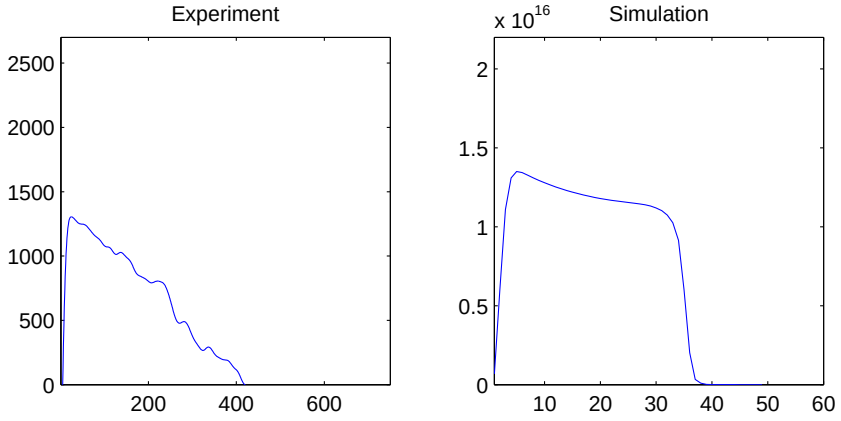

FIGURE 6.35: Movement of lithium ions into PEDOT

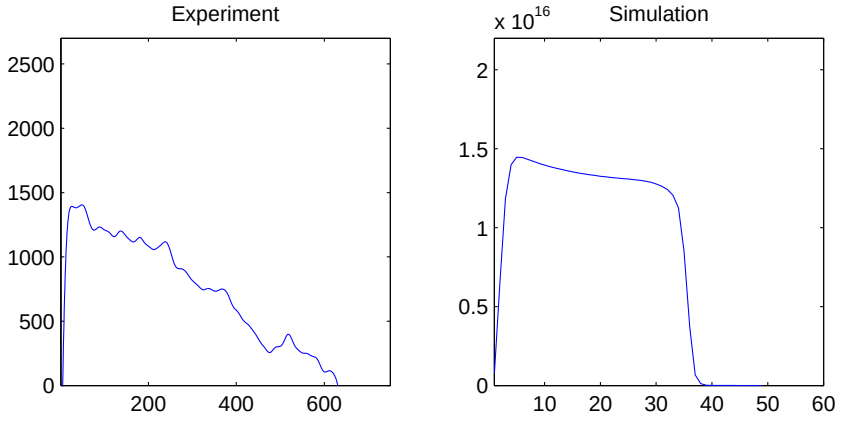

FIGURE 6.36: Movement of lithium ions into PEDOT

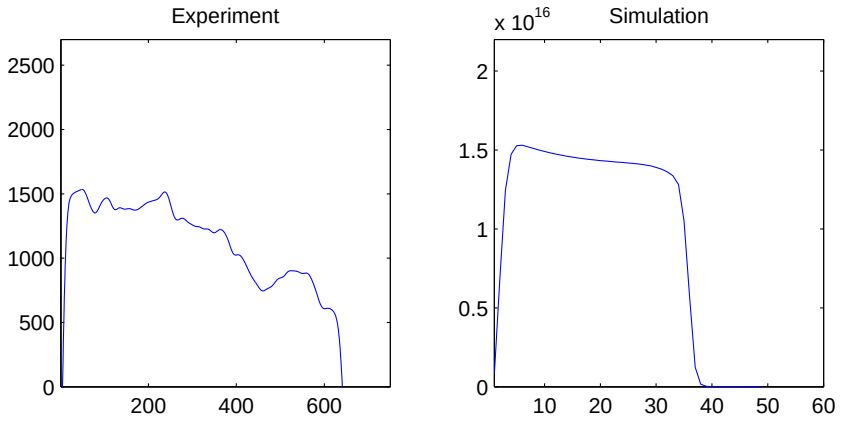

FIGURE 6.37: Movement of lithium ions into PEDOT

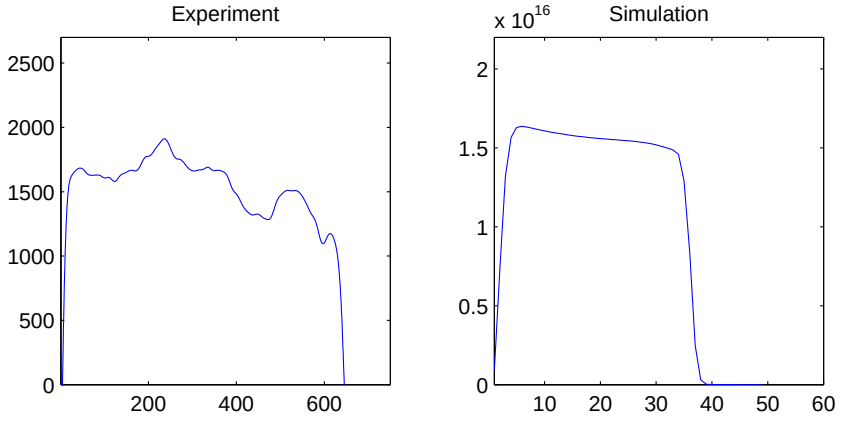

FIGURE 6.38: Movement of lithium ions into PEDOT

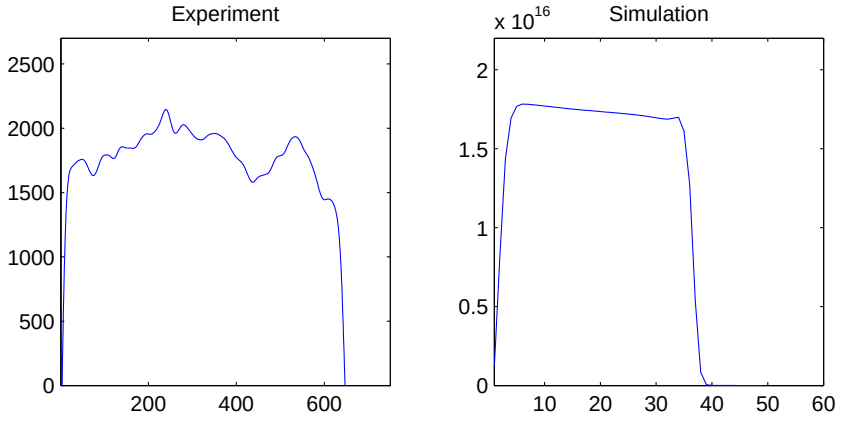

FIGURE 6.39: Movement of lithium ions into PEDOT

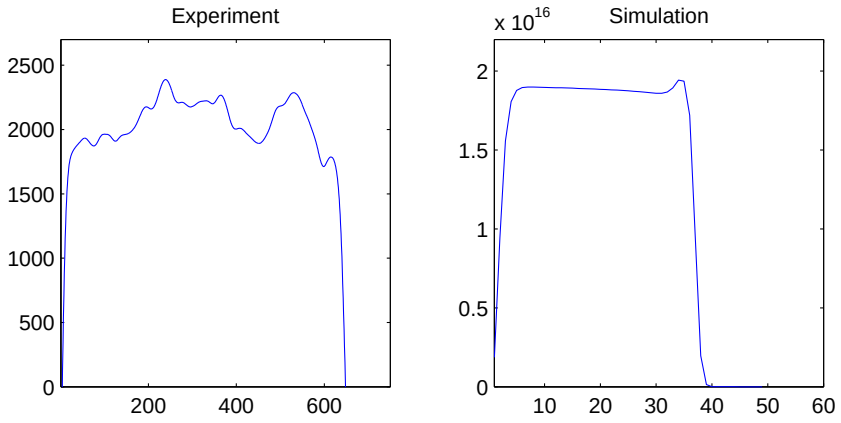

FIGURE 6.40: Movement of lithium ions into PEDOT

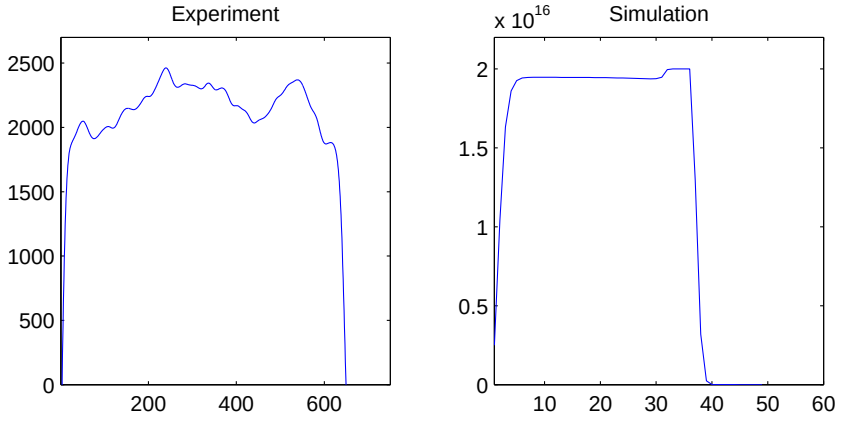

FIGURE 6.41: Movement of lithium ions into PEDOT

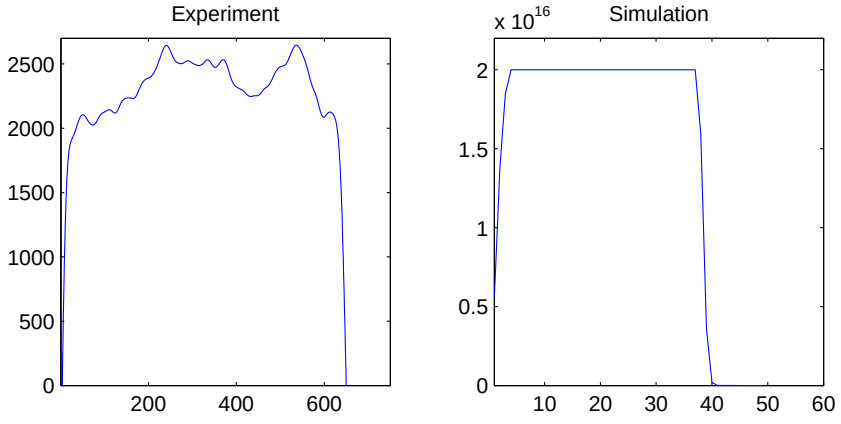

FIGURE 6.42: Movement of lithium ions into PEDOT

Chapter 7

Conclusion

The purpose of this thesis was to create a memristor model for computer simulation. We were able to model the change in conductivity through the movement of lithium and undoping of PEDOT. The transient simulation results match experimental data visually for both single channel and notched memristor. Although our simulation matched with the experimental data this model requires more work and can be improved through better numerical schemes, physical models and thorough experimentation. There are also few limitations of this model due to its size and physical features.

In terms of numerical methods there are a few down sides of using finite difference. The simulation for this device was done in 2-D instead of 3-D. This did not cause a lot of problems in our case since the structures we used were quite simple and produced reasonable results in 2-D. Unfortunately getting a transient response for devices using finite difference is computationally expensive. Even though we had a 100x100 grid, which is quite coarse, the simulation time was not less than 3 hours on a computer with multiple cores. Addition of another 100 points for a third dimension will make this simulation at least a 100 times longer. This makes 3-D simulations impractically long and very hard to test and optimize.

Another fundamental issue with this simulation arises from debye length. Maximum grid size in finite difference depends on the debye length, which is at least 5 or 6 orders of magnitude smaller than the device size. This means that we need at least 10^5 points in each direction in order to simulate this device. At this point the simulation becomes impossibly long so we had to compromise by either reducing the device size or carrier density.

The model we have developed is quite open for improvements on carrier transport models. A constant bulk mobility was used for holes in this model which is not the case in

an actual device. Holes move from site to site via hopping. Addition of lithium into PEDOT not only reduces the number of available holes but also decreases the number of possible sites through holes can move. A variable range hopping mechanism and thermal effects can be added into this model for a more complete simulation. Also PEDOT:PSS is a disordered material and the way it was deposited on a substrate can make a big difference on hole movement. Anisotropic hole mobilty can be implemented in order to account for this issue.

Overall we have showed that it is possible to simulate a memristor using a simple finite difference method which can be very useful model in understanding the way ions and holes move in PEDOT. Our results show a very promising start for a vast research and development opportunities on memristor and polymer conductors.

Appendix A

1-D Memristor Simulations

A.1 1-D Memristor (Cross section 2)

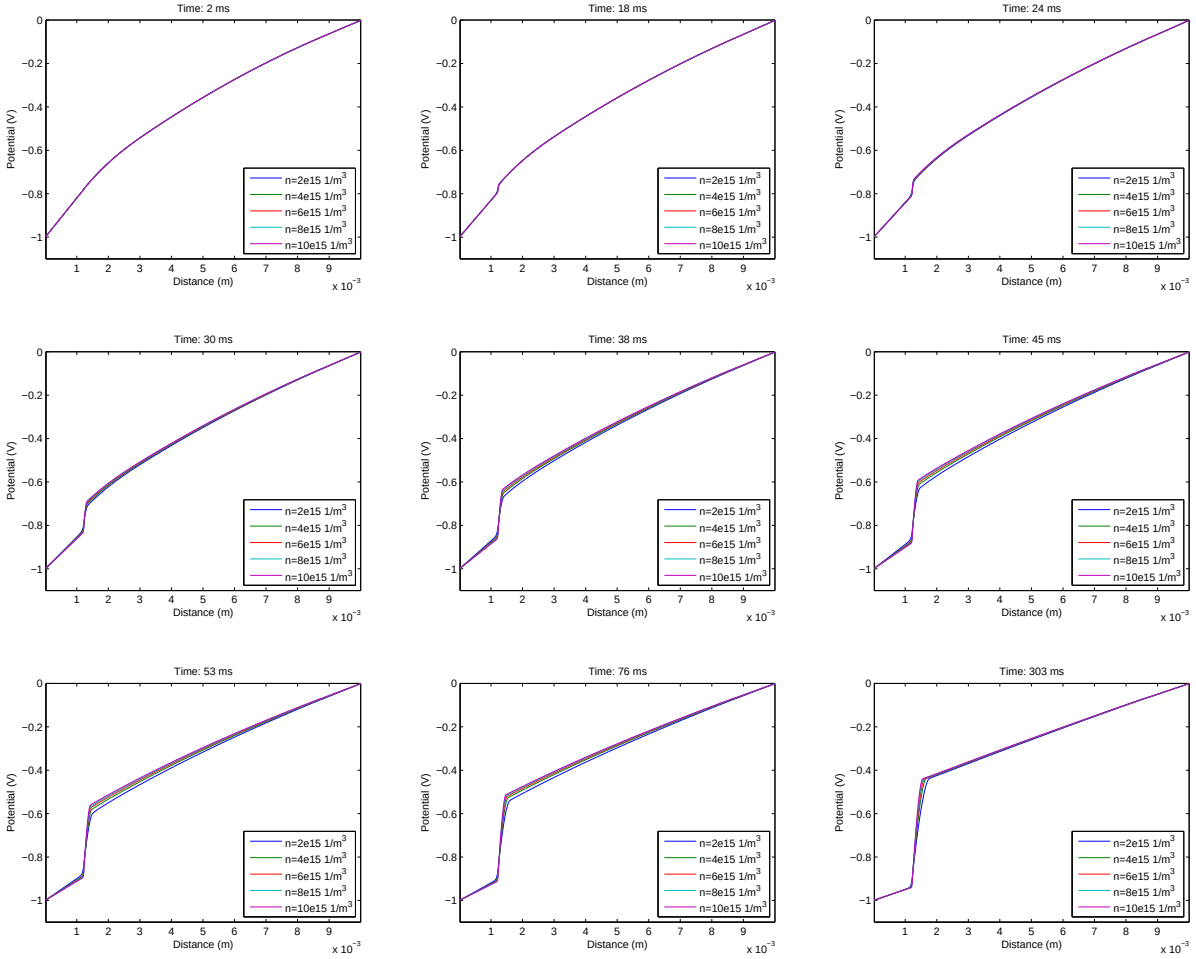

FIGURE A.1: 1-D Memristor potential distribution over time

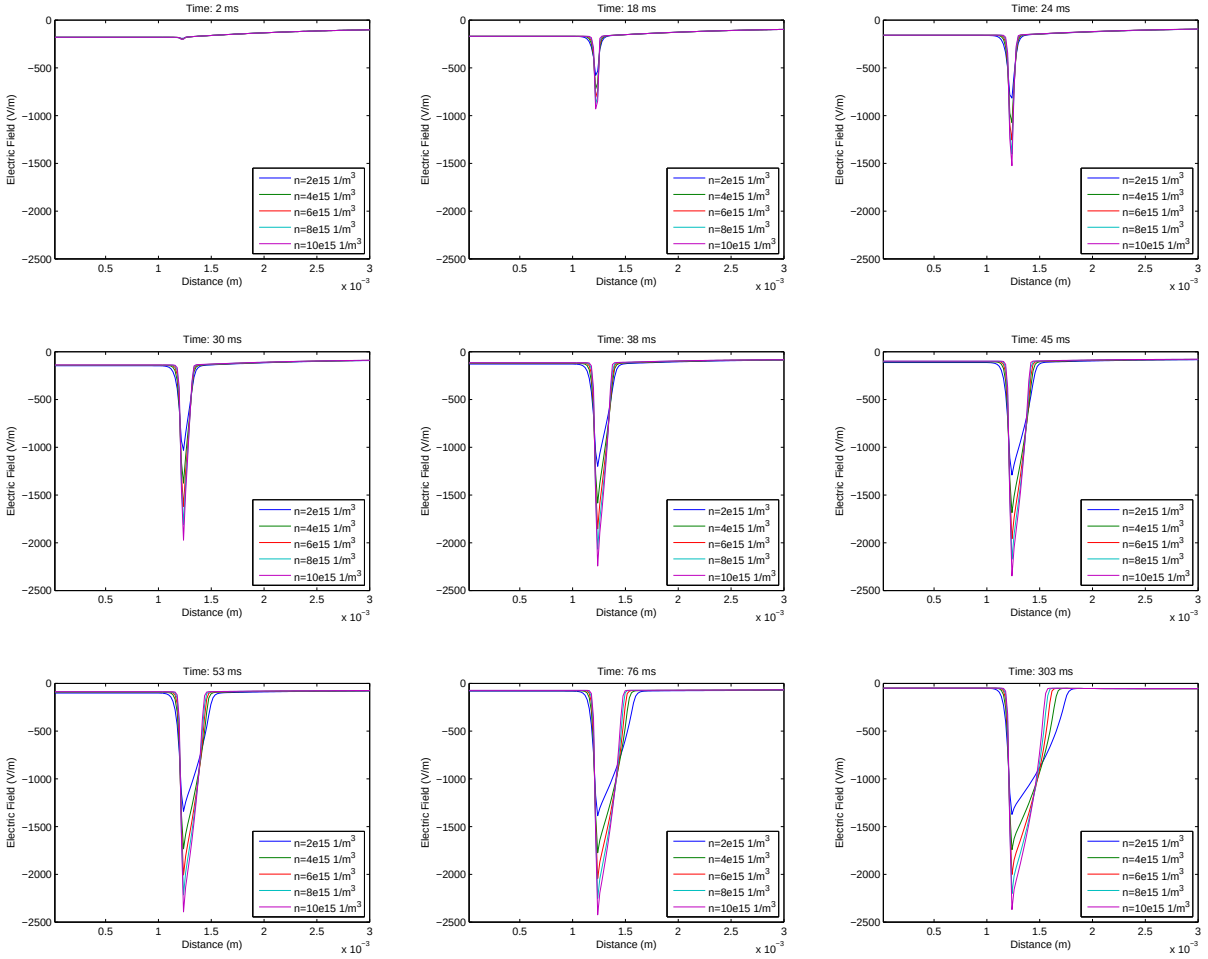

FIGURE A.2: Electric field distribution over time (Note:Not aligned with potential distribution for better visuals)

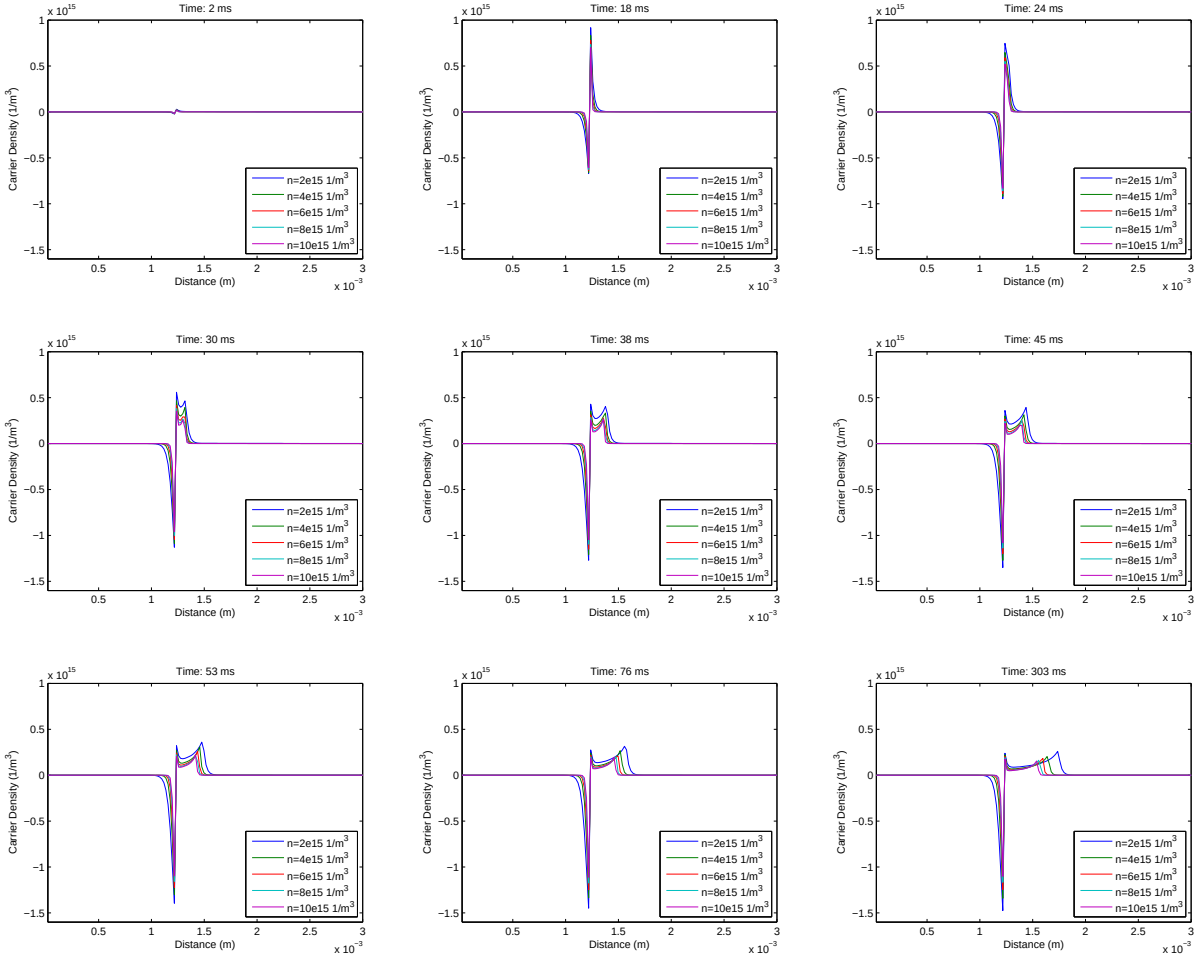

FIGURE A.3: Normalized net charge density distribution over time (Note:Not aligned with potential distribution for better visuals)

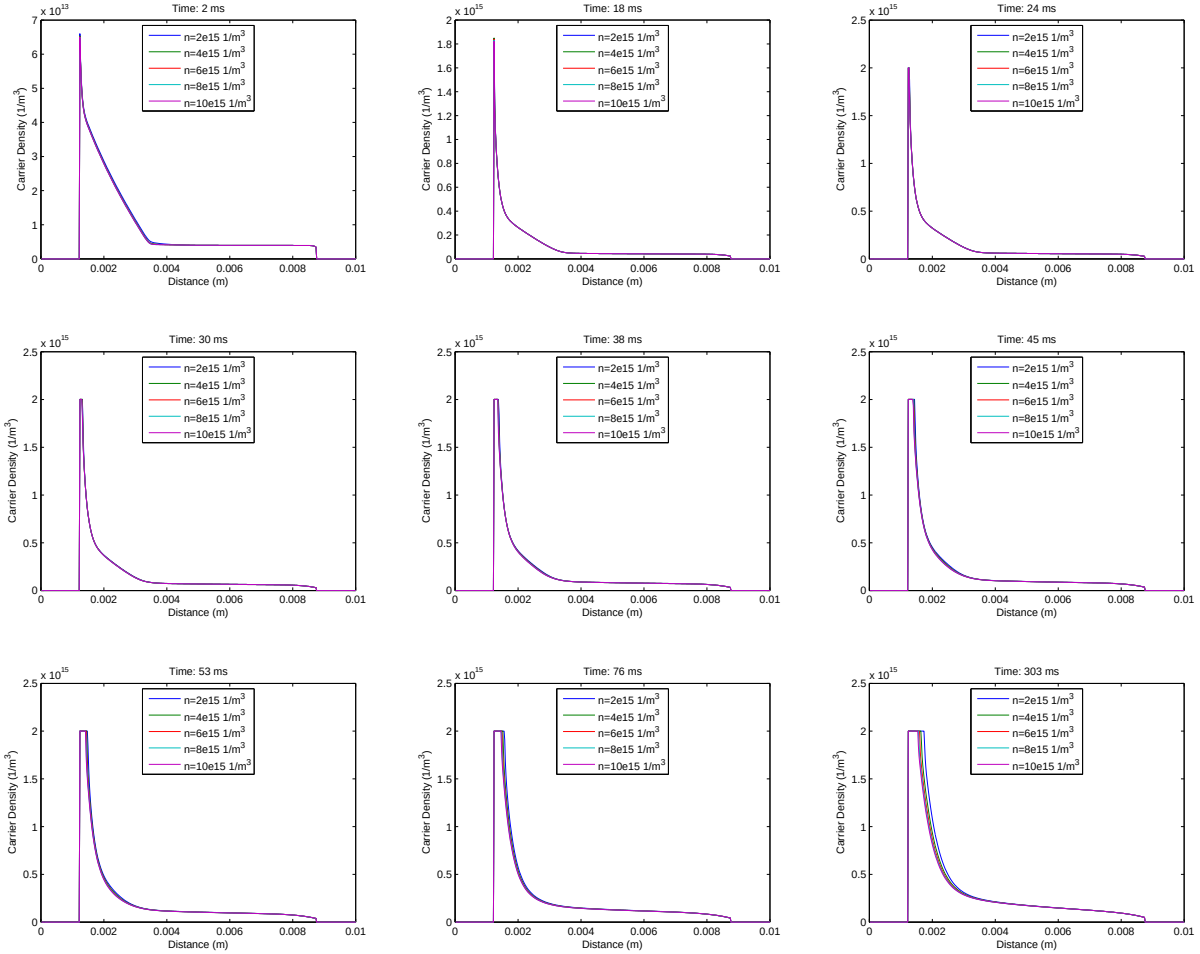

FIGURE A.4: Normalized lithium density distribution over time

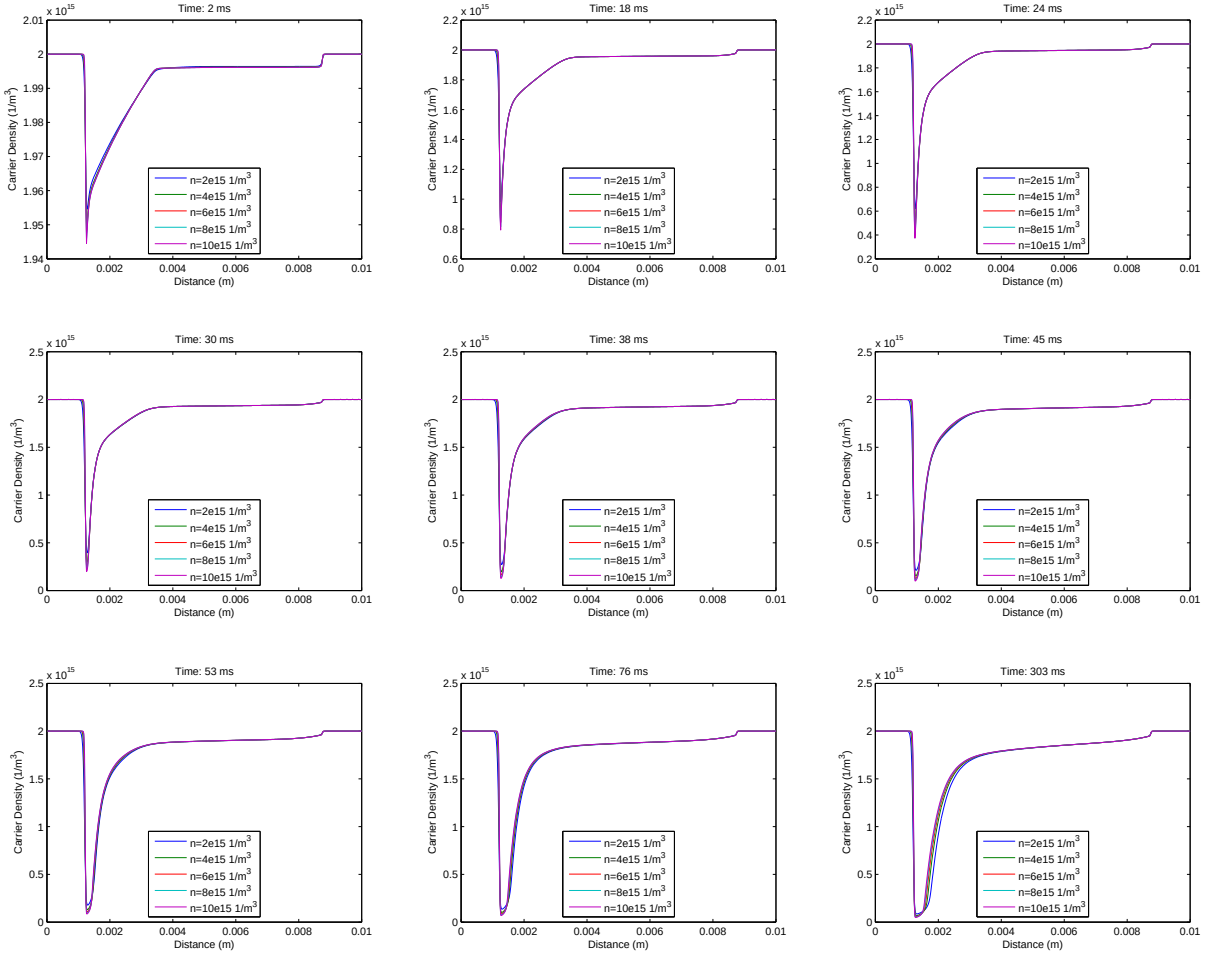

FIGURE A.5: Normalized hole density distribution over time

A.2 1-D Memristor with Notch (Cross section 2)

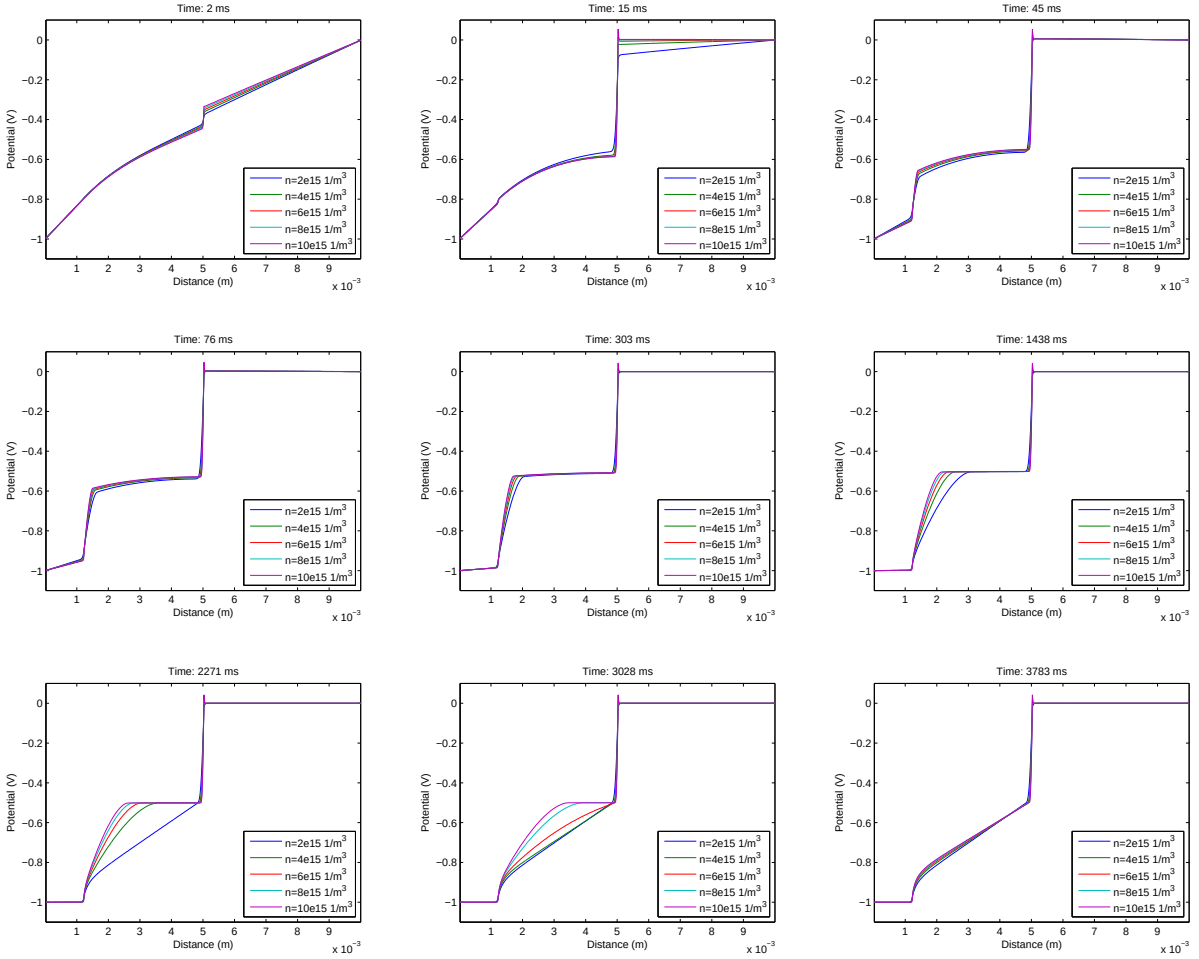

FIGURE A.6: Notched memristor potential distribution over time

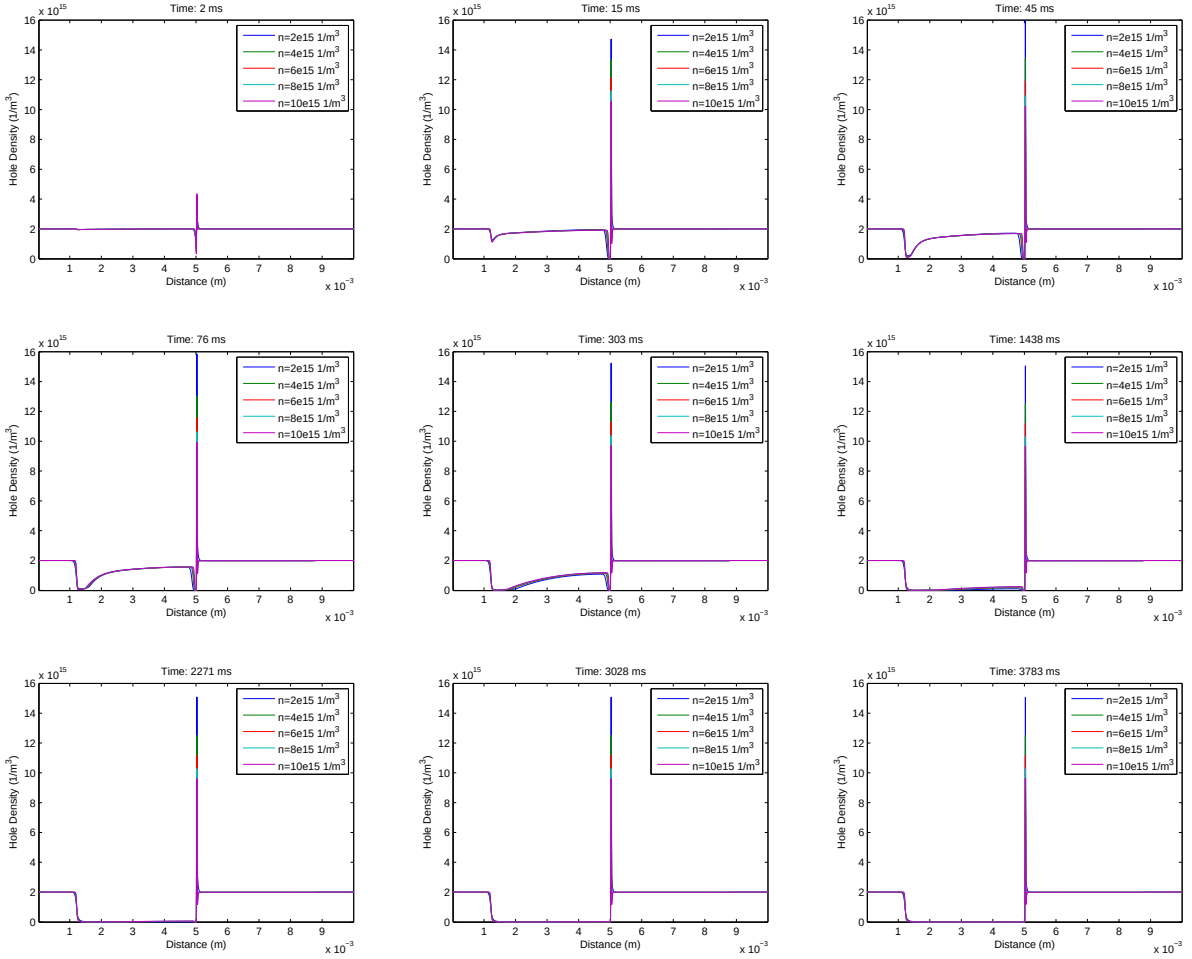

FIGURE A.7: Normalized hole distribution over time

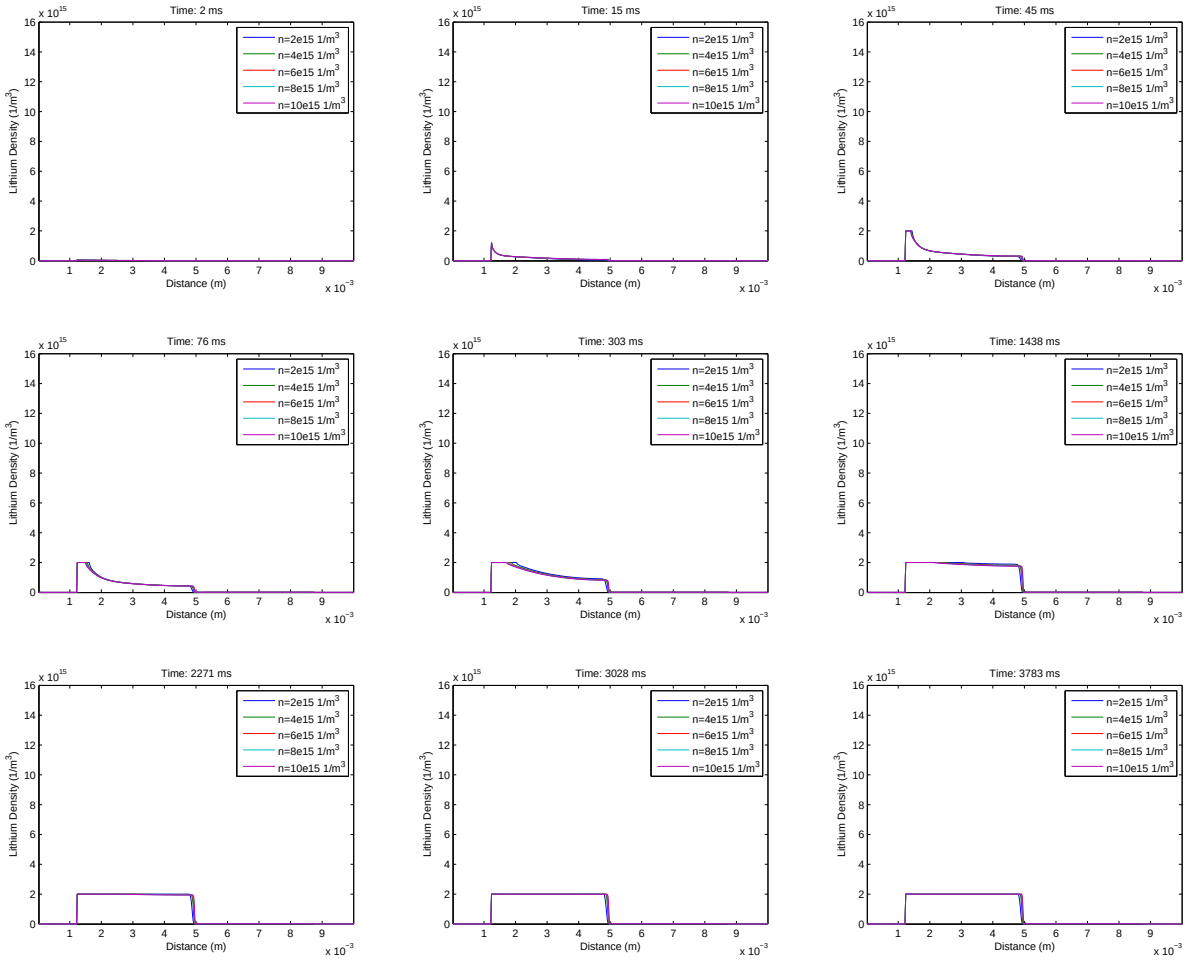

FIGURE A.8: Normalized lithium distribution over time

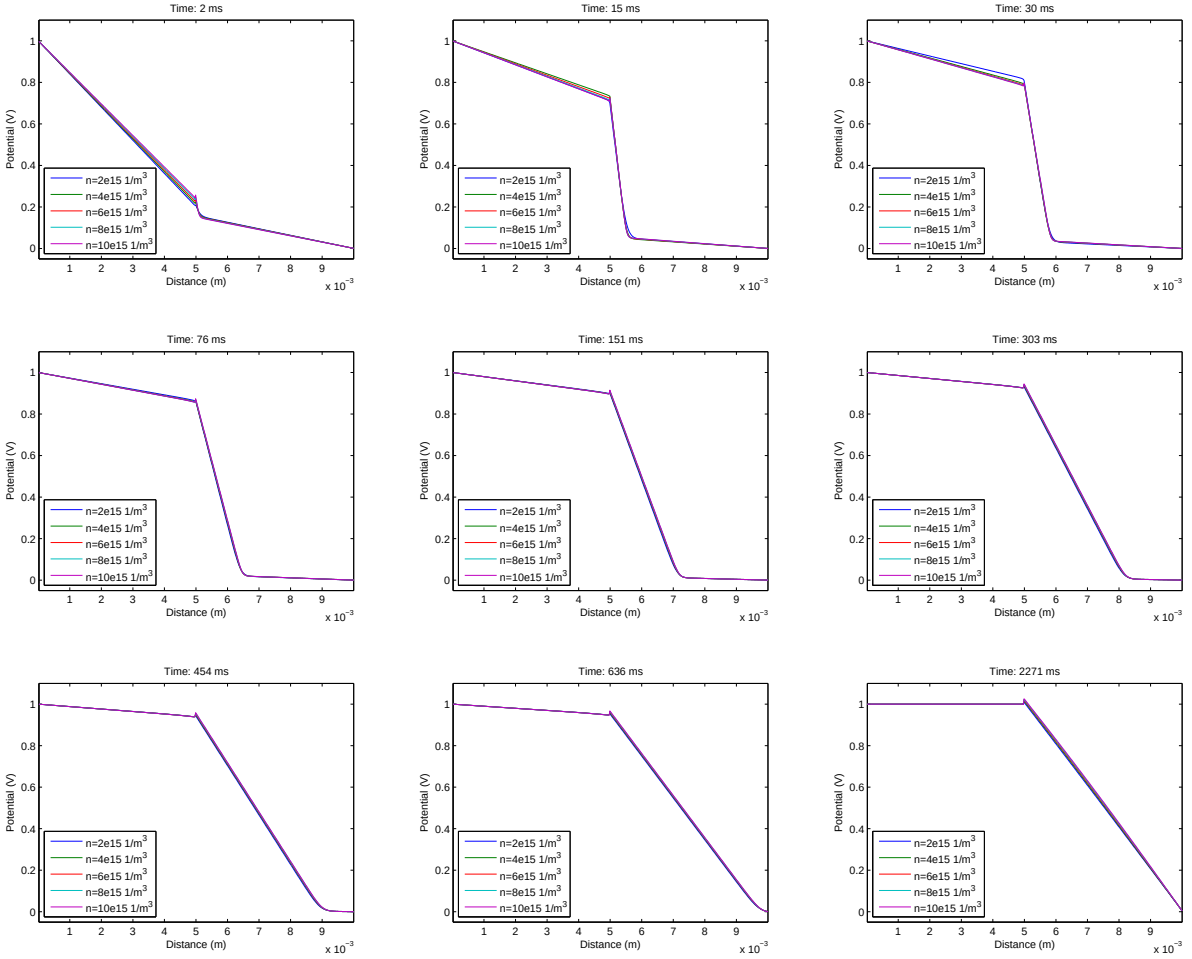

FIGURE A.9: Electrolyte/PEDOT interface potential distribution over time

A.3 Electrolyte/PEDOT Interface

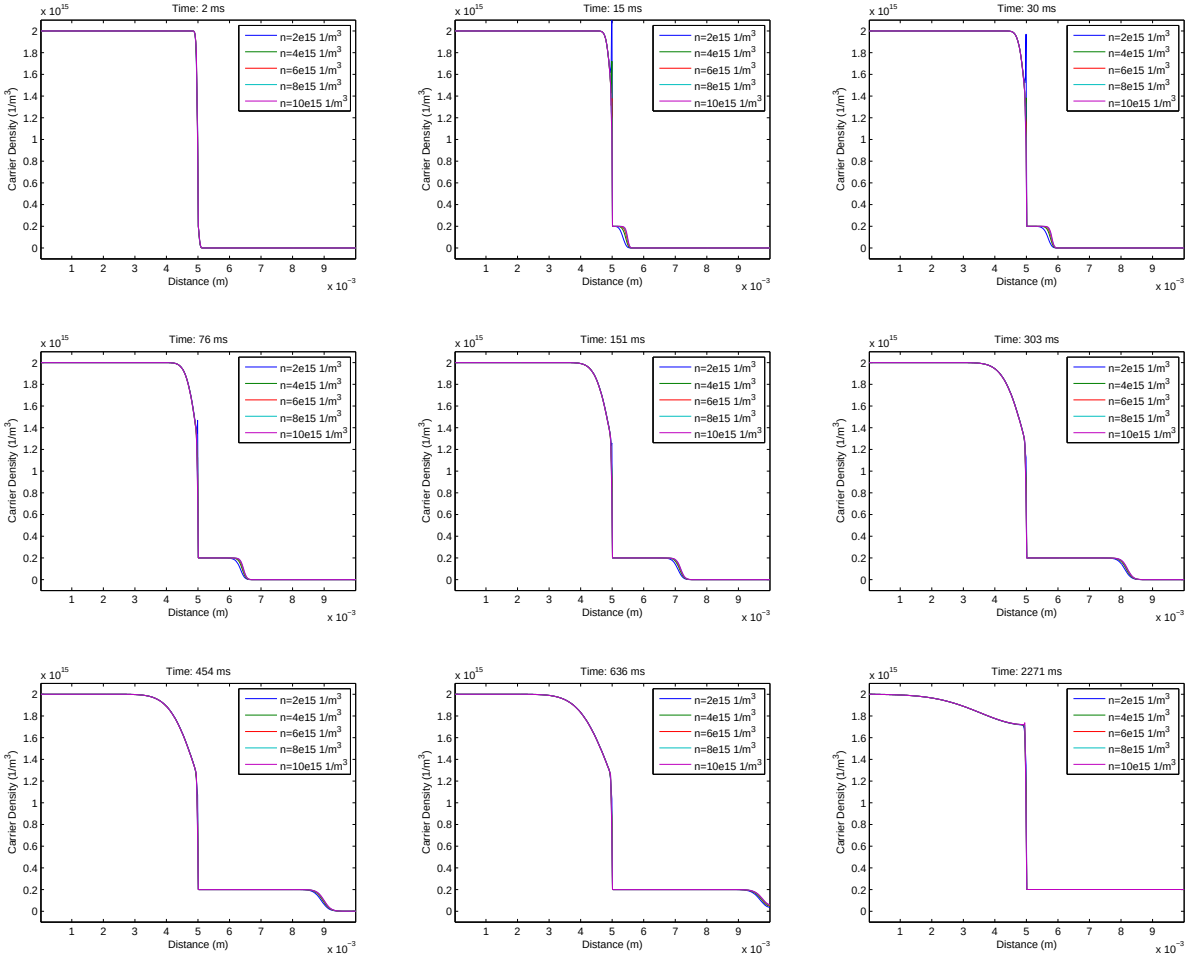

FIGURE A.10: Normalized lithium distribution over time

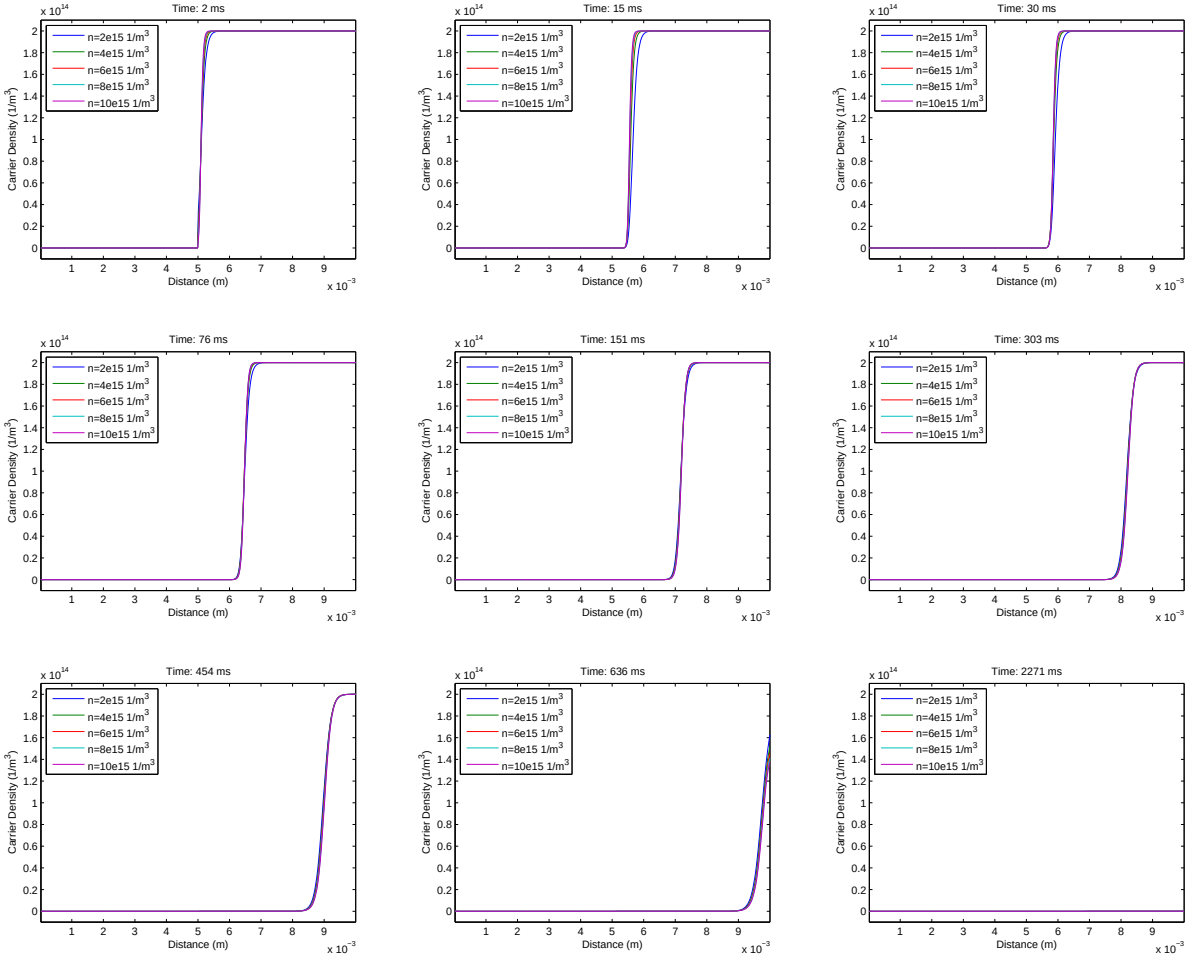

FIGURE A.11: Normalized hole distribution over time

Appendix B

Single Channel PEDOT Lithium and Hole Density

Appendix C

Title 3

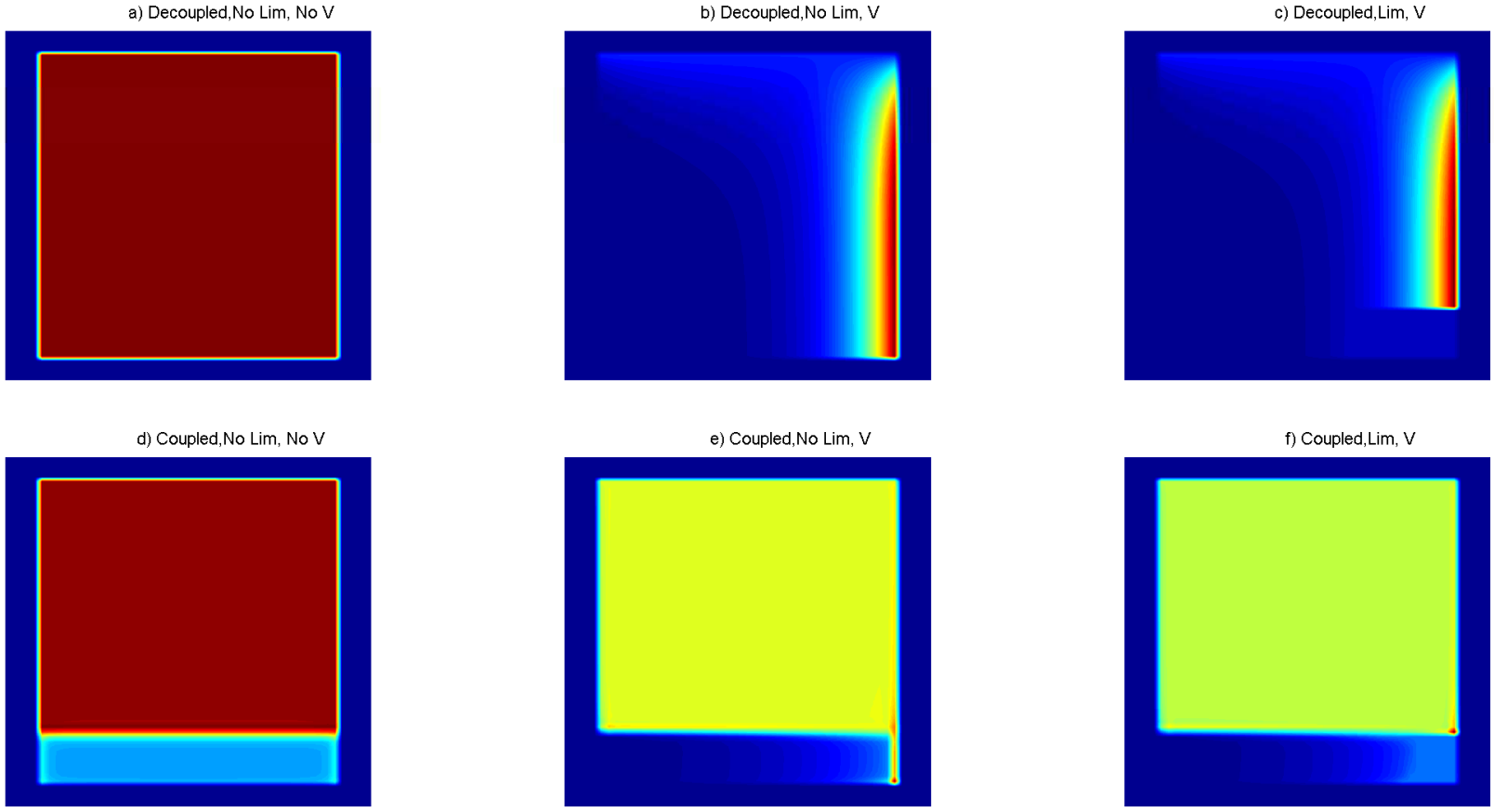

FIGURE C.1: Lithium Density in Steady State

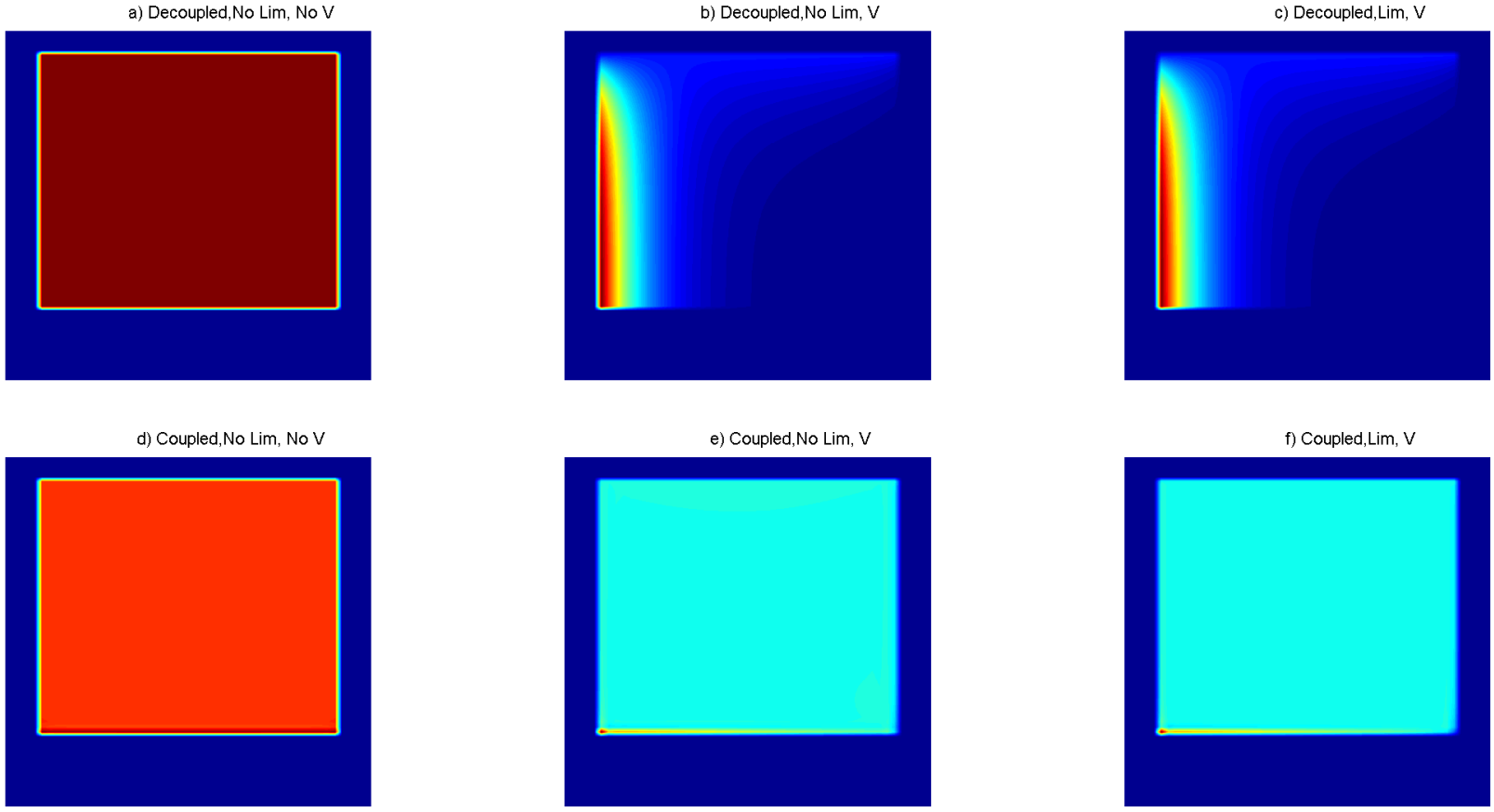

FIGURE C.2: Cadmium Density in Steady State

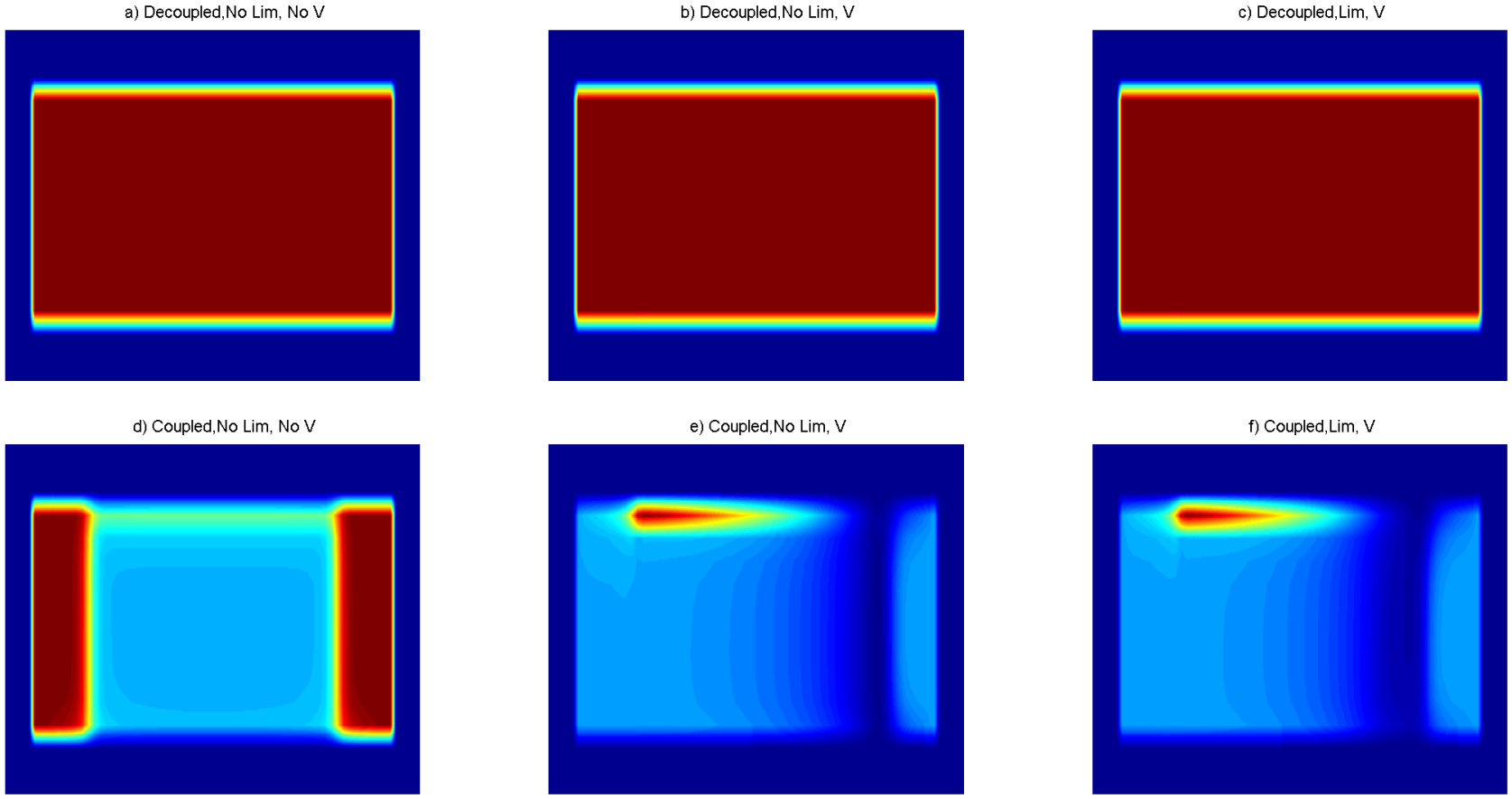

FIGURE C.3: Hole Density in Steady State

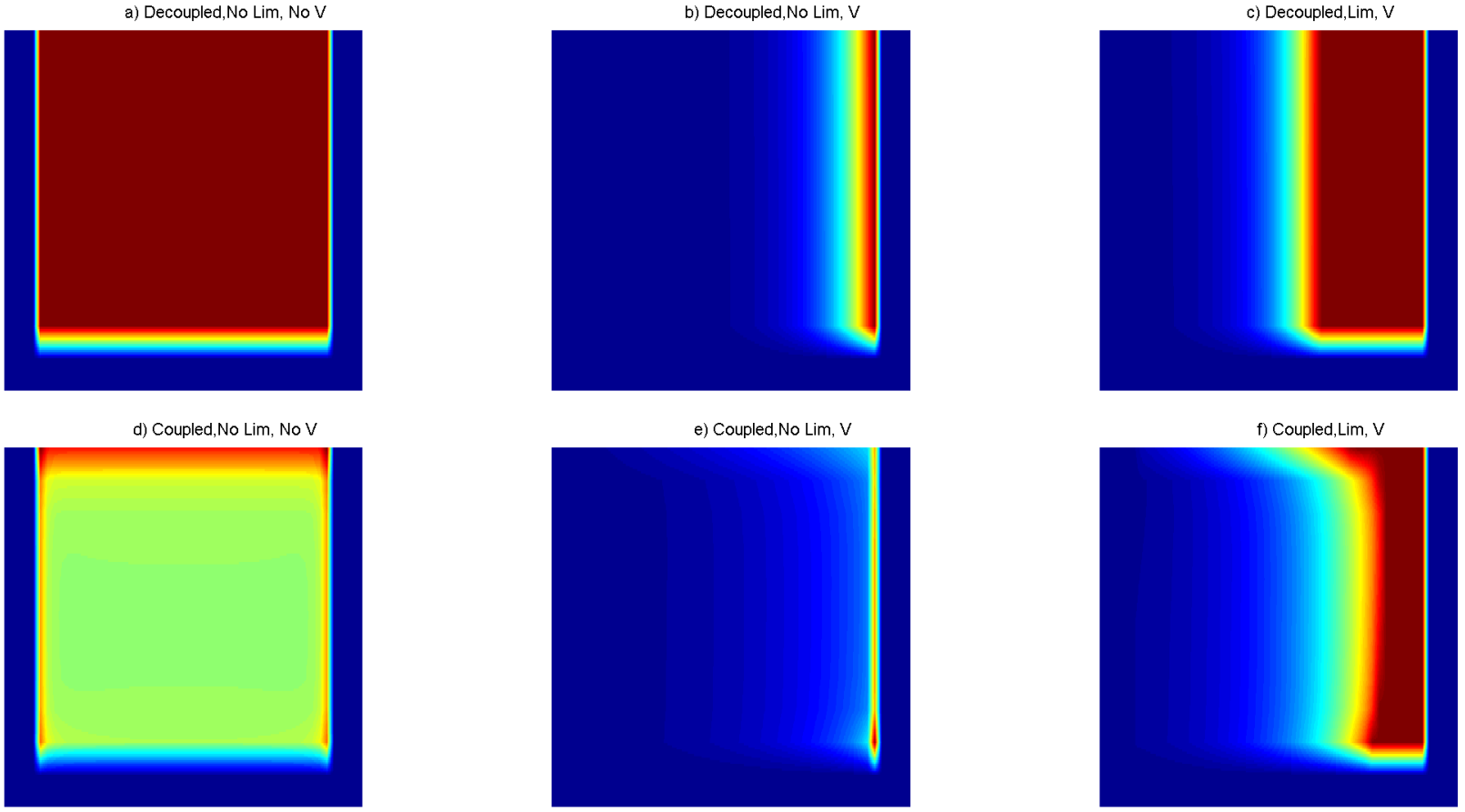

FIGURE C.4: 2d Lithium Steady State PEDOT

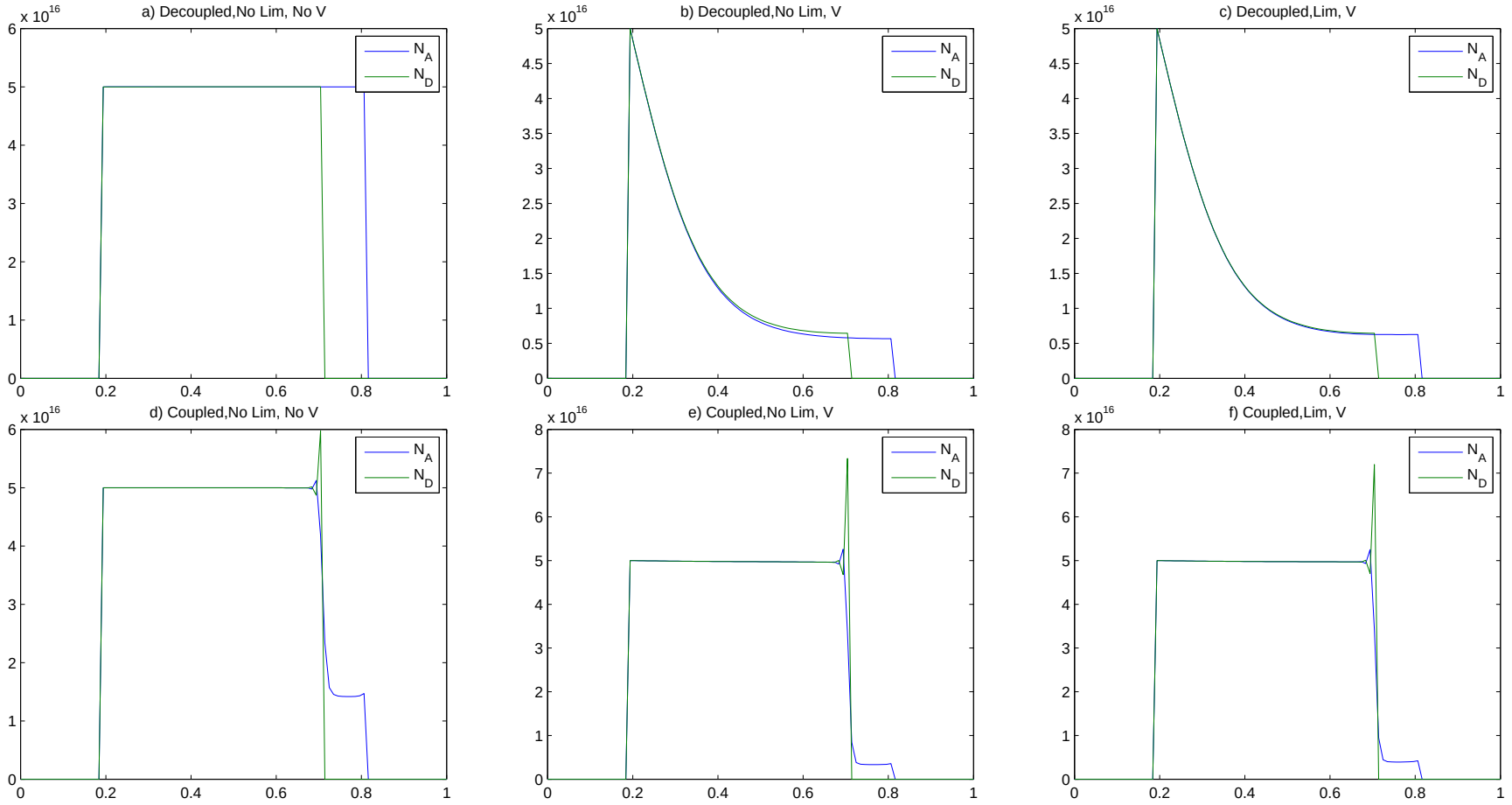

FIGURE C.5: 1D Nn Lithium Vertical

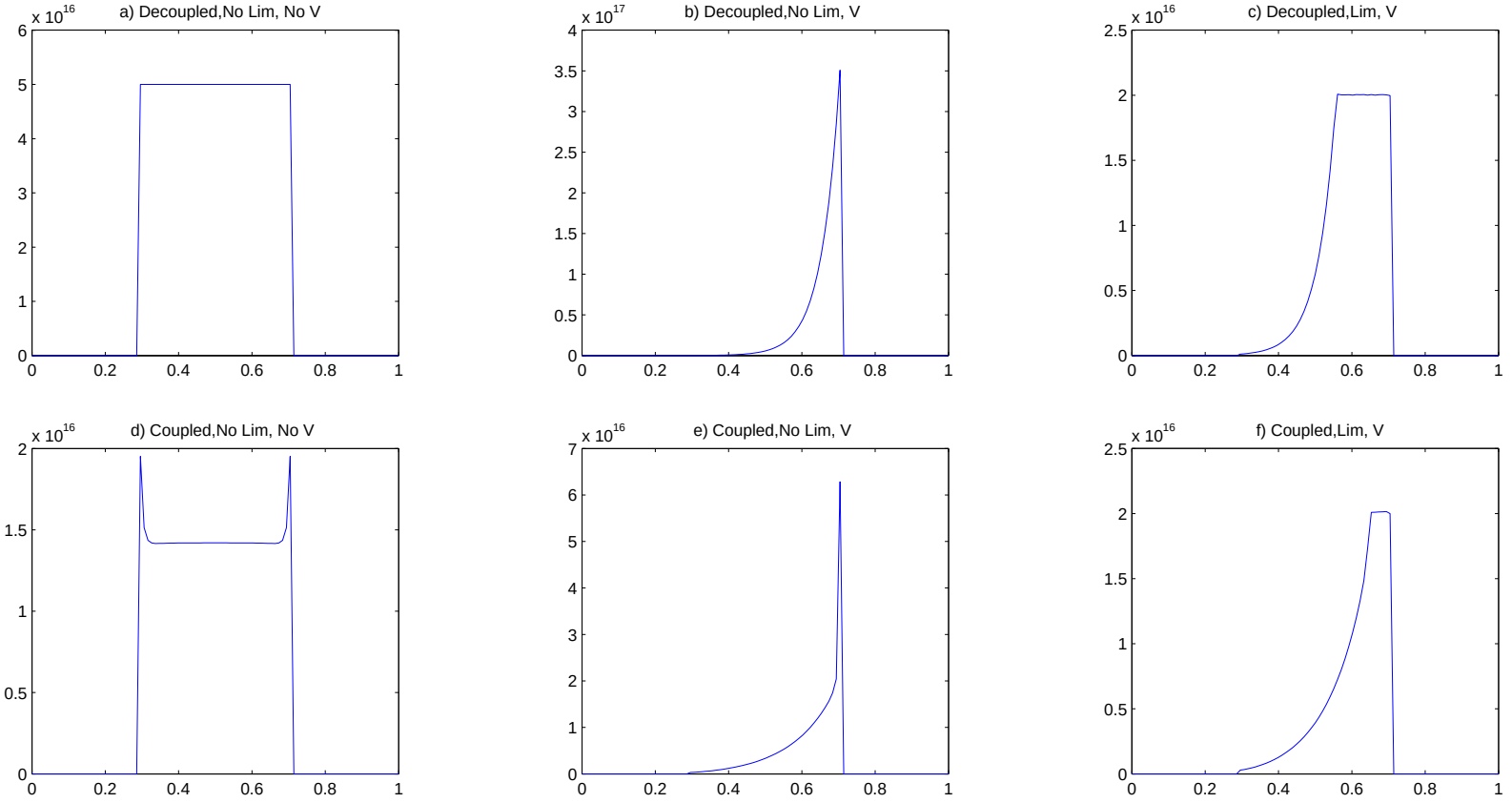

FIGURE C.6: 1d Lithium Horizontal

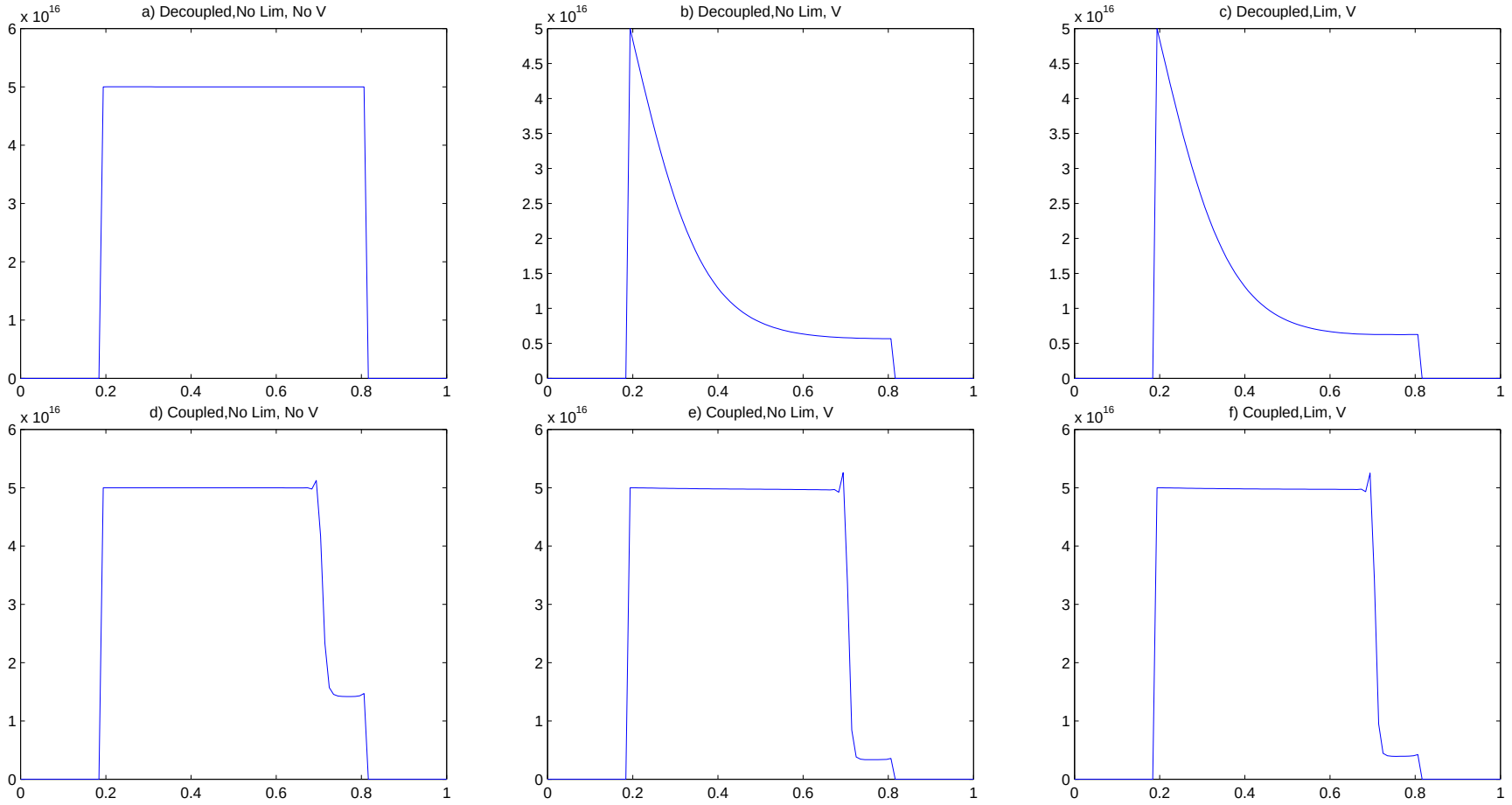

FIGURE C.7: 1d Lithium Vertical

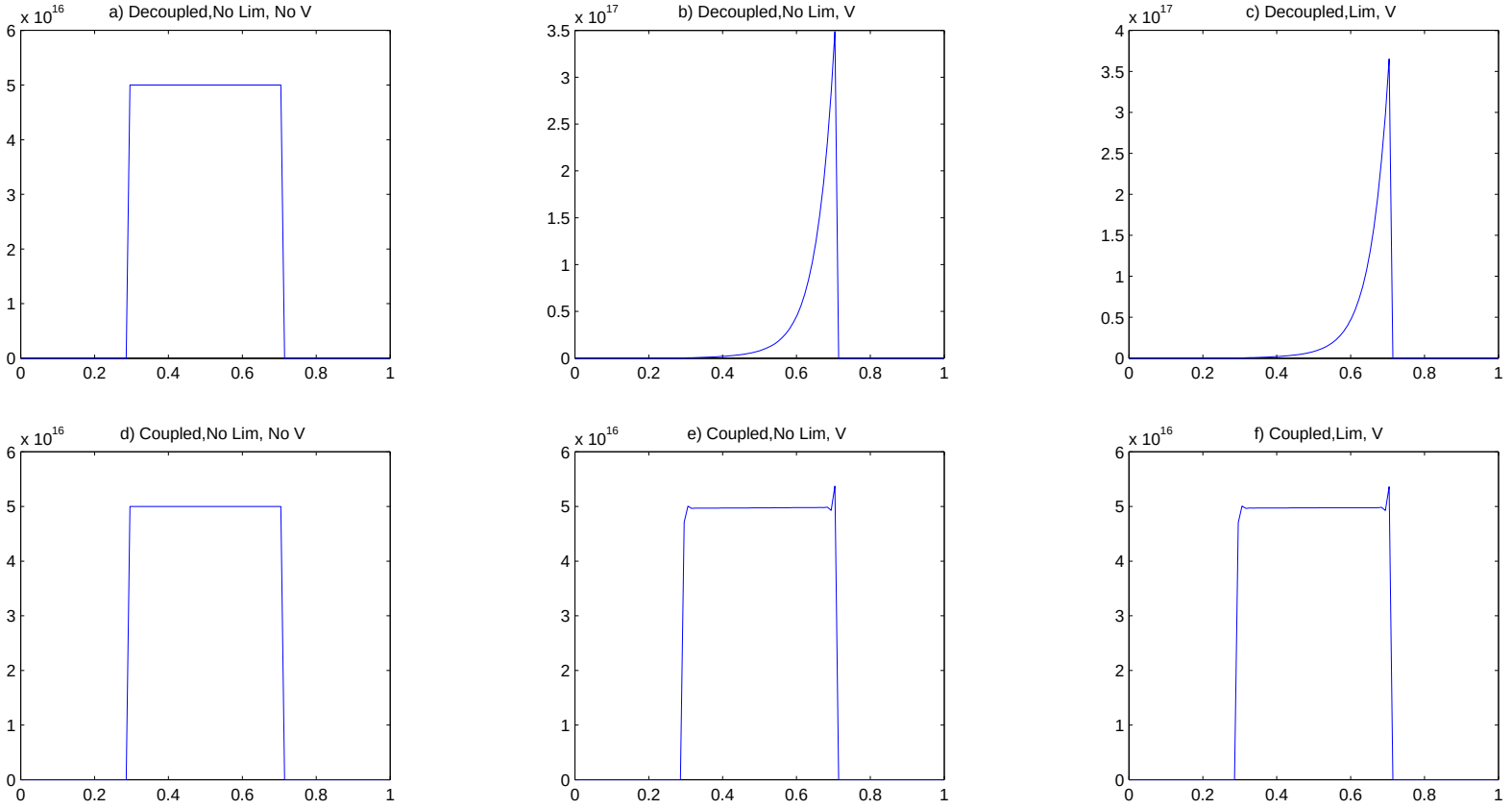

FIGURE C.8: 1D Nn Horizontal

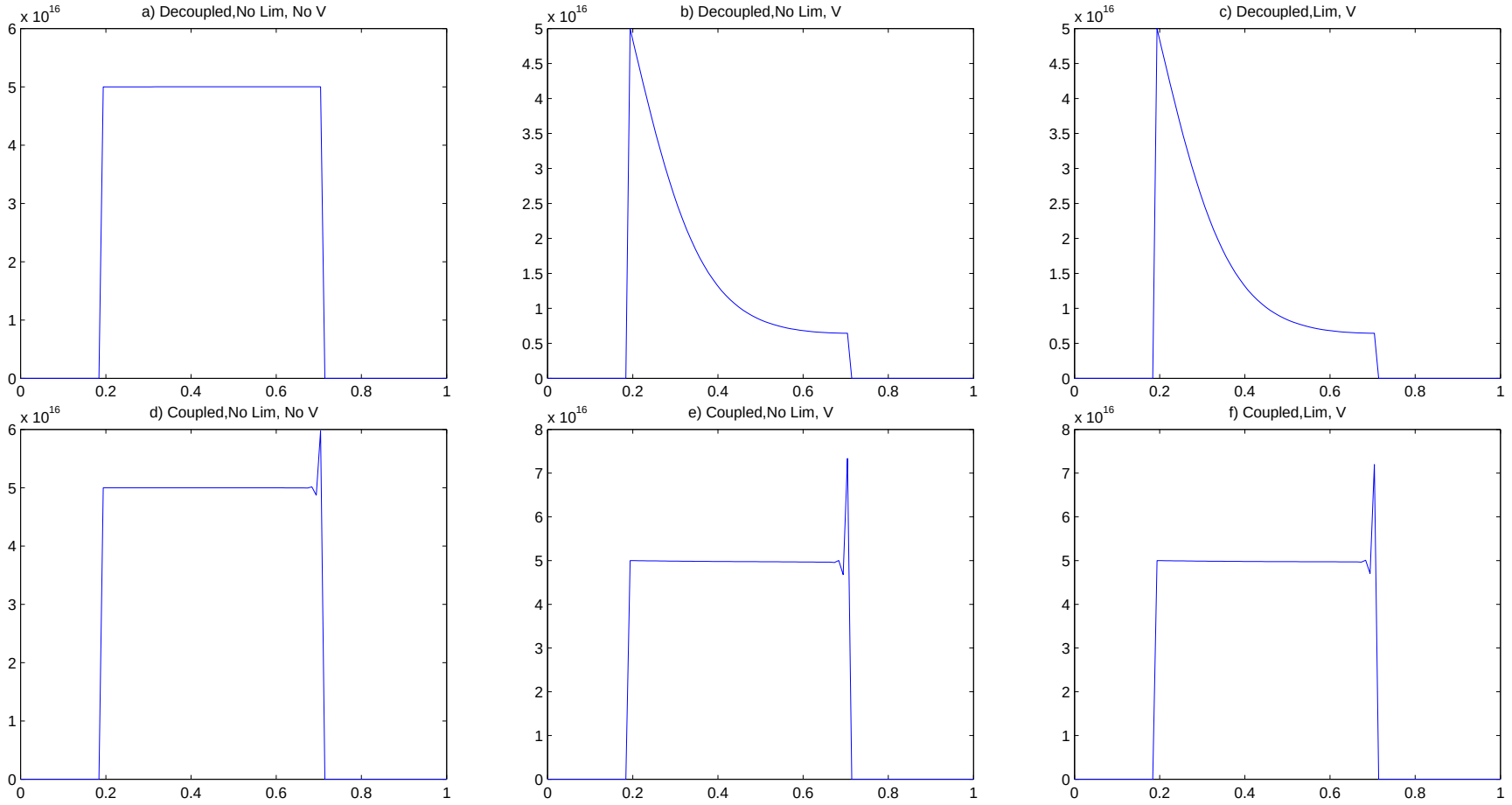

FIGURE C.9: 1D Nn Vertical

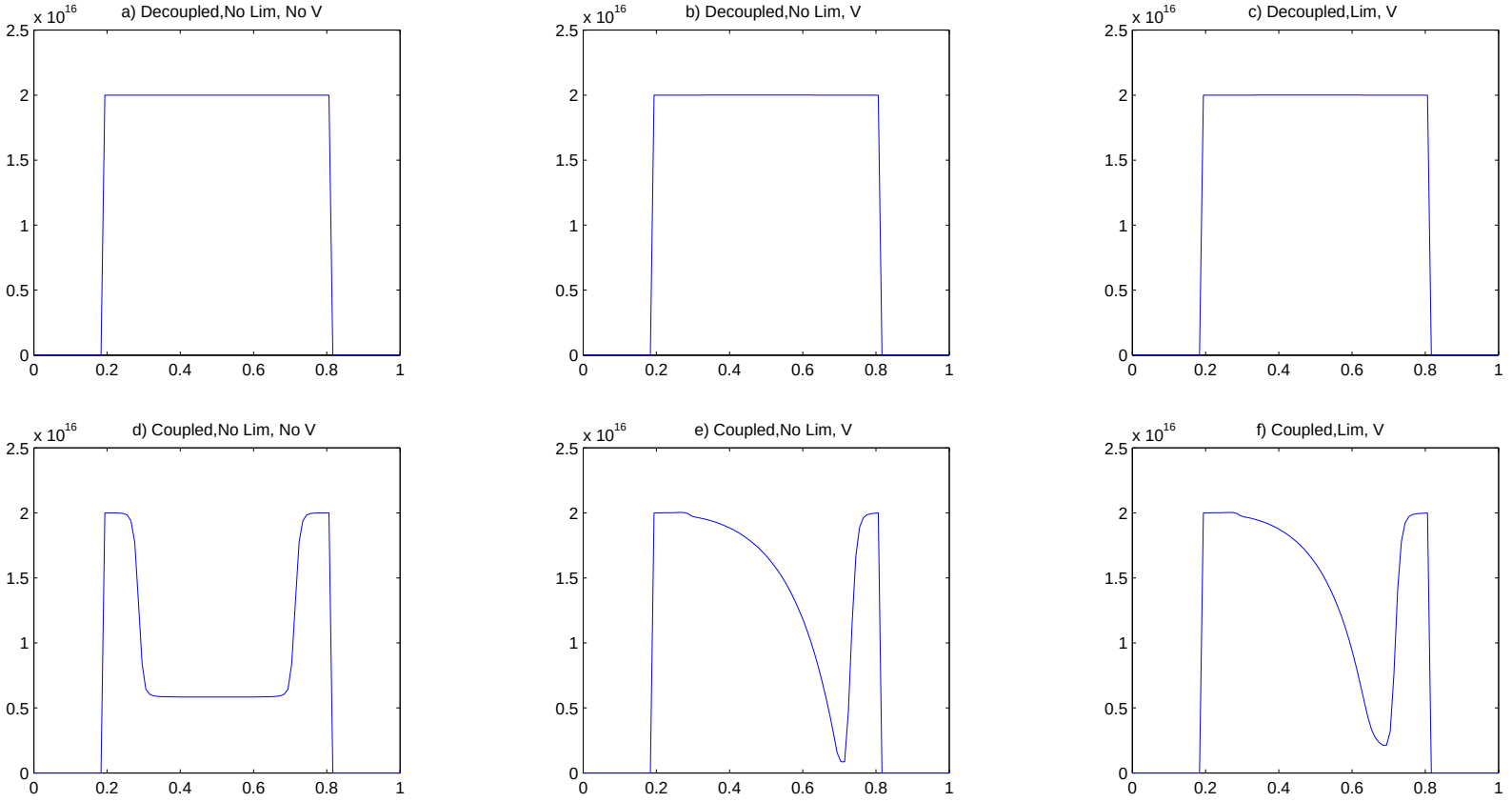

FIGURE C.10: 1-D Holes Vertical

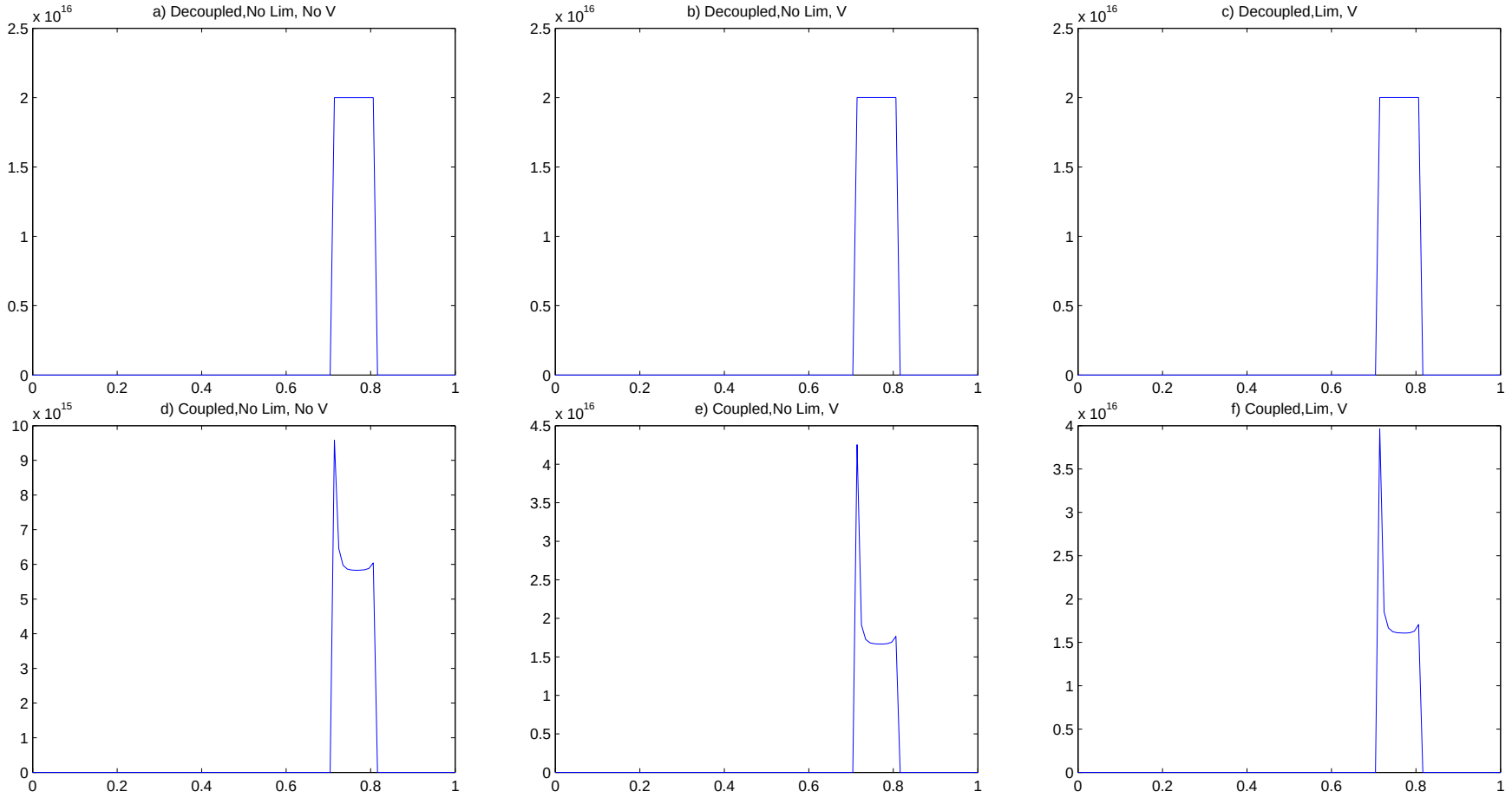

FIGURE C.11: 1 D Holes Horizontal

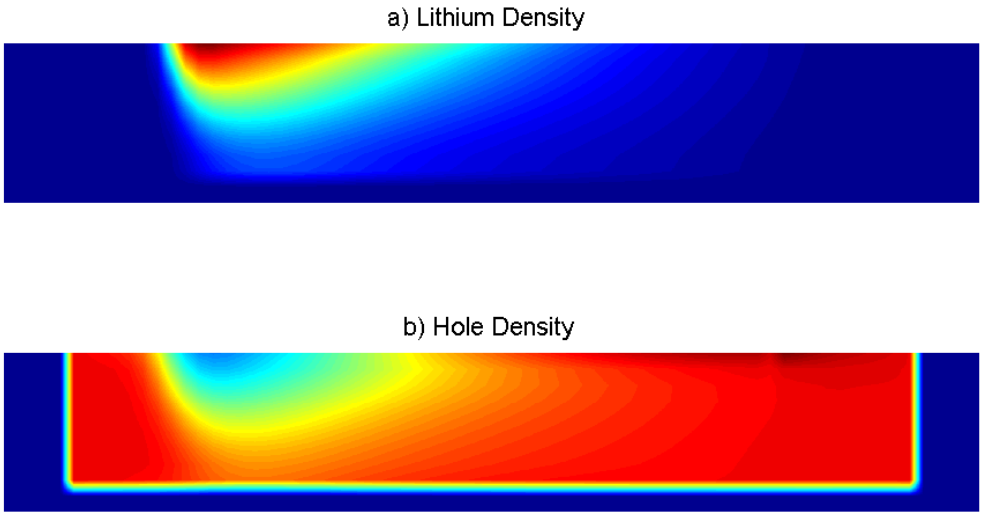

FIGURE C.12

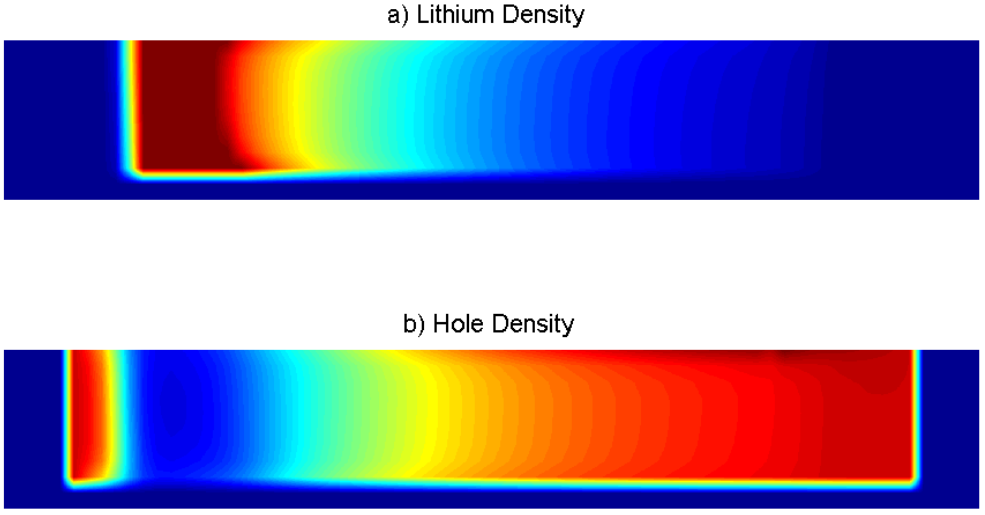

FIGURE C.13

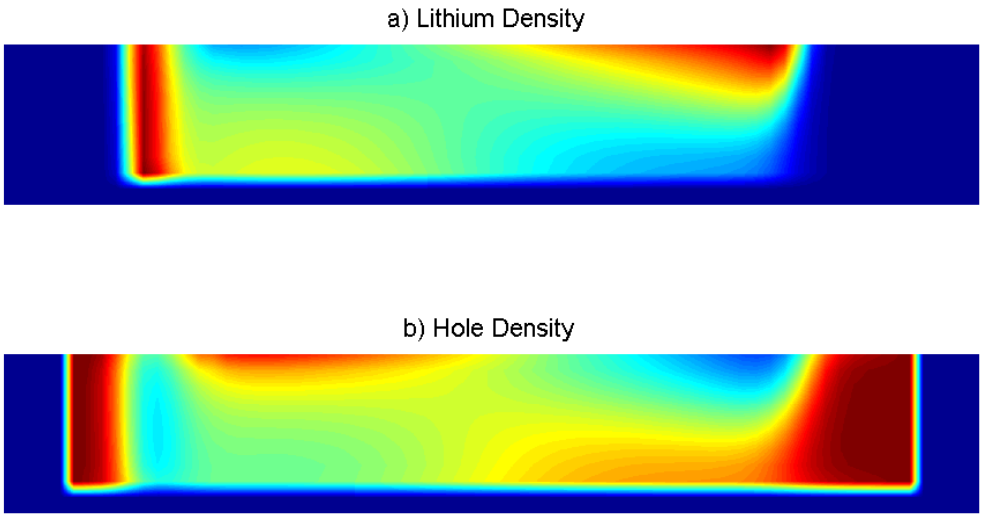

FIGURE C.14

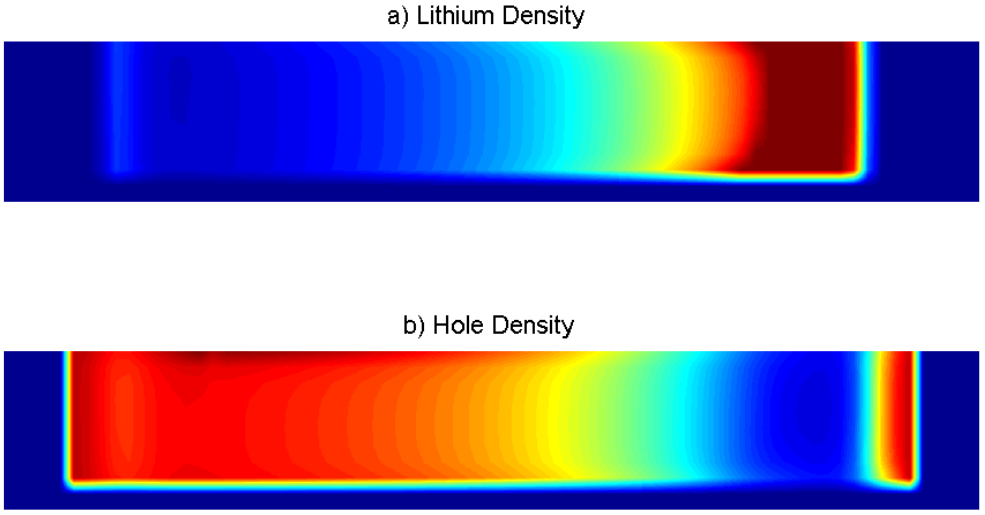

FIGURE C.15

Bibliography

[1] L.O. Chua. Memristor-the missing circuit element. *Circuit Theory, IEEE Transactions on*, 18(5):507–519, 1971. ISSN 0018-9324.

[2] Stephen M. Goodnick D. Vasileska. *Computational Electronics*. Morgan and Claypool, Arizona,United States, 2006.

[3] D.L. Scharfetter and H.K. Gummel. Large-signal analysis of a silicon read diode oscillator. *Electron Devices, IEEE Transactions on*, 16(1):64–77, 1969. ISSN 0018-9383.

[4] Mark H. Holmes. *Introduction to Numerical Methods in Differential Equations*. Springer Science,Business Media,, New York,United States, 2007. ISBN 978-0387-30891-3.

[5] Duncan R. Stewart R. Stanley Williams Dmitri B. Strukov, Gregory S. Snider. Missing memristor found. *Nature*, 453:80–83, 2008. ISSN 0028-0836.

[6] H. U. Schwarzenbach E. Knapp, R. Husermann and B. Ruhstaller. Numerical simulation of charge transport in disordered organic semiconductor devices. *J. Appl. Phys*, 108, 2010. ISSN 1089-7550.

[7] W. Lvenich U. Merker K. Reuter A. Elschner, S. Kirchmeyer. *Introduction to Numerical Methods in Differential Equations*. Taylor and Francis Group,, Florida,United States, 2011. ISBN 978-1-4200-6911-2.

[8] Snowden C.M. *Semiconductor Device Modelling*. Peter Peregrinus Ltd., London,United Kingdom, 1988.

[9] A.M. Nardes. *On the conductivity of PEDOT:PSS thin films*. PhD thesis, Technische Universiteit Eindhoven, Eindhoven, 2007.